Recent developments of $Na_4M_3(PO_4)_2(P_2O_7)$ as the cathode material for alkaline-ion rechargeable batteries: challenges and outlook

Aleksandra Gezović[a, #], Milica J. Vujković[b, # *], Miloš Milović[c], Veselinka Grudić[a], Robert Dominko[d,e], Slavko Mentus[b,f]

[a] Faculty of Metallurgy and Technology, University of Montenegro, Cetinjski put bb, 81000 Podgorica, Montenegro

[b] Faculty of Physical Chemsitry, University of Belgrade, Studentski trg 12-14, 11158 Belgrade, Serbia

[c] Institute of Technical Sciences of Serbian Academy of Sciences and Arts, Knez Mihajlova 35/IV, 11158 Belgrade, Serbia

[d] National Institute of Chemistry, Hajdrihova 19, SI-1000 Ljubljana, Slovenia

[e] FKKT, University of Ljubljana, Večna pot 117, 1000 Ljubljana, Slovenia

[f] Serbian Academy of Sciences and Arts, Knez Mihajlova 35, 11158 Belgrade, Serbia

# Contributed equally

*Corresponding author: Milica Vujković, Research Associate Professor

University of Belgrade, Faculty of Physical Chemistry

Studentski trg 12–14, 11158 Belgrade, Serbia

E–mail address: milica.vujkovic@ffh.bg.ac.rs;

Recent developments of $Na_4M_3(PO_4)_2(P_2O_7)$ as the cathode material for alkaline-ion rechargeable batteries: challenges and outlook

Aleksandra Gezović[a], Milica J. Vujković[b,*], Miloš Milović[c], Veselinka Grudić[a], Robert Dominko[d,e], Slavko Mentus[b,f]

Abstract:

Sodium ion batteries (SIB) present one of the most perspective post lithium technology and their progress strongly depends on the development of compounds having the structure which enables fast sodium insertion/deinsertion reactions. Polyanion compounds have been widely investigated as cathode materials for SIBs where they compete effectively to the usually used layered oxides. This survey is focused on the development of specific family of isostructural polyanion phases encompassed by the common chemical formula $Na_4M_3(PO_4)_2(P_2O_7)$. The comprehensive retrospective of their synthesis procedures, the kinetics and mechanism of sodiation/desodiation reactions, based on both experimental and theoretical results, is provided. First, the review summarizes the structural properties of variety of $Na_4M_3(PO_4)_2(P_2O_7)$ compounds in terms of its electrical, vibrational and surface properties. Then, the synthesis methods and sodium/lithium storage performance, of each type of $Na_4M_3(PO_4)_2(P_2O_7)$ compounds, are chronologically presented and discussed. Finally, the strengths and weaknesses of these mixed polyanion cathodes are outlined, with the aim to explain some discrepancies and unclarified issues encountered in the literature. Besides, this survey will make room for future development. It can be very useful for the future design of high-performance mixed polyanionic compounds as cathodes for alkaline-ion rechargeable batteries.

Keywords: polyanionic material, $Na_4M_3(PO_4)_2(P_2O_7)$, sodium-ion batteries, synthesis procedures, sodium redox processes.

1. Introduction

An increased utilization of intermittent renewable energy sources requires expansion of electrochemical energy storage systems (EESS) to a large scale, suitable to be integrated with renewable energy source devices into electrical grid. The state-of-the-art Li-ion batteries (LIBs) play the pivotal role, due to the capability of storing a large amount of energy, which is favorable for various applications such as portable electronics, electric vehicles and grid power stabilization units [1–9]. However, the demand for electrochemical storage devices keeps getting higher and higher, thus leading to an increased lithium consumption from limited resources and its steep price. To slow down this growth and control lithium supply, extensive studies on alternative systems, based on Na, Zn, Al, Mg, Ca, etc. [10–17], have been launched. The focus of these studies is actually on the development of cost-effective and environmentally friendly energy storage systems which would be capable of replacing Li-ion batteries, at least in the field where weight and/or volume are not a limiting factor. Among them, sodium-ion batteries (SIBs) have the great economic and energetic potential for grid-scale energy storage systems, due to the low cost and high sodium abundance in Earth's crust. Although SIBs theoretically possess less specific energy than Li ion batteries (the lower redox potential of Na^+/Na than Li^+/Li), the similarity between Li and Na chemistry and "rocking-chair" working principle caused their booming in recent years. Numerous studies have concentrated on the development of electrode materials and electrolytes through different synthesis methods and strategies, trying to get the best performance [18–25]. As a result, different anodes (hard carbon, metal oxides/sulfides…) [16,17,22,26] and cathode materials (oxides, polyanionic compounds…) [20,23,27–32] have been developed, which show not only ultra-fast sodium rate performance, but also the capability of storing larger amount of sodium than lithium ions.

Since Goodenough introduced $LiFePO_4$ olivine into the world of Li ion batteries [33–35], polyanionic-type materials (Fig. 1a) have been widely examined as cathode materials. Their three-dimensional framework, built on tetrahedral anions $(XO_4)^{n-}$ or their derivatives $(X_mO_{3m+1})^{n-}$ (X = P, Si, S, Se, Mo, W...) and corner - or edge-sharing MO_6 polyhedrons (M=transition metal), is suitable for diffusion of alkaline ions during charging/discharging and sufficient structural stability [30,36]. Sodium intercalation polyanionic structures based on phosphates ($NaMPO_4$, Nasicon type - $Na_3M_2(PO_4)_3$), fluorophosphates (Na_2MPO_4F, $Na_3M_2(PO_4)_2F_3$, $Na_3(VO)_2(PO_4)_2F$ …) and pyrophosphates ($Na_2MP_2O_7$…), where M is Fe, Mn, Co, V, etc., have experienced a huge expansion in the research field of alkaline-ion batteries [20,30,36–41]. The importance of investigating $NaFePO_4$ [31,32,39,40] should not be emphasized too much, bearing in mind the popularity of the commercial $LiFePO_4$ cathode material. Further, fluorine doping of phosphates is an effective way to increase redox potential via inductive effect and improve the kinetic of electrochemical reaction [30,42,43]. Also, pyrophosphates appear as promising cathode materials, possessing advantages over $MFePO_4$ in terms of offering 2D pathways for M^+ diffusion, higher voltage and higher thermal stability. On the other hand, their lower capacity, when compared to $MFePO_4$ compounds, can cause the lower energy density, if not compensated by the increased voltage [44,45].

Another group of pyrophosphates/phosphates with a mixed polyanionic group and a general formula of $Na_4M_3(PO_4)_2P_2O_7$ [46–48], have attracted an increased attention as novel Na-ion cathodes (Fig.1), due to low barrier for Na-ion diffusion and advantages over individual phosphate and pyrophosphate compounds.

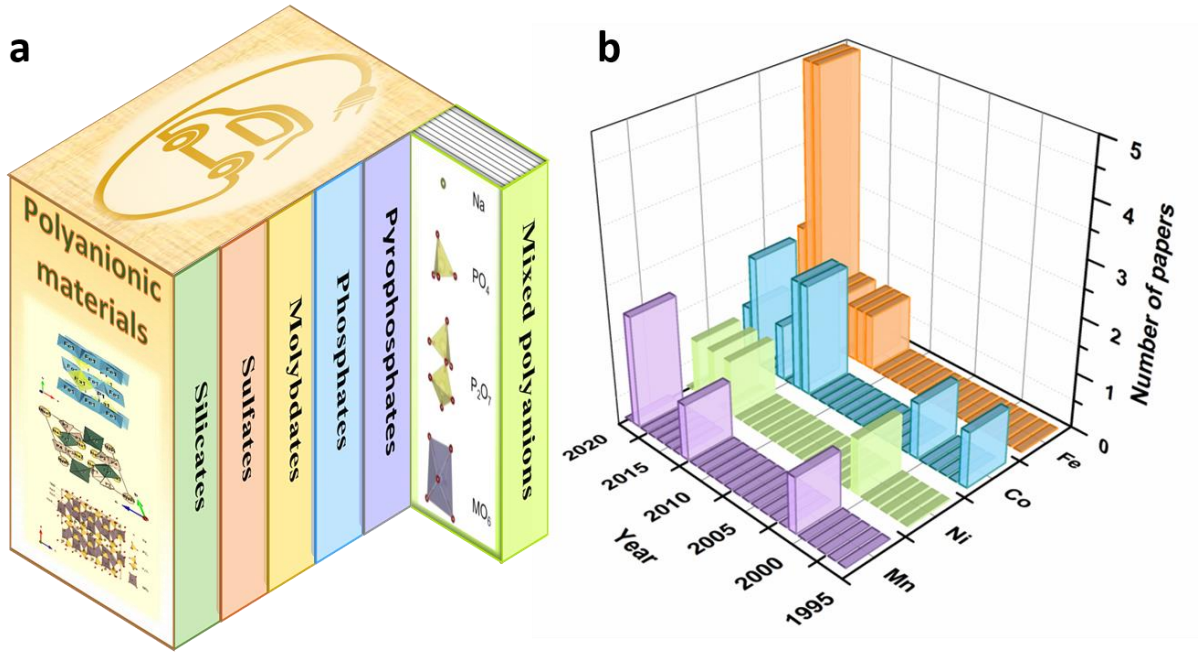

Fig. 1. The mixed-polyanionic compounds: a) the classification b) the recent development of $Na_4M_3(PO_4)_2(P_2O_7)$ where M=Co, Fe, Mn and Ni.

This mixed compound offers higher operating voltage and less volume changes than individual phosphates and pyrophosphate structures. For instance, the Fe^{2+}/Fe^{3+} redox potential increases following the order $FePO_4$, $NaFePO_4$, $Na_2FeP_2O_7$ or Na_2FePO_4F, $Na_4Fe_3(PO_4)_2P_2O_7$, amounting to 2,4 V, 2.7 V, 3V and 3.2 V versus Na^+/Na, respectively [36,49,50], as illustrated in Fig. 2a-c. The reason for the higher voltage of the mixed polyanionic compound agrees with the change of the M-O covalency strength via inductive effect from the neighboring polyanionic groups. The introduction of polyanionic units, in the structure, results in more resonance forms, thus causing a weaker (covalent) M-O bond and a shorter distance between bonding and antibonding orbitals. As a result, system with more polyanionic units will have a slightly higher voltage [51], despite the same nature of metal and polyanionic group. The control of electronegativity via polyanionic groups is an operative way to tune redox properties of the polyanionic cathode. The replacement of Fe in the mixed polyanion by some other transition metals such as Mn, Co, Ni, leads to the increase of the redox potential. In addition, the small volume change during Na^+ insertion/deinsertion is observed for $Na_4Fe_3(PO_4)_2P_2O_7$ (below 4%) [47], which is close to that for $Na_2FeP_2O_7$ (~ 2 %) [52,53], but significantly less than that for $NaFePO_4$ (~ 17 %) [54]. Furthermore, the issue of pyrophosphates' degradation, caused by reaction with moisture or CO_2,

as one of the crucial complications of pyrophosphates [55], is not pronounced for this type of mixed polyanion compounds.

Although these mixed phosphates have a higher molecular weight than individual phosphate or pyrophosphates, their three-dimensional (3D) channels could allow fast diffusion of sodium ions with low migration barrier (0.2-0.24 eV), while one Na^+ participates into electrochemical reaction of $NaMPO_4$ and $Na_2MP_2O_7$, thus diffusing through 1D and 2D channels, respectively [44,54,56]. Still, it should be noted that the Na^+ ion diffusion along the three principal axes of the $Na_2MP_2O_7$ material is also reported [57]. However, the diffusion barrier of mixed polyanion compound (0.2-0.24 eV) [58] is lower than those calculated for other polyanionic structures such as $NaMPO_4$ (for Fe 0.32 eV and 0.65 eV for Mn) [59,60], $Na_2MP_2O_7$ (0.49eV or 0.54 eV for Fe and 0.58 for Mn pyrophosphates) [56,57], Na_2FePO_4F (0.3 eV) [61] and $Na_3V_2(PO_4)_3$ (0.35 eV) [62], Fig. 2d. Based on the Arrhenius equation ($D= v\, e^{-Ea/kbT}$, D is diffusion coefficient, Ea is the activation diffusion barrier, k_b is Boltzman constant and v is the pre-exponential factor), this can be explained by the higher diffusion coefficients of mixed polyanionic compounds when compared to other polyanion structures. By using molecular dynamic (MC) simulations, Islam et al [58] calculated a high diffusion coefficient value of NFPP and NMPP amounting to 6.1×10^{-11} or 3.1×10^{-10} S cm^{-1}, which is in accordance with the experimentally obtained values ranging from 10^{-9} to 10^{-11} [63,64]. Experimental diffusion coefficients of some other polyanionic-type materials were found to be ~10^{-15} S cm^{-1} for $NaFePO_4$ [32], ~ 10^{-12} - 10^{-13} for Na_2FePO_4F [65], $2{,}79 \times 10^{-13}$ for $Na_2FeP_2O_7$ [44] and 6×10^{-13} - 2×10^{-15} S cm^{-1} for $Na_3V_2(PO_4)_3$ [66].

Phosphates/fluorophosphates have higher theoretical capacity than pyrophosphates (129 mAh g^{-1} vs. 97 mAh g^{-1} for Fe-based compounds) [23,44,67]. Nevertheless, this value is slightly lower than that for $NaMPO_4$ (129 mAh g^{-1} vs. 154 mAh g^{-1} for Fe) due to large differences in the molecular weights. If the mixed-polyanion has theoretical ability to exchange all four Na^+ [68,69], its capacity will be higher than that of $NaMPO_4$. The first principle calculation shows that the exchange of all Na^+ ions is possible in the case of $Na_4Co_3(PO_4)_2P_2O_7$, whereas deinsertion process of the last Na ion is followed by the electron transfer from the oxygen sublattice rather than the oxidation of Co^{3+} to Co^{4+} [70]. However, the process is found to be difficult due to channel's narrowing upon the last Na ion deinsertion. Moreover, the final extraction of the Na ion causes large volume changes, while the process itself occurs at very high potentials (4.93 V vs. Na^+/Na) where the electrolyte stability is the main issue. Nevertheless, theoretical capacity of NCPP is taken to be 170 mAh g^{-1} due to possible exchange of all four Na ions. So, this value would be larger than the one calculated for $NaCoPO_4$ amounting to 154 mAh g^{-1}. On the other hand, the cycling stability upon possible deinsertion of all four Na ions would be very challenging. Regarding $Na_4Fe_3(PO_4)_2P_2O_7$ structure, if the exchange of four Na^+ ions was possible, the oxidation of Fe^{2+} up to Fe^{4+} would happen. However, this process is not identified (so far at least). Moreover, Kim et al [71] observed that Na tunnels narrowed upon extraction of the third Na ion (Fe^{3+}-Fe^{3+} repulsion at the composition of $NaFe_3(PO_4)_2P_2O_7$), thus preventing further extraction of the last Na ion, which acts as a pillar. That is why the capacity of NFPP is calculated per three Na ions (based on Fe^{2+}/Fe^{3+} redox couple) and amounts to 129 mAh g^{-1}. If

the extraction of all Na^+ ions was achievable in real system (which in our opinion is not impossible), it would probably occur at such high potentials, while the structural collapse (due to removal of Na pillar) present the issue.

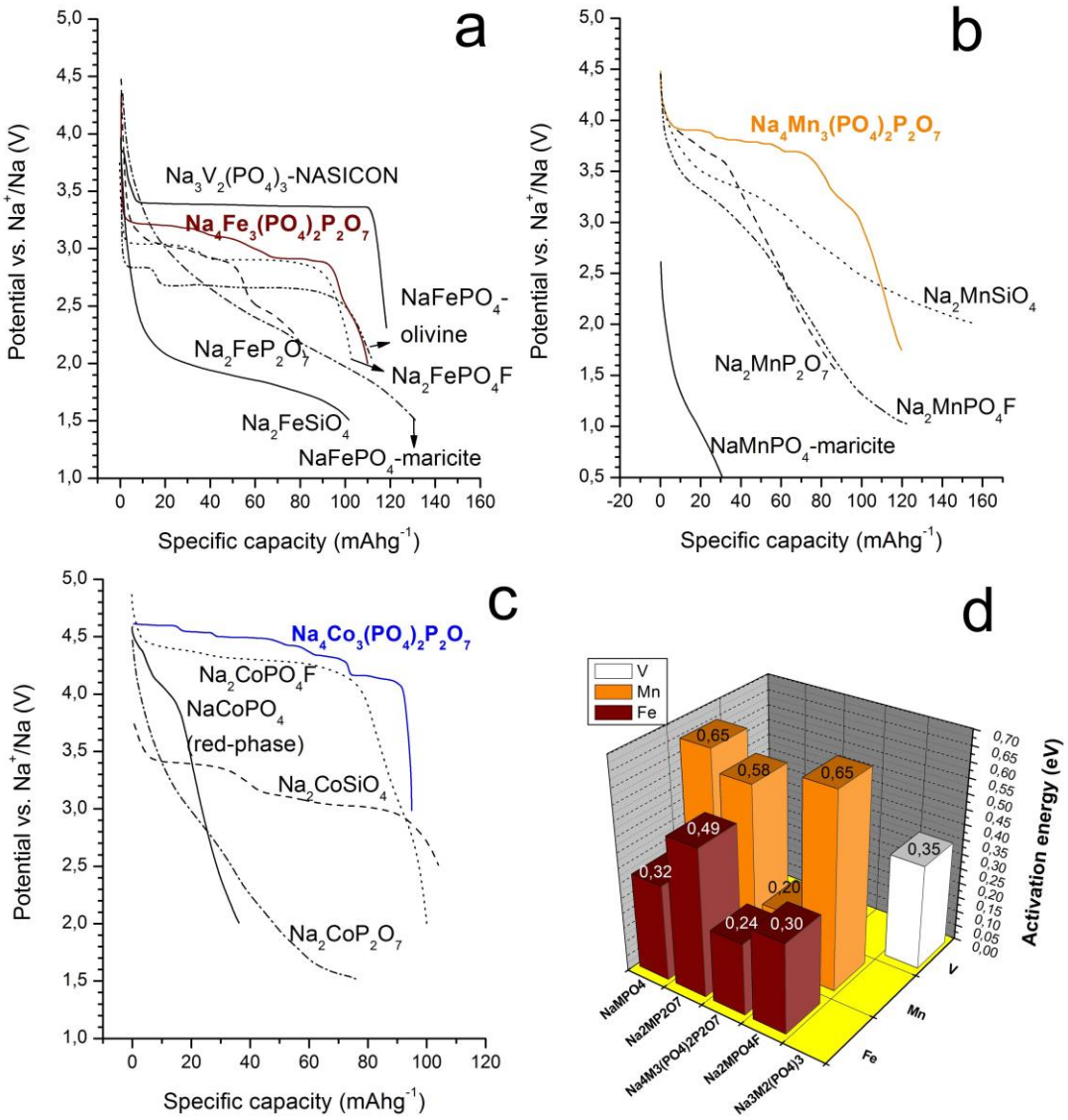

Fig. 2. Typical discharge profiles at low current densities (≤ C/10) of $Na_4M_3(PO_4)_2P_2O_7$ versus other polyanionic cathodes of Fe (a), Mn (b) and Co (c). Calculated activation barriers of Na^+ migration in various polyanionic compounds of Fe and Mn (d). Profiles are replotted with permission from [50] ($Na_4Fe_3(PO_4)_2P_2O_7$), [72] ($NaFePO_4$-olivine), [73] ($NaFePO_4$-maricite), [56] ($Na_2FeP_2O_7$), [74] (Na_2FeSiO_4), [75] ($Na_3V_2(PO_4)_3$-NASICON), [76] (Na_2FePO_4F), [77] ($Na_4Mn_3(PO_4)_2P_2O_7$), [78] ($NaMnPO_4$-maricite), [79] ($Na_2MnP_2O_7$), [80] (Na_2MnPO_4F), [81] (Na_2MnSiO_4), [68] ($Na_4Co_3(PO_4)_2P_2O_7$), [82] ($NaCoPO_4$ red-phase), [83] ($Na_2CoP_2O_7$), [84] (Na_2CoSiO_4) and [85] (Na_2CoPO_4F). DFT activation energy data are taken from [58] ($Na_4Fe_3(PO_4)_2P_2O_7$/$Na_4Mn_3(PO_4)_2P_2O_7$), [59] ($NaFePO_4$), [60] ($NaMnPO_4$), [57] ($Na_2FeP_2O_7$), [56] ($Na_2MnP_2O_7$), [61](Na_2FePO_4F) and [62] ($Na_3V_2(PO_4)_3$-NASICON).

`

Anyhow, all these comparative properties of these mixed polyanion compounds, emphasized as their strong and weak points are elaborated through this overview. Numerous review papers on the topic of sodium-ion batteries provide a general picture of all existing cathode materials [27–30,49,86–94]. Some of them are exclusively focused on the survey of polyanionic compounds [86,87,92–94] including novel cathode structures, such as these mixed phosphates. However, due to a large number of covered polyanionic structures in those studies, main points, related to the $Na_4M_3(PO_4)_2P_2O_7$, are outlined very briefly, thus leaving plenty of room for deeper discussion, more detailed insights and challenges for the specific structural composition. Therefore, this interesting $Na_4M_3(PO_4)_2(P_2O_7)$ structure containing 3d transition metals (such as Co, Fe, Mn and Ni) [46,48] needs to be further developed and improved as a cathode for SIBs. This paper offers the recent progress of each member of $Na_4M_3(PO_4)_2(P_2O_7)$ family (M=Co, Fe, Mn and Ni) starting from the synthesis methods, sodium insertion mechanism, to electrochemical behavior in both half-cells (vs. Na anode) and full coin-type configurations (vs. hard carbon anode). It summarizes the strengths and weaknesses of polyanionic cathodes and highlights main issues/contradictions from the literature, as directions for further research in this area.

2. Structure-to-property relations of $Na_4M_3(PO_4)_2P_2O_7$

2.1. Structure vs. electrochemistry

Sanz et al. [46,48] determined the crystal structure for different polymorphs of $Na_4M_3(PO_4)_2(P_2O_7)$. The $Na_4M_3(PO_4)_2P_2O_7$ compounds are isostructural and belong to orthorhombic space group No.33 ($Pn2_1a$) with similar lattice parameters and slight increase of the cell volume in order Ni<Co<Fe<Mn, as displayed in Table 1. It is the structure composed of alternating $\{M_3P_2O_{13}\}_n$ double layers built from edge- and corner-shared MO_6 octahedra and PO_4 tetrahedra (parallel to the b-c plane).

Table 1. Table comparing the unit call parameters of $Na_4M_3(PO_4)_2(P_2O_7)$ (M=Co, Fe, Ni, Mn)

Space group		$Pn2_1a$			
Space group no.		33			
Crystal System		orthorhombic			
M	Ref.	Cell parameters (Å)			Cell Volume (Å^3)
		a	b	c	
Ni	[47]	17.999(2)	6.4986(6)	10.4200(9)	1218.9(2)
Co	[49]	18.046(5)	6.533(2)	10.536(2)	1242.1(5)
Fe	[47]	18.07517(7)	6.53238(2)	10.64760(4)	1257.204(1)
Mn	[2]	17.991(3)	6.648(1)	10.765(2)	1287.6(3)

The $\{M_3P_2O_{13}\}_n$ layers are interconnected along a-direction by diphosphate P_2O_7 groups (acting as “pillars”) thus creating extensive tunnel network (along with three main crystallographic directions [100], [010] and [001]) that hosts Na cations. This stable framework is prone to small volume changes of just ~4 vol % (Fe) [71], ~ 7 vol % (Mn) [77], ~ 10 vol % (Co) [95] and ~ 2

vol % (Ni) [96] upon Na extraction. Three symmetrically distinguishable sites in octahedral coordination are reserved for a transition metal, while sodium ions are arranged in four crystallographic sites: Na(1), Na(2), Na(3) and Na(4), which are connected by channels (A, B and C) along all three axes (a, b, and c), as illustrated in Fig. 3. Na(2) atoms are located in the A1 channel, at the height of the $(Co_3P_2O_{13\infty})_y$ sheet, while the intersection of two tunnels B2xC1, A1xC1, and B1xC1, accommodates Na(1), Na(3) and Na(4), respectively, with a low activation barrier for all diffusion paths [47,58]. While the pathways, involving Na2 and Na3 sites, are essentially linear, those including Na1 and Na2 are curved ones [58]. The Na^+ ion diffusion coefficient (D_{Na}) of Fe and Mn-based compound is calculated to be in the range of 10^{-10} and 10^{-11} $cm^2\ s^{-1}$, respectively [47,58].

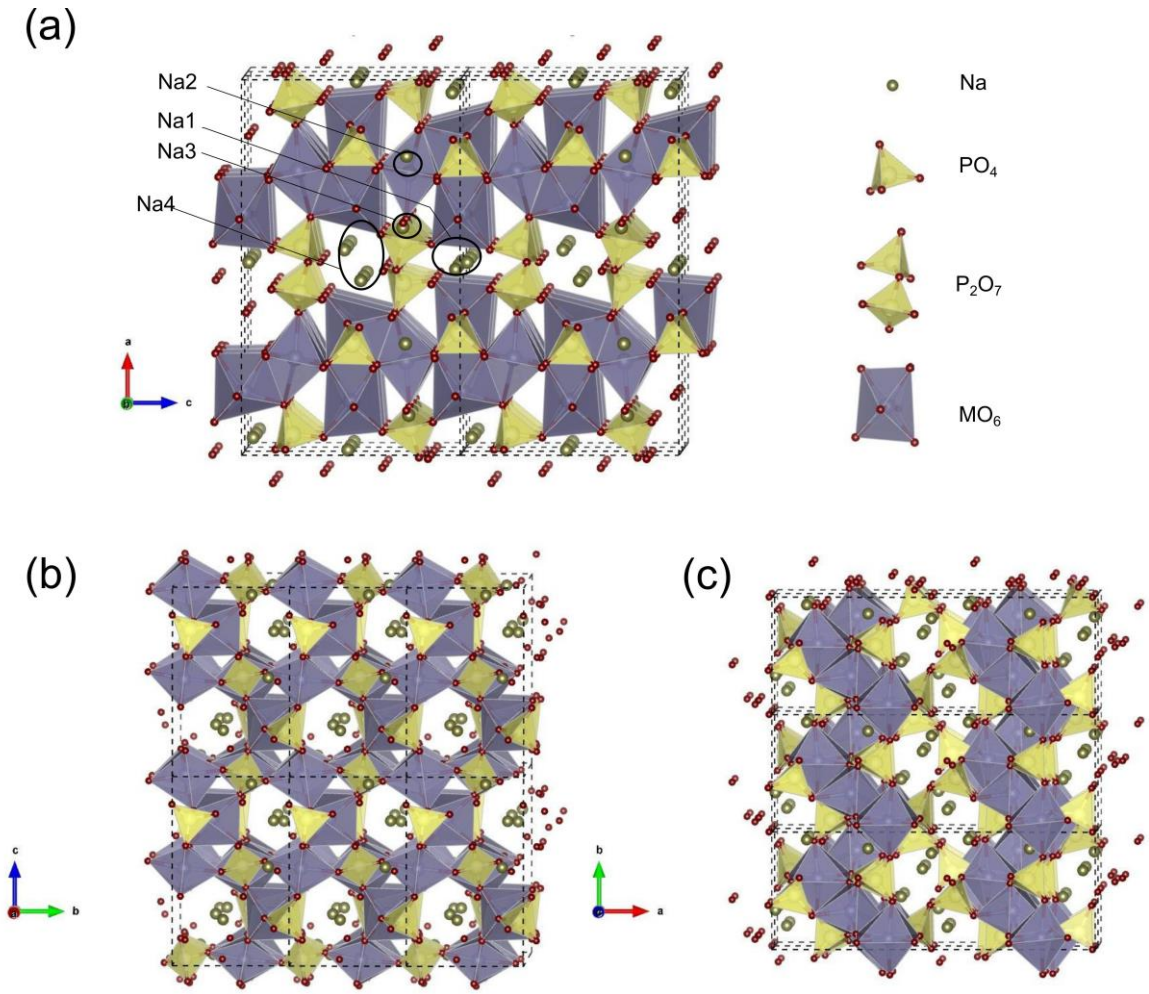

Fig. 3. The crystal structure of $Na_4M_3(PO_4)_2P_2O_7$ viewed along b-axis (a), a-axis (b) and c-axis (c); the structure is reproduced with permission from ref. [48].

The coordination number of Na sites is a matter of debate in the literature with no consent (see ref. [47,50,63,71,97]) and ranges from 5 to 7, but the majority of authors agrees that the lower coordinated sodium ions are extracted first. Anyhow, small changes in the crystal field, around different sodium atoms, noticeably affect potential of sodium intercalation, which is reflected as

the “stepped” discharge curve or as multiple redox peaks in cyclic voltammograms (or in dQ/dV profiles) of all $Na_4M_3(PO_4)_2P_2O_7$ compounds (Fig.3a,b). Except these small changes upon insertion, the discharge potential of M^{2+}/M^{3+} pair in $Na_4M_3(PO_4)_2P_2O_7$ follows the trend Ni>Co>Mn>Fe as a result of d-orbital splitting discrepancy, well-known from previous polyanion cathode compounds [51].

Reported ionic conductivities of the members of the $Na_4M_3(PO_4)_2P_2O_7$ family differ by several orders of magnitude (Fig. 4c). At 330 °C the ionic conductivity amounts to ~10^{-7}, ~10^{-6} and ~10^{-5} S cm^{-1} for $Na_4Ni_3(PO_4)_2P_2O_7$, $Na_4Co_3(PO_4)_2P_2O_7$ and $Na_4Mn_3(PO_4)_2P_2O_7$, respectively [46].

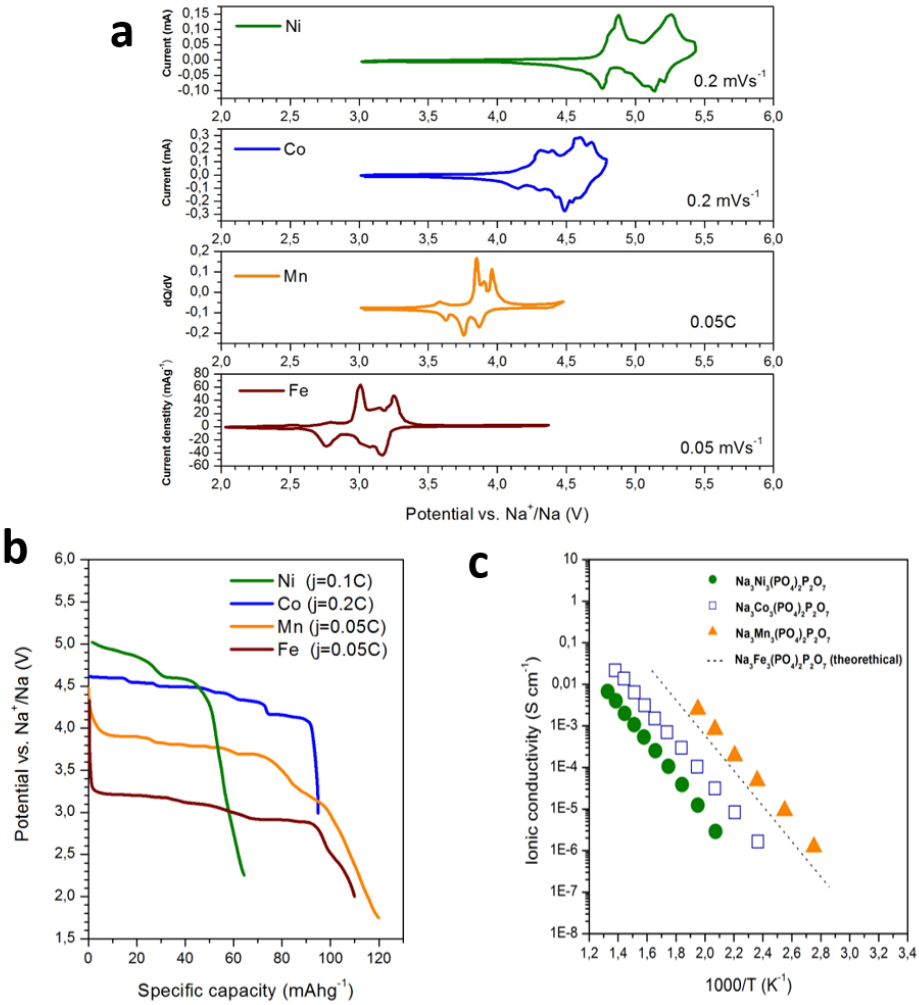

Fig. 4. a) Typical CV profile of $Na_4M_3(PO_4)_2P_2O_7$ (M=Ni, Co and Fe) and dQ/dV plot for M=Mn; b) Typical electrochemical discharge profile of $Na_4M_3(PO_4)_2P_2O_7$ (M=Ni, Co, Fe and Mn; the image is replotted with permission from [98] (for Ni), [67,68] (Co), [77] (Mn) and [50] (Fe); c) Arrhenius plots of the ionic conductivity of $Na_4M_3(PO_4)_2P_2O_7$ compounds; replotted with permission from [46] (for M=Co, Mn, Ni) and [58] (theoretically estimated for $Na_4Fe_3(PO_4)_2P_2O_7$).

Since diffusion of sodium dominantly takes place between $\{M_3P_2O_{13}\}_n$ layers in the bc-plane, the reported rise of conductivity is attributed to the increased dimensionality of the ionic conduction, i.e. to the facilitated transfer of sodium in a-direction and through $\{M_3P_2O_{13}\}_n$ layers. It is a result of channels' widening of the (larger Na2-O and N3-O distances) that go along this axis [46]. To date, however, there are no experimental reports for ionic conductivity values of the pure $Na_4Fe_3(PO_4)_2P_2O_7$ compound. Still, theoretically calculated Arrhenius plots of Na^+ diffusion coefficients suggest slightly lower ionic conductivity for $Na_4Fe_3(PO_4)_2P_2O_7$ than for $Na_4Mn_3(PO_4)_2P_2O_7$ [58]. So, the theoretically estimated values of sodium ion conductivity for the composition $Na_4Fe_3(PO_4)_2P_2O_7$ are also shown in the Fig. 4c.

2.2. DFT approach

The calculations based on DFT are now widely used investigation method of electrode materials for alkali-ion batteries. For calculations, usually Quantum Expresso or Vienna ab-initio simulation package (VASP) are used. Both software packages are based on plane-wave pseudopotential method, what implies a choice of a suitable pseudopotential function in input file formulation. Several other input data are necessary to run the software. The necessary crystallographic data (i.e. the coordinates of constituting atoms) are usually provided by X-ray diffractometry. The calculations with alkali iron phosphates and pyrophosphates [58,79,86] were successively performed using generalized gradient approximation (GGA) with the Perdew-Burke-Ernzerhof (PBE) exchange correlation functional. The Brillouin-zone integration is performed under suitable choice of Monkhorst-Pack grid. The criterion of good choice of input data is the convergence of the system total energy to a minimum. As explained in a recent review by Chakraborty et al [86] for a proposed crystallographic structure without or with defects, this method allows to determine the electronic structure, the enthalpy of formation of crystal lattice, the energy of formation of defects and the height of the ion migration barrier. Furthermore, assuming the closeness of enthalpy to the Gibbs free energy, one may calculate the open circuit potential for different charging degrees. Theoretical results could significantly save time for experiments serving as guidelines in materials engineering. As a good example, Park et al [79] searched the reasons of admirable $Na_2MnP_2O_7$ sodiation/desodiation kinetics relative to the monoclinic $Li_2MnP_2O_7$ by means of first-principle calculations. The explanation was found in the corner-sharing triclinic structure of $Na_2MnP_2O_7$ enabling the locally flexible accommodation of Jahn−Teller distortions on charging. On contrary, the edge sharing geometry of monoclinic $Li_2MnP_2O_7$ requires much larger atomic rearrangements during charging reaction, which slows down the reaction kinetics.

Several theoretical or combined experimental/theoretical studies relate just to the $Na_4M_3(PO_4)_2(P_2O_7)$ materials [58,70,71,99]

By combining experimental studies and DFT calculations, Kim et al [71,87,100] concluded that sodiation/desodiation reactions of the $Na_4Fe_3(PO_4)_2P_2O_7$ electrode proceed within a single phase. They experience very small volume change, less than 4%., while the oxidoreduction reactions of

Fe^{3+}/Fe^{2+} redox couple compensate the charge carried by sodium ions. This behavior is in contrast to that of individual phosphates ($NaFePO_4$) and pyrophosphates ($Na_2FeP_2O_7$), which possess two-phase electrochemical reaction.

Islam et al. [58] studied sodium storage mechanism in mixed phosphates $Na_4M_3(PO_4)_2P_2O_7$ (M = Fe, Co, Mn, Ni), using molecular dynamics (MD) and DFT simulations. The results of atomistic energy minimization demonstrated for all compositions that the most energetically favorable type of intrinsic defect are the Na/M anti-site pair. By means of mean square displacement inside the long-scale MD simulations, the sodium diffusion coefficients for Fe and Mn materials were determined. The results suggest that Na ions tend to diffuse across 3D migration pathways with a low activation barrier of 0.20−0.24 eV, allowing relatively high Na^+-diffusion coefficients of 10^{-10}–10^{-11} cm^2 s^{-1} at 325 K, suggesting good rate capability. The calculated trends of open circuit voltage for Ni doping in $Na_4Fe_{3-x}M_x(PO_4)_2P_2O_7$ show an increase in operational voltage from 3 to 4.9 V if x increases from 0 to 3.

Moriwake et al. [70] have also used the first principles DFT calculations to study the desodiation behavior of $Na_4Co_3(PO_4)_2P_2O_7$. Assuming a stepwise desodiation process, the removal of three Na ions (Na1, Na2 and Na4) down to $NaCo_3(PO_4)_2P_2O_7$ is found to be accompanied by oxidation of Co^{2+} to Co^{3+}. Further removal of the last Na (Na3) to give $Co_3(PO_4)_2P_2O_7$ requires oxidation of oxygen 2p orbitals in the P_2O_7 polyhedra instead of Co^{3+} being oxidized to Co^{4+}. Open circuit potentials have been calculated to increase from 4.05 to 4.33, 4.81 and 4.93 V (vs. Na^+/Na) for this stepwise desodiation.

Furthermore, Chen et al. [99] studied $NaFe_3(PO_4)_2P_2O_7$/C composite as cathode material. Structural investigations indicated low volume change of 4.0 % on charging/discharging cycle. Density functional theory (DFT) as well as bond valence sum (BVS) calculations were used to unveil possible sodium diffusion pathways. The authors discovered that the Na^+ ions can be assigned to three different types, based on their binding energies. The diffusion energy barriers, within the same Na^+ ion type, were found to be 0.553 eV, 0.02 eV, and 0.365 eV, respectively. These low barriers along all crystallographic axes allow three-dimensional diffusion pathways.

More comprehensive overview of theoretical calculations, regarding Na storage sites, Na diffusion sequence during deinsertion/insertion and migration barriers, will be elaborated within the following section 3, for each type of $Na_4M_3(PO_4)_2P_2O_7$ separately. The comparison of theoretical data with the experimental observations will be discussed as well. We would like to get the ball rolling by pointing out discrepancies which occur between different theoretical and experimental approaches.

2.3. Spectroscopic Study

The structural characterization of $Na_4M_3(PO_4)_2P_2O_7$ compounds is usually examined by FTIR, Raman and XPS methods. Vibrational spectrum of these mixed phosphate compounds consists

of the characteristic PO_4 and P_2O_7 bands [97,101], as presented in Fig. 5a,b. Vibrations of PO_4 group include symmetric and asymmetric stretching νP-O and bending δO-P-O modes. Vibrations of P_2O_7 (or O_3P-O-PO_3) are assembly of vibrations of PO_3 group and P-O-P bridges. The first one includes above mentioned νP-O and δO-P-O modes (as in PO_4) and the latter includes symmetric and asymmetric νP-O-P vibrations. The overlap of certain modes complicates the precise interpretation of the $Na_4M_3(PO_4)_2P_2O_7$ spectrum. For the sake of simplicity, the spectral region (1400-450 cm^{-1}) can be divided into several regions [97,101], as shown in Fig. 5. The 1200-990 cm^1 spectral region includes asymmetric stretching vibrations ν_{as}(P-O) in PO_3 and PO_4, while corresponding symmetric stretching vibrations contribute to the 990-900 cm^{-1} region. Further, the multiple bands, in the lowest frequency range of 500-680 cm^{-1}, have been assigned to the bending O-P-O vibrational modes (δ_{as}O-P-O). Also, Fe-O vibration mode of FeO_6 units contributes to this region. The position of this vibrational band is found to be 543 cm^{-1}, but for isolated FeO_6 octahedra [99]. Two bands, belonging to symmetric and asymmetric P-O-P vibrations in $P_2O_7^-$ group appear in the frequency range 900-700 cm^{-1}. According to Kosova [97], these modes are located at ~ 737 cm^{-1} (ν_s) and ~879 cm^{-1} (ν_{as}). However, there are some divergences/shifting regarding the assignation of these modes, since their positions have been found either at 721 (ν_s) and 956 cm^{-1} (ν_{as}) [102] or at 710 and 905 cm^{-1} [63]. It can be concluded that interpretation of the spectrum strongly depends on the sample's composition, i.e. on the presence of small fraction of the secondary phases and their nature.

To the best of our knowledge, infrared spectra of Ni-, Co- and Mn-based compounds of this family have not been reported yet. Due to close structural similarities of the compounds, it is expected that their respective spectra practically match the spectrum of $Na_4Fe_3(PO_4)_2P_2O_7$. Fe replacement with a more electropositive metal shifts the bands towards lower wavenumber values, Ni>Co>Fe>Mn (based on experience with phosphate [103] and pyrophosphate [104,105] family).

Raman spectroscopy and XPS are usually used for the surface characterization of the $NaM_3(PO_4)_2(P_2O_7)$. Raman spectra of Ni-based mixed polyanion (Fig.5b) reveals characteristic modes of mixed phosphates, positioned at ~1105 cm^{-1} , ~1056 cm^{-1} (the stretching modes of PO_4), ~958 cm^{-1} , ~718 cm^{-1} (the bridge P-O-P modes), 570 cm^{-1} and 348 cm^{-1} (the deformation of PO_4 and P-O-P), which are barely detected in the composite with carbon [106]. However, one can notice inconsistencies regarding other assignations, performed for $NaFe_3(PO_4)_2(P_2O_7)$/C [63,99], which are not mutually consistent. For instance, Chen et al [99] have identified typical Raman bands at 218.7 cm^{-1}, 288 cm^{-1} (belonging to stretching and banding vibrations of PO_4 units) and 402.1 cm^{-1} (belonging to the stretching vibrations of FeO_6 octahedra), while Pu et al [63] have recognized typical bands of FeO_4, PO_4 and P_2O_7 units at 451 cm^{-1}, 709 cm^{-1} and 1040 cm^{-1}, respectively. We are convinced that not only the quality of carbon layer contributes to these differences but also the chemical composition of the synthesized sample (in terms of the type and fraction of the secondary phase).

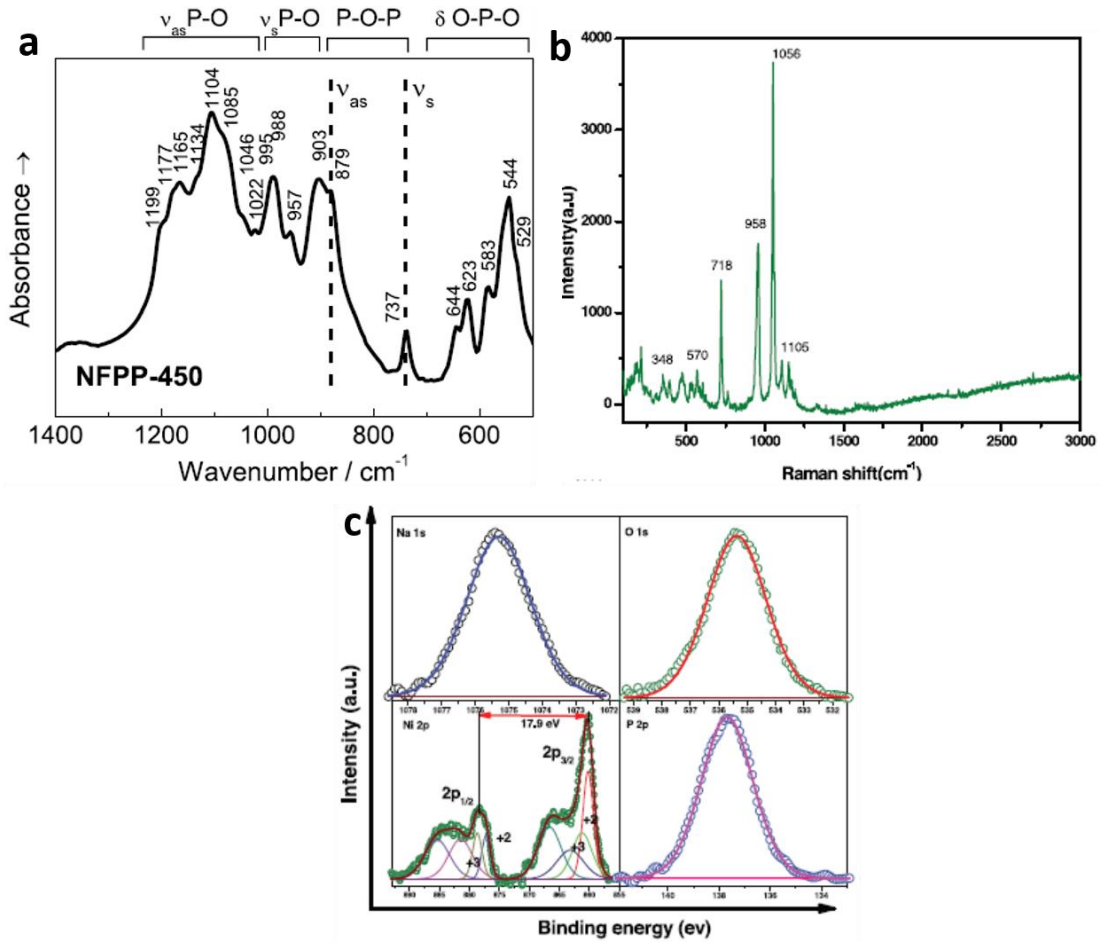

Fig. 5. a) FTIR spectrum of $Na_4Fe_3(PO_4)_2P_2O_7$, Reprinted with permission from ref.[97], Copyright 2018, Elsevier, b) Raman and c) XPS spectrum of $Na_4Ni_3(PO_4)_2P_2O_7$ Reprinted with permission from ref [106], Copyright 2015, Elsevier.

Furthermore, the typical XPS spectrum of the mixed polyanionic compound, such as $NaNi_3(PO_4)_2(P_2O_7)$ (Fig. 5c), shows that Ni 2p appears as a doublet of Ni $2p_{3/2}$ (~ 878.1 eV) and Ni $2p_{1/2}$ (860.2 eV), including satellite peaks at 866.3 eV and 883.3 eV as well. Each peak is resolved into two peaks, which correspond to Ni^{+2} and Ni^{+3} states. Also, Fe2p splitting into two major peaks, at the binding energies of ~ 711 eV (Fe $2p_{3/2}$) and ~ 725 eV (Fe $2p_{1/2}$) [63,107], indicates a divalent state of Fe in the $NaFe_3(PO_4)_2(P_2O_7)$ sample. It should be emphasized that the Raman and XPS analyses, of these isostructural polyanionic compounds, have been focused on the carbon analysis [102,107], as the most intensive feature in the spectrum. In some Raman spectra, the main phase cannot even be recognized, due to its coverage by the surface carbon layer [102,107,108].

An overview of each $NaM_3(PO_4)_2(P_2O_7)$ compound (M=Co, Fe, Mn and Ni), with the emphasis on the synthesis procedure, electrochemical behavior and sodium redox mechanism, will be provided in the following section.

3. The influence of the transition metal cations

3.1 $Na_4Co_3(PO_4)_2(P_2O_7)$ - NCPP

Although Sanz et al [48] determined the structure of $Na_4Co_3(PO_4)_2(P_2O_7)$ (NCPP) in 1996, the electrochemical behavior of this mixed polyanionic material has been examined since 2013, when the interests in sodium-ion batteries began to attract attention once again. In this regard, the sol-gel is the most commonly used synthesis method [67–69,95,109,110], while the spray-drying process [111] has also been reported. Let us provide, chronologically, an overview of the $Na_4Co_3(PO_4)_2(P_2O_7)$ electrochemical behavior and its sodium redox mechanism (the sequence of sodium deinsertion/insertion, the type of phase transition, etc.), which strongly depends on the synthesis conditions (type of precursors, temperature, the carbon source, etc.).

3.1.1. Sol-gel method

In 2013, Nose and co-workers [68,110] first reported the redox behavior of $Na_4Co_3(PO_4)_2P_2O_7$ (NCPP) for sodium ion batteries, by using the typical sol-gel method which includes mixing of the diluted nitrate solution of $(CH_3COO)_2Co$, $Na_4P_2O_7$ and $NH_4H_2PO_4$ and glycolic acid (to suppress the particle growth). By heating the gel at 700 ^oC, they have produced the $Na_4Co_3(PO_4)_2(P_2O_7)$ polycrystal (~ 3µm in diameter) consisting of submicron-sized primary particles, with the reversible capacity of 95 mAh g^{-1} (2.2. Na^+) at 34 mA g^{-1} (i.e 0.2 C, based on the theoretical capacity for 4 Na^+ which corresponds to the value of 170 mAh g^{-1}) and an average potential of 4.5 V vs. Na^+/Na. This comes from the multi redox peaks/plateaus, observed within the high potential region 4.1-4.7 V vs. Na^+/Na in $NaPF_6$/EC+DEC, which belong to Co^{2+}/Co^{3+} redox process (Fig. 6a). The full capacity was considered unattainable due to activity of Co^{3+}/Co^{4+} redox couple at potentials above 4.8 V vs. $Na^{+/}Na$. In addition to negligible capacity decrease after 100 cycles, Nose et al. [68] have also demonstrated the high rate capability of NCPP (10 C – 25 C), as evidenced by reaching the capacity of ~ 80 mAh g^{-1} at 25 C**.** A very small polarization of NCPP charge/discharge curves at these high current rates revealed its prominent advantage among reported Na^+ intercalation materials. By combining this material as a cathode, with a hard carbon as an anode, the authors have assembled 4 V-class sodium ion battery (C/$NaPF_6$//EC+DEC//$Na_4Co_3(PO_4)_2P_2O_7$), with the initial capacity of ~ 90 mAh g^{-1} and long-term cyclability (93% after 50 cycles and 83% even after 100 cycles). By doping Co sites with Ni and Mn [69], through the same sol-gel procedure, they have further managed to procure improved electrochemical properties of polyanionic cathode, within the potential region of 3-5.1 V in $NaPF_6$/EC+DEC. The $Na_4Co_{2.4}Mn_{0.3}Ni_{0.3}(PO_4)_2P_2O_7$ compound (with accompanied traces of $NaCoPO_4$ amounting to 0.5%) was capable of delivering specific discharge capacity of 106 mAh g^{-1} at 2 C and 103 mA hg^{-1} at 5 C (1 C=170 mA g^{-1}) (Fig. 6b). The capacity retention was 93 % and 88 % at 2 C and 5 C, although the authors showed only ten cycles. Unlike the multi-redox peaks of $Na_4Co_3(PO_4)_2P_2O_7$, two redox pairs of $Na_4Co_{2.4}Mn_{0.3}Ni_{0.3}(PO_4)_2P_2O_7$, narrow (~ 4.2 V) and broad (~ 4.6 V), were observed (Fig. 6b), as a consequence of mixing potentials of simultaneous Co, Mn and Ni redox processes (Co^{2+}/Co^{3+}, Mn^{2+}/Mn^{4+} via Mn^{3+} and Ni^{2+}/Ni^{3+}).

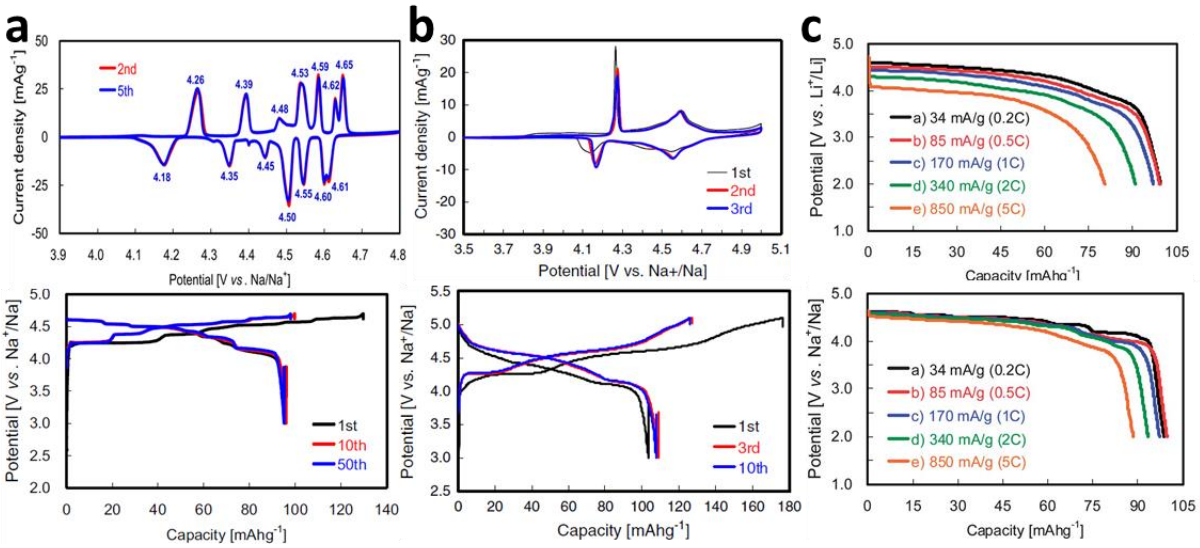

Fig. 6. a) CV and galvanostatic profiles of $Na_4Co_3(PO_4)_2(P_2O_7)$ measured at 0.01 mV s^{-1} and 0.2 C, respectively. (Reprinted with permission from ref [68] , Copyright 2013, Elsevier,); b) CV and galvanostatic profiles of $Na_4Co_{2.4}Mn_{0.3}Ni_{0.3}(PO_4)_2P_2O_7$ in $NaPF_6$/EC+DEC at 0.01 m V s^{-1} and 0.2 C, respectively (Reprinted with permission from ref [69], Copyright 2013, Elsevier); c) Discharge profiles of $Na_{1.4}Co_3(PO_4)_2P_2O_7$ at various C-rates in Li- and Na-ion cells (Reprinted with permission from ref. [109], Copyright 2014, The Royal Society of Chemistry); (1 C=170 mA g^{-1}).

In the next study, Nose et al. [109] showed that the lithiated form of the mixed polyanionic compound ($Li_4Co_3(PO_4)_2P_2O_7$) cannot be obtained chemically by the same sol-gel process. So, these authors have examined the lithium insertion capability of electrochemically desodiated form of $Na_4Co_3(PO_4)_2(P_2O_7)$, prepared by the deep anodic oxidation up to 4.8 V vs. Na^+/Na (corresponding to the capacity of 115 mAh g^{-1} or 2.6 Na^+). Such obtained $Na_{1.4}Co_3(PO_4)_2P_2O_7$ material shows the rapid Li^+ and Na^+ ion insertion capability. Its discharge capacity, measured in $LiPF_6$/EC+DEC solution, is close to 100 mAh g^{-1} at 0.2 C and 80 mAh g^{-1} at 5 C (2.4 Li^+ and 1.9 Li^+, respectively), while the corresponding discharge capacity in $NaPF_6$/EC+DEC solution amounts to 99 mAh g^{-1} and 89 mA hg^{-1}, respectively. So, the lithium and sodium storage capacity of this Na-extracted material are comparable at 0.2 C, while the better Na vs. Li capacity retention (90% vs. 80%) with the current rate increase to 5 C was observed (Fig. 6c). The higher operating voltage of sodium versus lithium redox process and the faster kinetics (which is attributed to the stronger interaction of Li^+-O^{2-} than Na^+-O^{2-}), have been verified. The lithium insertion capability (from the electrolyte) of this polyanionic compound is also proved in the full battery cell, which is composed of $Na_4Co_3(PO_4)_2(P_2O_7)$ as a cathode, $Li_4Ti_5O_{12}$ as an anode and $LiPF_6$/EC+EMC+DMC solution as the electrolyte. Such 3 V-class hybrid battery delivers reversible capacities of ~ 80 mAh g^{-1} at 0.2 C, ~ 65 mAh g^{-1} at 2 C and ~ 50 mAh g^{-1} at 5 C, with low coulombic efficiency at a low rate of 0.05 C (1-5 cycles), which is attributed to the irreversible decomposition of the organic electrolyte at the high potential of the positive electrode. An additional reason could be the deficit of Li ions since the electrolyte in this configuration is the only source of mobile ions.

With the aim to comprehend deeply the sodiation/desodiation behavior of this material, Moriwake et al. [70], in collaboration with Nose and co-workers, [68,109] have simulated each step of the $Na_4Co_3(PO_4)_2P_2O_7$ deinsertion process (the battery charging) by using the first principles calculations. They have reported the sequence of sodium deinsertion, from different sodium sites, as follows Na2, Na1 and Na4. Na2, The Na1 and Na4 deinsertion from $Na_4Co_3(PO_4)_2P_2O_7$, $Na_3Co_3(PO_4)_2P_2O_7$ and $Na_2Co_3(PO_4)_2P_2O_7$ phases, respectively, occurs at the potentials of 4.05, 4.33 and 4.81 V versus Na^+/Na, which reproduces experimentally obtained charge/discharge profile [68]. These authors have confirmed that these sodium deinsertion processes are accompanied by Co^{2+} to Co^{3+} oxidation (one third per each Na atom), with all Co^{3+} ions in highly spin state. The removal of the last Na atom (that is Na3 site occupied on A1xB1 tunnel intersection) from the $NaCo_3(PO_4)_2P_2O_7$ structure (happen at the highest potential of 4.93 V vs. Na) requires oxidation of oxygen 2p orbitals in the P_2O_7 polyhedra (verified through the formation of immobile holes at O^{2-} anions) rather than $Co^{3+} \rightarrow Co^{4+}$ oxidation. The absence of Co^{3+} to Co^{4+} oxidation, while the same one occurs in $LiCoO_2$, is explained by the less-densely packed phosphate structure (Fig. 7a). Small structural parameter changes (less than 3%) have been calculated upon deinsertion of three sodium ions. The removal of the last Na ion (from Na3 site) causes the narrowing of the Na channel, which along with the holes' strong self-trapping in P_2O_7 units, is considered to render kinetics of desodiation at the highest potentials. This is an explanation for the difficult deintercalation of all four Na atoms from the structure and achievement of the full theoretical capacity. Unlike these DFT studies [70] which showed the full extraction of the specified Na ion upon each redox process, experimental observations carried out by Zarrabeitia et al. [95] revealed that all four Na ions were partially extracted during redox processes within the voltage range 4.0-4.7 V vs. sodium. These authors have observed four biphasic regions (α-β, β-γ, γ-δ, δ-ε) during redox process of $Na_4Co_3(PO_4)_2(P_2O_7)$/C by the means of operando X-ray diffraction (XRD). That is evidenced by multiple-redox plateaus (more than three), which are followed by the solid-solution reaction at the highest potential (at the end of the charge), Fig. 7b. By using synchrotron XRD of the oxidized $Na_4Co_3(PO_4)_2(P_2O_7)$/C (at 4.67 V), three phases (α, β and δ) are evidenced (γ is not observable due to the used high current rate), where the sequence of Na^+ extraction is identified as follows: Na(4) progressively leaves the structure until it has been emptied in the δ phase (occ Na4 in α, β and δ phases is 0.68, 0.28 and 0) , Na1 is simultaneously removed, but at lower rates since ¼ remains in δ phase (occ Na1 is 0.82, 0.66 and 0.23), while Na2 and Na3 deinserted simultaneously at certain Na content (occ Na2 is 1, 1 and 0.64 and occ Na3 is 0.68, 0.28 and 0 in α, β and δ phases, respectively), with the partial occupation of Na2 in δ phase. The proposed Na^+ extraction sequence including all four Na ions, which is not in line with DFT study of Moriwake [70], has been confirmed by using the theoretical, bond valence energy landscape (BVEL) approach. Additionally, very low values of charge transfer resistance, Rct (< 7Ω) and its changes (2% variation between the lowest and the highest Rct value) have been identified upon occurrence of mentioned successive structural transitions.

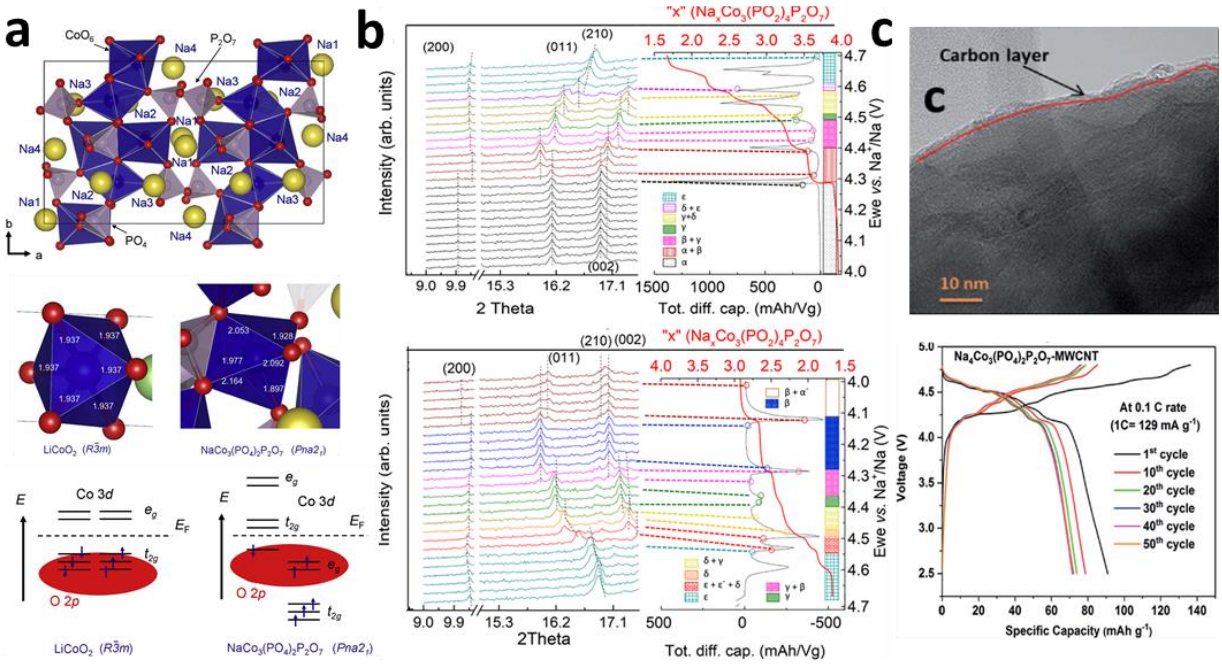

Fig. 7. a) Local environment of Co ions in $LiCoO_2$ and $Na_4Co_3(PO_4)_2(P_2O_7)$ structures and their Fermi energy, E_F (Reprinted from with permission ref [70], Copyright 2016, Elsevier,) b) Combined operando XRD and EIS data which show the evolution of the phase transitions (Reprinted with permission from ref. [95], Copyright 2019, American Chemical Society); c) TEM of $Na_4Co_3(PO_4)_2(P_2O_7)$-MWCNT and its galvanostatic profile measured in $NaPF_6$/EC+DMC at 0.1 C, at room temperature (1 C =129 mA g^{-1}). (Reprinted with permission from ref. [67], Copyright 2020, The Royal Society of Chemistry).

Furthermore, Kumar et al [67] have prepared the composite of $Na_4Co_3(PO_4)_2(P_2O_7)$ with multiwalled carbon nanotubes (NCPP - CNT), with the particle size of 200 nm, by modifying procedure developed by Nose et al [68]. They have used an aqueous solution instead of diluted nitric acid solution and the temperature of 650 ºC instead of 700 ºC. Also, the CNTs were added (instead of the glycolic acid) to provide ~ 16 wt% of the carbon in the composite. The redox behavior of the composite was found to depend on the composition of used electrolyte such as 1 M $NaPF_6$/EC+DMC and 1 M $NaClO_4$/PC+5% fluoroethylene carbonate (FEC), due to the difference in their electrochemical stability window (1-6 V and 1 - 4.8 V, respectively). Six anodic/cathodic peaks, positioned at 4.3/4.15 V, 4.4 /4.3 V, 4.5/4.42 V, 4.55/4.48 V, 4.6/4.53 V and 4.7/4.6 V, which correspond to Co^{2+}/Co^{3+} redox process are defined in CV of NCPP-CNT in $NaPF_6$/EC+DMC, while these peaks are poorly defined in $NaClO_4$/PC+FEC (the explanation is provided in the section 5). As a result, the initial specific capacity of NFPP-CNT in $NaPF_6$/EC+DMC solution was higher and amounted to 138 mAh g^{-1} (charge) and 92 mAh g^{-1} (discharge) at a current rate of 0.1 C (Fig. 7c). Unlike mentioned observations by Nose [68], these authors have estimated C_{theor} at 129 mAh g^{-1}, taking into account three Na^+ ions. The reversible specific capacity amounts to 80 mAh g^{-1}, thus retaining ~ 90 % of its own value after 50 cycles of charging/discharging. The similar capacity value was measured at 55 ºC (78 mAh g^{-}

[1] for 45 cycles), but with the lower coulombic efficiency (~ 85 %) due to the accelerated kinetics, at elevated temperature, during the charging process. The discharge capacity of NFPP-CNT at higher current rate of 1 C, 2 C, 5 C, 10 C and 20 C amounted to 55, 48, 39, 31 and 20 mAh g^{-1}, respectively. When the NCPP-CNT is used as cathode in the $NaTi_2(PO_4)_3$-MWCNT//$NaPF_6$/EC+DMC//NCPP-CNT full cell, it is capable of delivering the capacity of 75 mAh g^{-1} (the initial value) and 50 mAh g^{-1} (after 40 cycles) at 0.2 C rate, with a very low coulombic efficiency of 85%, which is probably due to the electrolyte degradation. Still, the measured capacities are b elow those observed by Nose [68] for the full SIB, using the pure NCPP as a cathode.

3.1.2. Spray-drying pyrolysis

One can see from previous studies that the sodium storage capacity of sol-gel synthesized NCPP lies noticeably below theoretical value (even if calculated for three Na ions), while the rate capability has been limited to 20C and capacity retention to 100 cycles. Liu et al. [111] have improved both rate capability and cyclic stability of $Na_4Co_3(PO_4)_2(P_2O_7)$ by Al doping of Co sites (on account of Na^+ vacancy generation), through the spray-drying method using $Co(NO_3)_2$, $Al(NO_3)_3$, $NaH_2PO_4x2H_2O$ and $C_6H_8O_7xH_2O$ as raw materials and CNT as the carbon source. The Al doping was found to increase ***a, b*** and ***c*** lattice parameters despite smaller Al^{3+}(0.535Å) than Co^{2+} (0.65Å) radius, while it improves ionic conductivity, charge transfer and structural stability thus maintaining the multiple redox behavior of an active phase (Fig. 8 a-c). A moderate amount of Al increases the sodium storage properties (from 82.8 to 99.5 mAh g^{-1} at 0.5 C for x=0.15 in $Na_{4-x}Co_{3-x}Al_x(PO_4)_2P_2O_7$) (Fig. 8c, left), while the excessive Al dopant reduces the electrochemical activity (85 mAh g^{-1} at 0.5 C for x=0.2) (Fig. 8c, middle). The $Al_{0.15}$-NCPP hollow microspheres (inset in Fig. 8c) with the size of 0.5-3 μm and shell thickness of 465 nm, composed of NCPP nanoparticles and CNT conductive network, can deliver the highest discharge capacity in $NaPF_6$/EC+DEC+FEC electrolyte, amounting to 99.5, 93.2, 89.2, 85.8 and 83.2, 80.3, 77.7 and 73.4 mAh g^{-1} at 0.5, 1, 2, 5, 10, 20, 30 and 50 C (1 C =170 mA g^{-1}). Its capacity retention of 98.4 % (after 800 cycles at 5 C) or 96.3 % (after 900 cycles at 10C) is higher than one observed for Al-free sample (91.1 % and 80.3 %, respectively). Superb capacity retention of 82.7 % was measured over 8000 cycles at an extremely high current rate of 30 C (Fig. 8c, right). Excellent rate capability of the full battery cell C//$NaPF_6$/EC+DEC+FEC//$Al_{0.15}$-NCPP (88.1 mAh g^{-1} at 5 C and 70.6 mAh g^{-1} at 30 C) and outstanding cycling stability (95 % of capacity maintaining after 200 cycles at 1 C), was also demonstrated. However, it should be taken into account that such a high rate capability is achieved under a quite small electrode loading (1.3 mg cm^{-2}). To meet the practical demands, such high C-rate properties need to be achieved under much higher loadings, which remains the challenge for this type of material.
It can be concluded that there is a need for further improvement of Co-based mixed polyanionic compound, especially at high current rates, through the development of different synthesis/strategies. They should primarily aim at reducing particles to nanodimensions. Besides, the issue of C-value should be addressed since the comparison of the specific capacity between different reported materials is not adequate due to different C-values taken.

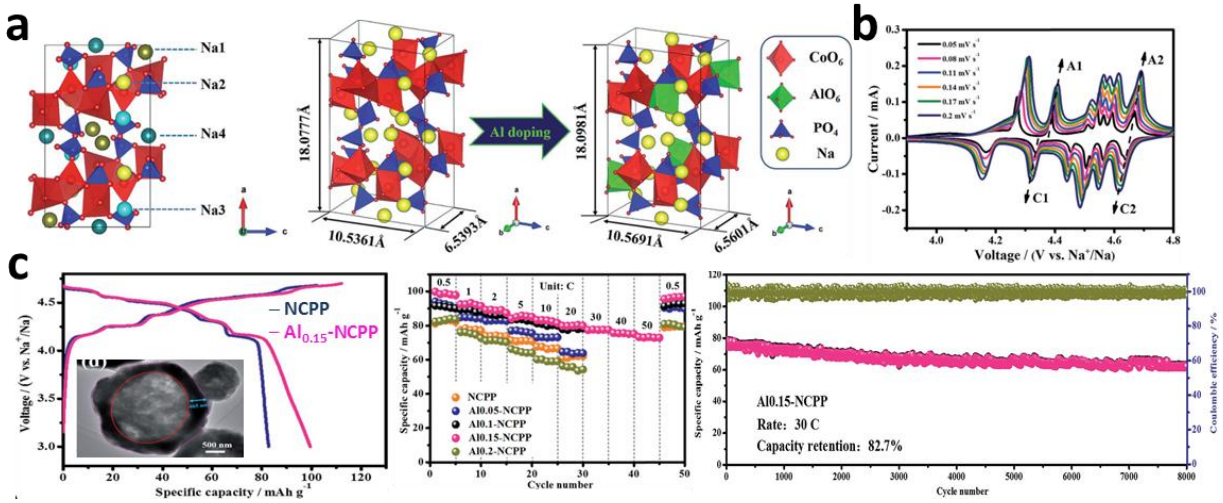

Fig. 8. a) The $Na_4Co_3(PO_4)_2(P_2O_7)$ and $Na_{3.85}Co_{2.85}Al_{0.15}(PO_4)_2P_2O_7$) ($Al_{0.15}$-NCPP) structures b) Cyclic voltammograms and c) Charge/discharge performance of $Al_{0.15}$-NCPP performed in $NaPF_6$/EC+DEC+FEC at different scan rates and current densities, respectively (1 C = 170 mA g^{-1}); Inset in c) shows $Al_{0.15}$-NCPP hollow microspheres observed by TEM (Reprinted with permission from ref. [111], Copyright 2019, The Royal Society of Chemistry).

3.2 $Na_4Fe_3(PO_4)_2(P_2O_7)$ - NFPP

3.2.1. Solid-state method

Solid-state synthesis of $Na_4Fe_3(PO_4)_2(P_2O_7)$ (NFPP) powder [47,71,97,112–115] usually employs $Na_4P_2O_7$, $Fe_2C_2O_4{\cdot}2H_2O$, and $NH_4H_2PO_4$ or $(NH_4)_2PO_4$ as Na, Fe and P sources. Kim et al [47,71] have proposed the NFPP crystalized in the orthorhombic crystal structure ($Pn2_1a$ space group) as a promising mixed-polyanion cathode for Na rechargeable batteries (Fig. 9). Simple, two-step solid-state synthesis method (ball milling at 70 ^{o}C + solid-state reaction at 500 ^{o}C) was used to obtain NFPP particles (100-200 nm), with the small fraction of accompanied maricite $NaFePO_4$ phase (~ 4 %). While the NCPP phase can be obtained at 700 ^{o}C, NFPP undergoes thermal decomposition above 530 ^{o}C, thus producing different Na-rich and Na-poor phosphate or pyrophosphate phases, depending on the sodium content [71]. In $NaClO_4$/PC electrolyte, solid-state prepared NFPP showed an average operating voltage of ~ 3.2 V and the initial specific capacity of ~ 113 mAh g^{-1} at C/40 (~ 88 % of the C_{theor}) and ~ 106 mAh g^{-1} at C/20 (i.e. ~ 82 % of the C_{theor}). Authors showed only 15 cycles (the capacity is estimated per NFPP mass unlike that shown in Fig. 9c), respectively (1 C = 129 mAg^{-1}), Fig. 9b,c. The significant P_2O_7 distortion in lattice occurs at the last stage of charging (caused by Fe^{3+}- Fe^{3+} repulsion at the composition of $NaFe_3(PO_4)_2P_2O_7$), thus leading to a shift from edge to corner sharing of FeO_6 polyhedra between the Fe1 and Fe3 sites. It results in the contraction of Na diffusion tunnels and mobility reduction of the remaining Na ion [71]. That is why three Na ions from $Na_4Fe_3(PO_4)_2(P_2O_7)$ were found to participate in the electrochemical reaction during charging/discharging. Therefore, the theoretical capacity is calculated to be 129 mAh g^{-1} (based on possible exchange of three sodium ions). The same authors [47] also reported the

$Li_3NaFe_3(PO_4)_2(P_2O_7)$, prepared by chemical Na-Li exchange of $Na_4Fe_3(PO_4)_2(P_2O_7)$ (three Na were exchanged by Li cations), with an average potential of 3.4 V and initial capacity of ~119 mAh g^{-1} at C/20 measured in 1 M $LiPF_6$/EC+DMC (Fig. 9d). The lithium storage capacity of this electrode is capable of being improved to ~ 140 mAh g^{-1} (at C/5) by increasing the temperature of the Li-cell to ~ 60 ° C, thus retaining 86% of its value after 100 cycles (Fig. 9e). The high energy density of both Na-ion ($Na//NaClO_4$-PC//$Na_4Fe_3(PO_4)_2P_2O_7$) and Li-ion cells ($Li//LiPF_6$/EC+DMC//$Li_3NaFe_3(PO_4)_2P_2O_7$) amounted to energy densities of 380 Wh kg^{-1} and 460 Wh kg^{-1}, respectively (based on the materials' level).

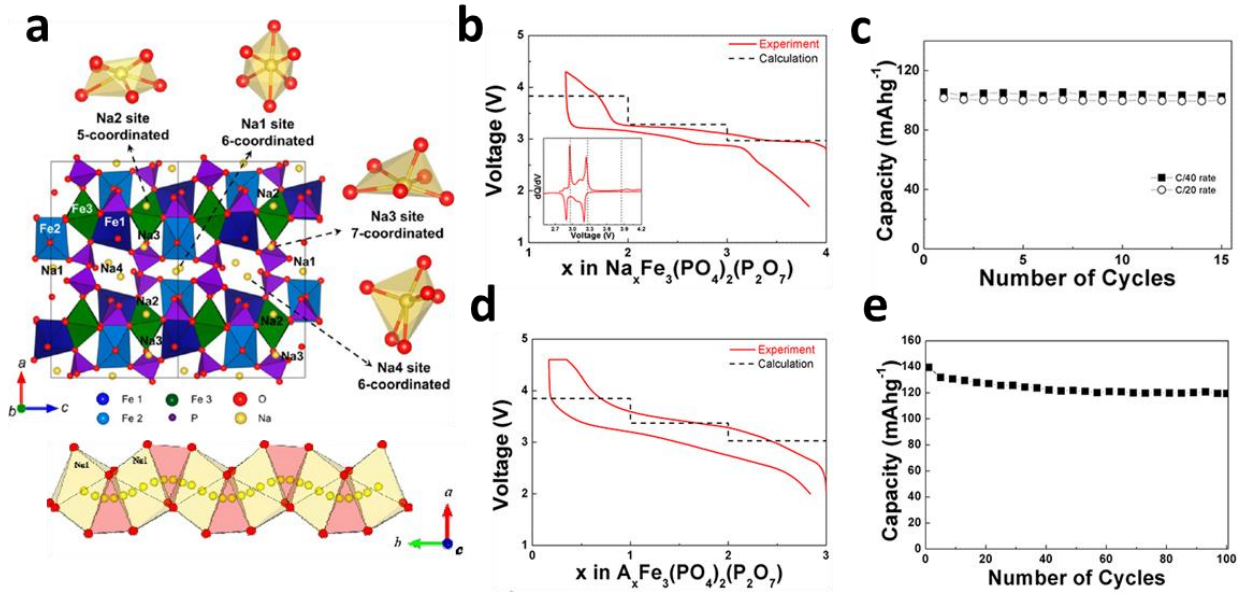

Fig. 9. a) Schematic representation of $Na_4Fe_3(PO_4)_2(P_2O_7)$ structure, its Na diffusion channel along the b-axis and different Na sites; b) Charge/discharge profile and c) cyclic performance of solid-state prepared $Na_4Fe_3(PO_4)_2(P_2O_7)$ in $NaClO_4$/PC at C/40 (b, c) and C/20 (b); (1 C = 129 mAh g^{-1}); d, e) Charge/discharge profile and cycle performance of $Li_3NaFe_3(PO_4)_2(P_2O_7)$ in $LiPF_6$/EC+DMC at C/20 (~ 25 ° C) and C/5 (~ 60 ° C), respectively. Reprinted with permission from ref. [47,71] Copyright 2012, 2013, American Chemical Society).

By investigating the electrochemical mechanism of $Na_xFe_3(PO_4)_2(P_2O_7)$ ($1 \leq x \leq 4$) through combined computation and experiments, Kim et al. [71] showed that this material underwent one-phase Fe^{2+}/Fe^{3+} electrochemical reaction (without formation of intermediate phase), with an exceptionally small volumetric change (less than 4%), unusual for larger Na ions. It is explained by the capability of P_2O_7 dimers to rotate and distort (provided by the open 3D framework) to accommodate structural changes. Four distinguishable Na sites, with a low activation barrier for all diffusion paths are identified, whereas the Na sinusoidal diffusion in the large tunnel along the b-axis (from Na1 site to another Na1 site) shows the lowest activation energy of 256 meV (Fig. 9a). Very low energy barrier for three-dimensional diffusion pathways of Na ions was also confirmed by Chen et al. [99], who calculated the values of 0.553 eV, 0.02 eV and 0.365 eV, thus revealing the barrier-less diffusion of Na^+ ions along ***a*** direction. Based on the first principle calculations, Kim et al. [71] have determined the sequence of Na extraction: I. Na ions are first

extracted from the Na2 site (5-coordinated); II. After their complete extraction, half of Na ions in both Na1 (6-coordinated) and Na4 sites (6-coordinated) are simultaneously extracted and III. The half of Na ions from Na3 site (7-coordinated) and remaining half of Na ions from Na1 site (6-coordinated) are deinserted thus leaving the half of Na ions in both Na3 and Na4 sites which do not participate in electrochemical reaction. Still, the exact order of the Na ion deinsertion/insertion is still unknown. Let us express some discrepancies here. Wu et al. [50] and Kosova et al [97] have exposed different Na sites coordination and arrangement, pointing out the preference of extracting Na ions with lower coordination number. Based on the results of solid-state NMR spectroscopy, Wu et al. [50], reported the next Na extraction sequence: Na3 (five-coordinated) and Na1 (six-coordinated), followed by Na4 (six-coordinated), while the Na ions from seven-coordinated Na2 hardly participate in the electrochemical reaction. Furthermore, Kosova et al. [97] have confirmed "non-activity" of Na2 positions, thus suggesting (based on the Rietveld refinement of the XRD pattern) different coordination numbers of Na1, Na2, Na3 (6-coordinated) and Na4 sites (7-coordinated) than those in references [50,71] and indicating that the insertion of Na ions happens opposite to the deinsertion (i.e. the charging process), following the order Na4, Na1, Na3. These authors indicate an imparity of three Fe different sites (relying on the results of 57Fe Mössbauer measurements), which does not go along with Kim's observations [71] based on equal distribution of Fe ions between three sites.

Solid-state synthesis procedure, developed by Kim, has been adopted in further studies [97,112–115] aimed at improving the electrochemical properties of NFPP, either through the selection of an appropriate electrolyte [112,115] or through the carbon addition/coating [97,113,114]. By using the mixture of ethylene carbonate and propylene carbonate (EC+PC), as a solvent for $NaClO_4$, Jang et al. [112] measured the initial specific capacity of NFPP very close to the theoretical value, amounting to 128 mAh g^{-1} at C/20, as shown in Fig. 10a. About 97 % of the initial capacity can be retained after 100 cycles of charging/discharging. The use of electrolytes with 1 M $NaClO_4$ in the combination with EC and PC solvents instead of EC and DEC in the Na/NFPP cell leads to the higher discharge capacity and columbic efficiency. This can be attributed to higher ionic conductivity, lower reactivity with Na metal and higher stability under high voltage conditions of 1M $NaClO_4$/EC+PC, when compared to 1M $NaClO_4$/EC+DEC (Fig. 10a). Ropero et al. [114] modified the solid-state procedure [47,71,112] by adding the conducting carbon into reagent mixture, to produce the $Na_{3.97}Fe_3(PO_4)_2(P_2O_7)$/3.04wt%$NaFePO_4$/7.8wt%C composite with an extended potential of application in terms of high current performance (up to 1 C) and aqueous batteries. Actually, the synthesized composite may deliver the initial discharge capacity of 99 mAh g^{-1} at 1C in $NaClO_4$/EC+PC (Na metal as an anode) and 84 mAh g^{-1} in an aqueous solution of 1 M Na_2SO_4 (the aqueous type of cell with AC as an anode), thus retaining 99 % and 74 % of the initial value after 50 cycles, respectively (Fig. 10b,c). The less capacity retention of NFPP in an aqueous than in an organic cell could be attributed to the material solubility in an aqueous electrolyte (more precisely the hydrolysis of pyrophosphates which lead to iron oxides and sodium phosphate) and the sample oxidation upon the discharge process. The sodium storage capacity of this mixed polyanionic cathode, in an aqueous electrolyte, exceeds the capacity of other materials such as $Na_2FeP_2O_7$ (55 mAh g^{-1}), $NaFePO_4$ (70 mAh g^{-1}), $Na_{0.5}Ti_{0.5}Mn_{0.5}O_2$ (46 mAh g^{-1}) and

$Na_3MnTi(PO_4)_3$ (58 mAh g^{-1}), also measured in the aqueous-based electrolytes, while the capacity retention is below that measured for $Na_2Fe_2P_2O_7$ (86 % after 300 cycles) or $NaFePO_4$ (90 % after 30 cycles) [114].

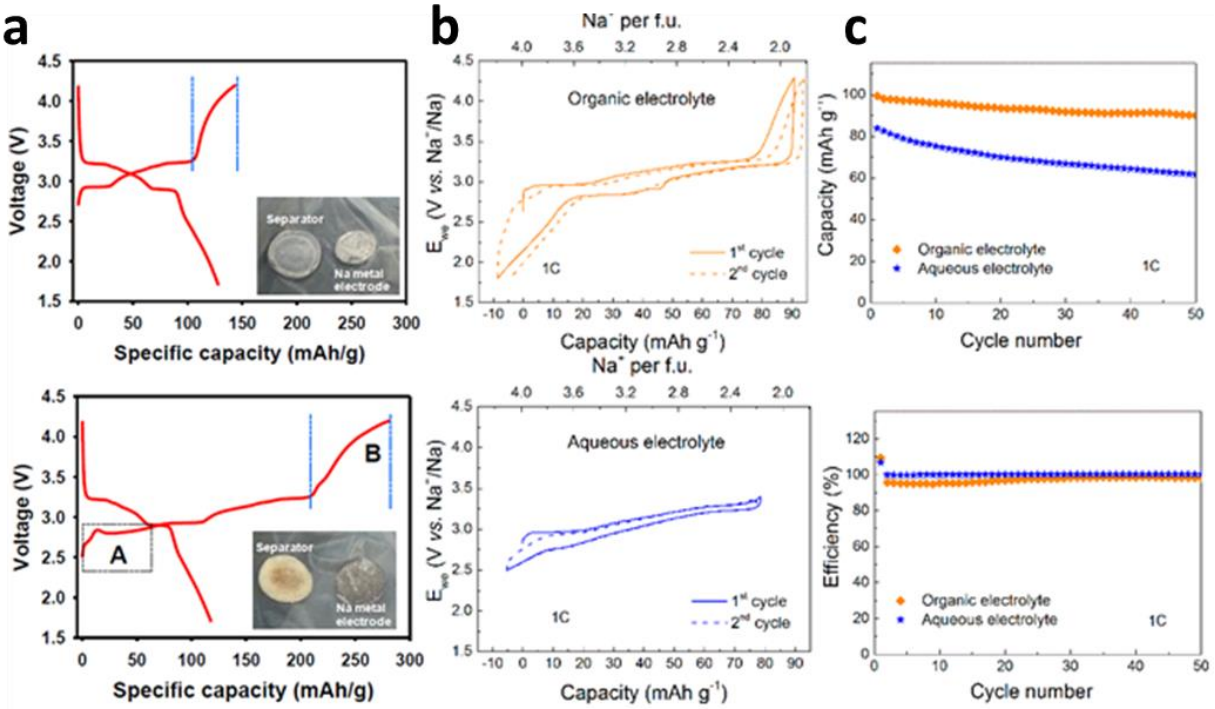

Fig. 10. a) The initial charge/discharge curves of solid-state prepared $Na_4Fe_3(PO_4)_2(P_2O_7)$ measured in $NaClO_4$/EC+PC (top) and $NaClO_4$/EC+DEC (bottom); (Reprinted with permission from ref. [112], Copyright 2014, Elsevier); b) galvanostatic profiles and c) cyclic performance of $Na_{3.97}Fe_3(PO_4)_2(P_2O_7)$/3.04wt%$NaFePO_4$/7.8wt%C measured in an organic ($NaClO_4$/EC+PC) and aqueous electrolyte (Na_2SO_4), at a current rate of 1 C (1 C = 129 mAh g^{-1}); (Reprinted with permission from ref. [114], Copyright 2018, American Chemical Society).

Recently, Kang and his collaborators [115] have demonstrated an excellent NFPP performance in the highly concentrated aqueous electrolyte of $NaClO_4$ (17 M), capable of providing a high-voltage aqueous-type of sodium ion batteries. In both 1 M and 17 M $NaClO_4$ aqueous solutions the NFPP showed the discharge capacity of 90-100 mAh g^{-1} at 1 C and an average redox voltage of 3.2 V vs. Na^+/Na, which is very similar to the performance in an organic electrolyte. What is very important is that the oxygen evolution reaction (OER) at NFPP is not induced before 4.2 V vs. Na^+/Na in 17 M $NaClO_{4aq}$, while the oxygen evolution in 1M $NaClO_{4aq}$ was observed at 3.9 V vs. Na^+/Na (the theoretical oxygen evolution potential corresponds to 3.5 V vs. Na^+/Na). With the aim to demonstrate the practical application of NFPP in the aqueous Na-ion battery of an extended voltage, Kang's team constructed the cell containing NFPP as a cathode, $NaTi_2(PO_4)_3$ as an anode and the aqueous salt of $NaClO_4$ as an electrolyte. The capacity of this battery using 1 M $NaClO_{4aq}$ decreases rapidly, from the initial 44 to 8 mAh g^{-1} after 50 cycles (calculated per both anode and cathode masses) or from 87 to 17 mAh g^{-1} if the capacity is calculated per NFPP cathode mass. Poor capacity retention (18%) and columbic efficiency (from the initial 87 % up to

68 % after 50 cycles), measured in 1 M $NaClO_{4aq}$, are considerable disadvantages. However, notable improvement of this battery was achieved using 17 M $NaClO_{4aq}$ as the electrolytic solution, where the capacity retention after 200 cycles and coulombic efficiency were found to be 75 % and 99 % at 1C, respectively. The constructed $NaTi_2(PO4)_3$//17M $NaClO_{4aq}$//$Na_4Fe_3(PO_4)_2(P_2O_7)$ full cell is capable of delivering an energy density such as 36 Wh kg^{-1}, outperforming the state-of-the-art experimental sodium batteries based on super-concentrated $NaCF_3SO_3$ electrolyte solution.

Kosova et al. [97,113] also adopted mechanochemically assisted solid-state method [47,71] to get $Na_4Fe_3(PO_4)_2(P_2O_7)$ particles (the average size of 100 nm) covered by carbon layer of ~ 2-3 nm (NFPPC) (Fig. 11a). Unlike the proposed synthesis procedure, in mentioned Kim's papers [47,71], the soot is used as a carbon source and the time of mechanical milling of reagent mixtures (under Ar atmosphere) is shortened to only 5 min. Kosova's study [97] indicates the strong influence of the synthesis conditions on the phase purity of targeted $Na_4Fe_3(PO_4)_2(P_2O_7)$ phase and its structural arrangement. First, the solid-state reaction, without mechanical treatment, does not cause the formation of $Na_4Fe_3(PO_4)_2(P_2O_7)$ phase (the mechanical milling facilitates the solid state-reaction). Second, the chemical composition of the solid-state reaction prepared sample significantly varies, depending on the temperature of heating. Actually, the temperature selection, within the 400 - 600 ^{o}C range, determines the type and fraction of secondary phases in the sample, as shown in Table 2.

Table 2. The chemical composition of the solid-state prepared NFPP determined by XRD Rietveld refinement; Replotted with permission from ref. [97].

Sample	XRD Rietveld refinement		
	NFPP, %	$NaFePO_4$, %	$Na_2FeP_2O_7$, %
NFPP-600	56.7	25.3	18.0
NFPP-500	64.2	22.7	13.1
NFPP-450	89.1	10.9	-
NFPP-450 (quenching)	93.8	6.2	-
NFPP-400	61.8	28.9	9.3

The highest fraction of NFPP phase and one type of secondary phase (maricite $NaFePO_4$) is obtained at 450 ^{o}C (NFPP-450). Third, the quenching of this sample leads to the increase of the NFPP fraction (96 : 6 = NFP : $NaFePO_4$ for 450 ^{o}C), but results in the higher structural distortion of FeO_6 octahedra (due to the partial $Fe^{2+} \rightarrow Fe^{3+}$ oxidation), as evidenced by X-ray, Mossbauer and FTIR measurements, and lower electrochemical performance.

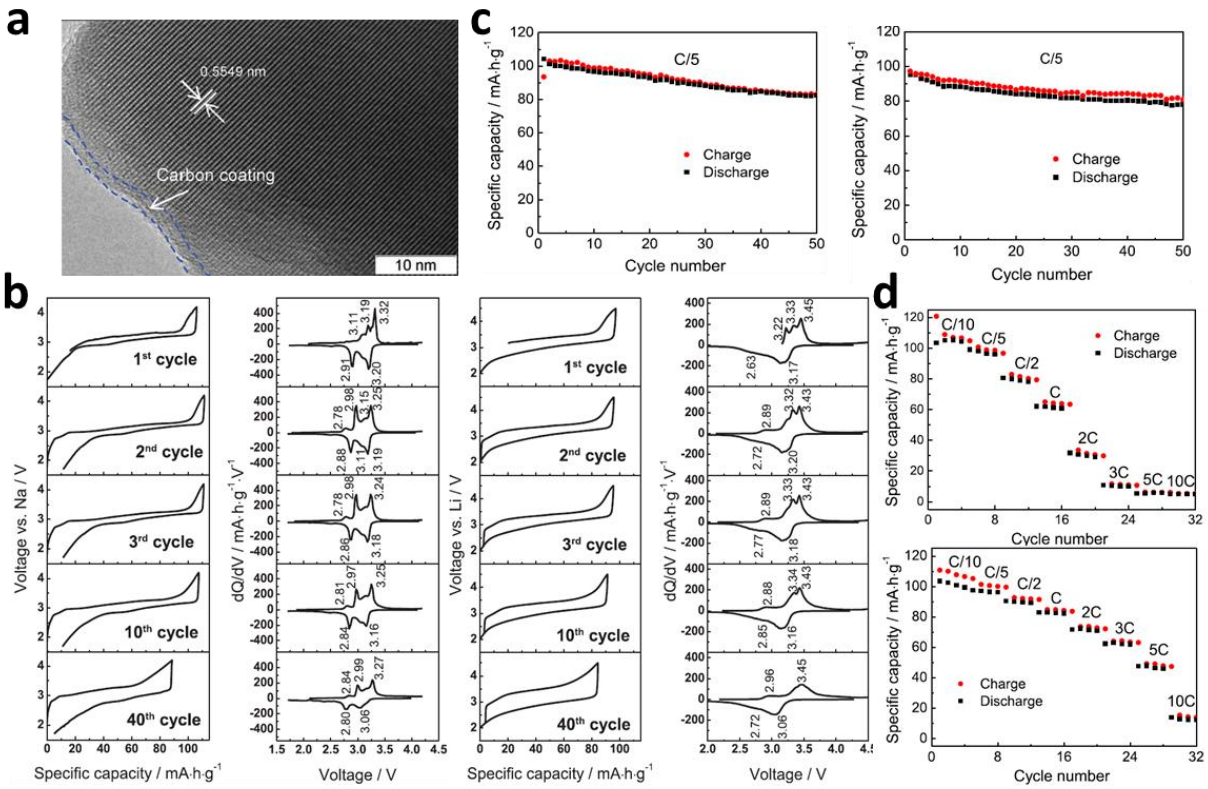

Fig. 11. a) TEM image of NFPP-450 sample; b) Galvanostatic and dQ/dV profile of NFPP-450 measured in $NaClO_4$/EC-PC (left) and $LiPF_6$/EC-DEC (right) at C/5 rate; c) Cyclic stability of NFPP-450 measured in Na-cell (left) and Li-cell (right); d) The specific capacity of NFPP-450 measured in Na-cell (top) and Li-cell (bottom) at different current rates up to 10 C (1 C = 129 mAh g^{-1}) (Reprinted with permission from ref. [97], Copyright 2018, Elsevier).

The best electrochemical properties are obtained for the sample heated at 450 ° C and cooled slowly (89 % NFPP / 11 % $NaFePO_4$), where the irreversibility upon the first charge process is observed due to the structural rearrangement. In a Na-cell, one can see three anodic/cathodic redox peaks of NFPP-450 (2.98/2.88, 3.15/3.11 and 3.25/3.19 V vs. Na^+/Na for the second cycle), which correspond to Na deinsertion/insertion from/in different crystallographic sites. In a Li-cell, one can see three anodic peaks at ~ 3.22, 3.32 and 3.43 V vs. Li^+/Li and one broader cathodic peak at ~ 3.17 V vs. Li^+/Li (the second cycle) belonging to simultaneous deinsertion/insertion of both Li and Na ions (Fig. 11b). The initial discharge capacity of NFPP-450, measured in $NaClO_4$/EC-PC and $LiPF_6$/EC-DMC solutions, reaches ~ 90 % (~ 116 mAh g^{-1}) and ~ 83 % (107 mAh g^{-1}) of the theoretical value at the rate of C/5 (capacities are re-estimated per mass of NFPP phase) (Fig. 11c). Its sodium storage capacity is somewhat better than one for NFPP in $NaClO_4$/PC reported by Kim et al. (the latter is also ~ 90 % of C_{theor} but it is measured at significantly lower current rate of C/40) [47], however, it is lower than the value in $NaClO_4$/EC-PC solution reported by Jang (~ 105 vs. ~ 125 mAh g^{-1} at C/10) [112]. Although slightly lower initial capacity of NFPP-450 was measured in Na than in Li-salt electrolyte, better cyclic and rate capability were evidenced in the Li cell (Fig. 11c,d). Namely, the specific

capacity, after 50 cycles, is decreased by ~ 21 %, in the Na-, and by ~ 18 %, in the Li-salt electrolyte, while the capacity decrease with the cycling rate increase (from C/10 to 1 C) is almost two times less in the Li cell. The capability of NFPP, to withstand very high current rates (from 1 C to 10 C), was demonstrated for the first time in the Kosova' papers [97,113] (Fig. 11c), which is probably related to the carbon coating. Still, very small capacities were measured at 10 C.

By investigating the mechanism on Na-Li exchange within NFPP, tZhese authors showed [97] that the full process of Na-Li exchange of $Na_4Fe_3(PO_4)_2P_2O_7$, either chemically or electrochemically, cannot be achieved, but it results in the formation of the mixed Li/Na compound. By the cycling of $Na_4Fe_3(PO_4)_2P_2O_7$ in Li electrolyte, one part of Na ions (~ 1.2 Na^+ ions per f.u) remains in the structure, acting as a pillar throughout cycling (according to the ref. [50,97] these ions belong to Na2 sites), the other part (~ 1.6 Na^+ ions per f.u) deinserts during the first charge cycle, thus remaining in the electrolyte, while the last part (~ 1.2 Na^+ ions per f.u) participates in the electrochemical reaction, together with the approximately same fraction of Li ions. This simultaneous Na/Li participation in electrochemical reaction improves electrochemical properties. By continuing the studies of the Li-Na redox mechanism, Kosova et al. [113] reveal that the addition of Na-salts into Li-salt electrolyte actually improves the capacity, especially rate capability of NFPP, since Na sites are not completely suitable for Li ions. This makes the composite an excellent cathode material for hybrid Li/Na batteries. Actually, the initial specific discharge capacities of the NFPP in Li electrolyte, the desodiated NFPP in Li electrolyte and the desodiated NFPP in mixed 0.9 Li - 0.1 Na electrolyte, measured at C/5, were found to be 95 mAh g^{-1}, ~ 105 mAh g^{-1} and ~ 106 mAh g^{-1}, respectively (desodiated sample is obtained by the previous extraction of three Na ions upon the cell charging). The capacity drop, after 45 cycles, is 16.4 %, 33.4 % and 8.9 %, respectively. After cycling, the lowest capacity is obtained for the system with the lowest Na fraction, which confirms instability of the Li^+ ions in the NFPP structure. At higher current rates, the capacity of desodiated carbon coated NFPP in mixed 0.9 Li - 0.1 Na electrolyte is found to be 91 mAh g^{-1} (1 C) and 65 mAh g^{-1} (3 C). The capacity at 1 C is in the range of the capacity measured by Ropero et al [114] for NFPP (also modified with carbon), but these authors did not report the current rate above 1 C. Still, at lower current such as C/10, the capacity of this hybrid Li/Na battery is inferior to the capacity of Na battery reported by Jang et al [112].

3.2.2. Solution combustion synthesis

Bascar et al. [116,117] have reported 200 nm thick pulsed laser deposited $Na_4Fe_3(PO_4)_2(P_2O_7)$ film as the promising electrode for thin sodium-ion microbatteries, due to its excellent rate-capability (125 mAh g^{-1} and 110 mAh g^{-1} at ~ 2 μA cm^{-2} and ~ 10 μA cm^{-2}), cyclic stability (over 500 cycles) and high coulombic efficiency (~ 100 %). The pure $Na_4Fe_3(PO_4)_2(P_2O_7)$ powder (Fig. 12a), which is crystallized into orthorhombic structure, of $Pn2_1a$ space group, was firstly synthesized by the facile solution combustion process using $Fe(NO_3)_3 \cdot 9H_2O$, NaH_2PO_4 (as the Fe and P sources) and $C_6H_8O_6$ (as a fuel and carbon source) and then, in the form of pallet, subjected to the pulsed laser deposition to make the thin film, with a fairly smooth surface (the roughness is 11 nm) and the thickness of ~ 220 nm, consisting of poorly agglomerated, well-

crystalized grains (65-75 nm). The specific discharge capacity of such obtained NFPP film, measured in 1 M $NaClO_4$/EC+DMC, amounts to ~ 118 mAh g^{-1} (stable upon 100 cycles), which is similar to the value of its carbon-coated $Na_4Fe_3(PO_4)_2(P_2O_7)$ parent obtained by the combustion route (126 mAh g^{-1} for the 1st and 121 mAh g^{-1} for 2nd cycle at 0.1 C), Fig. 12b. The charge/discharge plateaus, belonging to Fe^{2+}/Fe^{3+} redox reactions, are better defined and more stable (during cycling) for 220 (three distinct plateaus at ~ 3.2, ~ 2.9 and ~ 2.5 V vs. Na^+/Na) than for 300 nm thick film (plateaus merging), Fig. 12b. There is no capacity fade of ~ 220 nm thin film sample upon 500 cycles at 1 C, Fig. 12c.

In an additional study, Bascar et al. [118] have reported the reversible K^+ intercalation of the $Na_4Fe_3(PO_4)_2(P_2O_7)$ powder, prepared by the solution-combustion method. Compared to the sodium redox behavior, the larger number of redox peaks, corresponding to the K^+ insertion/deinsertion processes, is evidenced. The high irreversibility after the first charge cycle is the indication of structural arrangement caused by K^+ intercalation. The initial potassium storage capacity of the gel-combustion synthesized powder, measured in KPF_6/EC+DEC, amounts to 121 mAh g^{-1} at C/20, which is very close to the corresponding sodium storage capacity (126 mAh g^{-1} at C/20). Its value decreases in the second cycle to the value of 116 mAh g^{-1} (sodium discharge capacity in the second cycle is ~ 121 mAh g^{-1}), thus remaining stable during ten consecutive charge/discharge cycles [118].

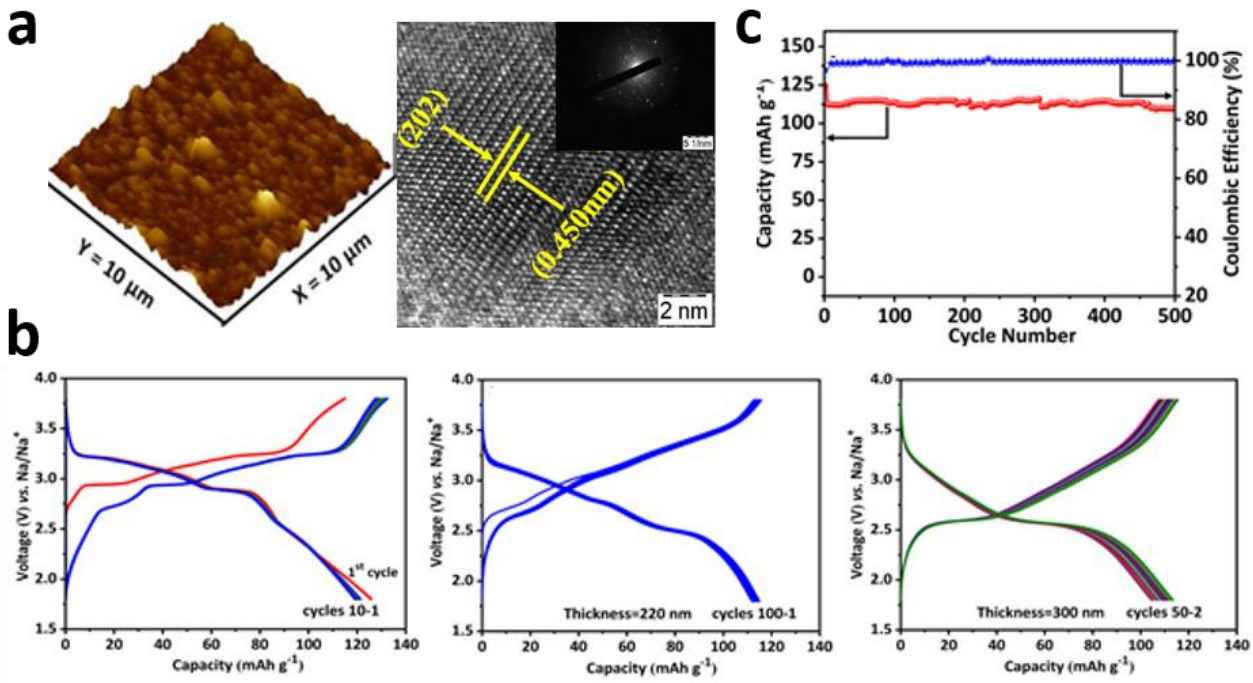

Fig.12 a) AFM image of the solution-combustion prepared bulk $Na_4Fe_3(PO_4)_2(P_2O_7)$ powder; b) Charge/discharge profiles of the bulk $Na_4Fe_3(PO_4)_2(P_2O_7)$ powder (left) and thin $Na_4Fe_3(PO_4)_2(P_2O_7)$ film with a thickness of 220 nm (right); (Reprinted with permission from ref. [117], Copyright 2020, American Chemical Society).

3.2.3. Sol-gel method

The use of sol-gel method for the NFPP synthesis has been reported firstly by Wu's group and further developed by other groups [99,107,119]. The synthesized sol-gel structures are capable of overcoming the barrier of solid-state prepared NFPP, related to the issue of the limited rate capability.

Wu and colleagues [50] have synthesized the NFPP/C particles (100-150 nm) of the orthorhombic structure ($Pn2_1a$ space group), using an stoichiometric ratio of Fe, citric acid and ethylene glycol as well as NaH_2PO_4 as the only source of phosphorus. These authors showed that the thermal stability of NFPP can be achieved within the temperature region 400 - 600 ^{o}C, while the excess of undesired pyrophosphate can be avoided with a stoichiometric ratio of phosphate and iron. The amorphous carbon (8.3 wt.% for 400 ^{o}C and 8.7 wt.% for 500 ^{o}C) is found to cover NFPP particles in the form of 7 - 8 nm layer (Fig. 13a). The characteristic redox profile of NFPP is recognized through the three galvanostatic plateaus/redox peaks and irreversible change in the first charge cycle. Nanocomposite, heated at 500 ^{o} C (NFPP/C-500), shows an excellent high rate performance (Fig. 13b), thus delivering the higher discharge capacity in 1 M $NaClO_4$/PC+FEC solution (78 mAh g^{-1} at 25 ^{o} C and 81 mAh g^{-1} at 55 ^{o} C under 10 C) than that measured for the sample obtained by the solid-state synthesis [113]. This material can retain 89 % of the initial discharge capacity after 300 cycles of charging/discharging at 0.5 C. By using combined in-situ synchrotron-based time-resolved X-ray diffraction (Fig. 13c) and solid-state nuclear NMR measurements, Wu's group identified sequence of Na extraction (indicated above), thus suggesting that the sodium extraction from NFPP is an imperfect solid-solution (evidenced by the local lattice distortion at the end of the charge process) rather than an ideal solid-solution reaction.

By introducing graphene oxide into the reaction solution of the sol-gel process [50] (Fig. 13d) and heating the gel at 500 ^{o}C in Ar/5%H_2, Ma et al. [107] have obtained amorphous carbon (AC)-coated $Na_4Fe_3(PO_4)_2(P_2O_7)$ particles (50 - 100 nm with 6 nm AC layer) embedded into cross-linked reduced graphene oxide ($Na_4Fe_3(PO_4)_2P_2O_7$@AC/rGO) (Fig. 12e), with improved sodium storage performance compared to that of NFPP@AC composite. Such improvement is more pronounced at high current rates (10 - 50 C) and low temperature (- 15 ^{o} C), Fig. 13f. Cross-linked rGO network plays a pronounced role in the suppression of particles aggregation and the increase of both carbon content (10.8 % vs. 8.8 %) and porosity. As a result, the NFPP@AC/rGO is capable of withstanding ultra-fast diffusion of Na ions, thus delivering the high and stable sodium storage capacity in a wide temperature range. Its average discharge capacity in 1 M $NaClO_4$/PC+FEC solution amounts to 107, 99, 85, 78 and 66 mAh g^{-1} (at 30 ^{o} C) and 97, 89, 53, 42 and 29 mAh g^{-1} (at - 15 ^{o} C), at 0.5, 1, 10, 20 and 50 C, respectively (Fig. 13f). These values are higher than the corresponding discharge capacities of NFPP@AC composite amounting to 95, 62, 51, and 37 mAh g^{-1} (at 30 ^{o} C) and 60, 28, 18 and 9 mAh g^{-1} (at - 15 ^{o} C), respectively. The capacity retention of rGO-modified NFPP@AC after 300 cycles is 83 % (30 ^{o} C) and 89 % (-15 ^{o} C) at 20 C, which is also better than that measured for NFPP@AC amounting to 69 % and 61.2 %, respectively (Fig. 13g). Outstanding high-rate performance is the consequence of the high contribution of pseudocapacitive effects. The full battery with the composition of hard carbon//$NaClO_4$/PC+FEC//NFPP@AC/rGO is capable of powering 42 red

light-emitting diode (LED) lights, thus delivering the average capacities of 95, 82, 64 and 50 mAh g^{-1} (calculated per mass of cathode) at 0.5 1, 2 and 5 C, respectively. The energy density of this cell amounts to 250 Wh kg^{-1}, based on the mass of cathode active material. By developing simple sol-gel-based dip coating method, followed by heat treatment at 500 °C under Ar/H_2 (v/v=95:5) atmosphere, Ma et al. [119] also have recently developed core-double shell structured $Na_4Fe_3(PO_4)_2P_2O_7$@$NaFePO_4$@C composite grown on a carbon cloth (CC) substrate (NFPP@NFP@C-CC), with an improved rate capability (up to 100 C). This binder-free and self-supported cathode is capable of delivering capacities of 127, 118, 113, 104, 97, 89, 75 and 68 mAh g^{-1} in 1 M $NaClO_4$/PC+5% FEC, at current densities of 0.5, 1, 2, 5, 10, 20, 50 and 100 C, respectively. The capacity fade is not observed over 3000 cycles at the current rate of 10 C. The full battery cell, composed of NFPP@NFP@C-CC as cathode, HC as anode and 1 M $NaClO_4$/PC+FEC solution as electrolyte, can deliver the initial charge/discharge capacity of 125 /114 mAh g^{-1} , thus retaining 97.2 % capacity after 110 cycles of charging/discharging [119].

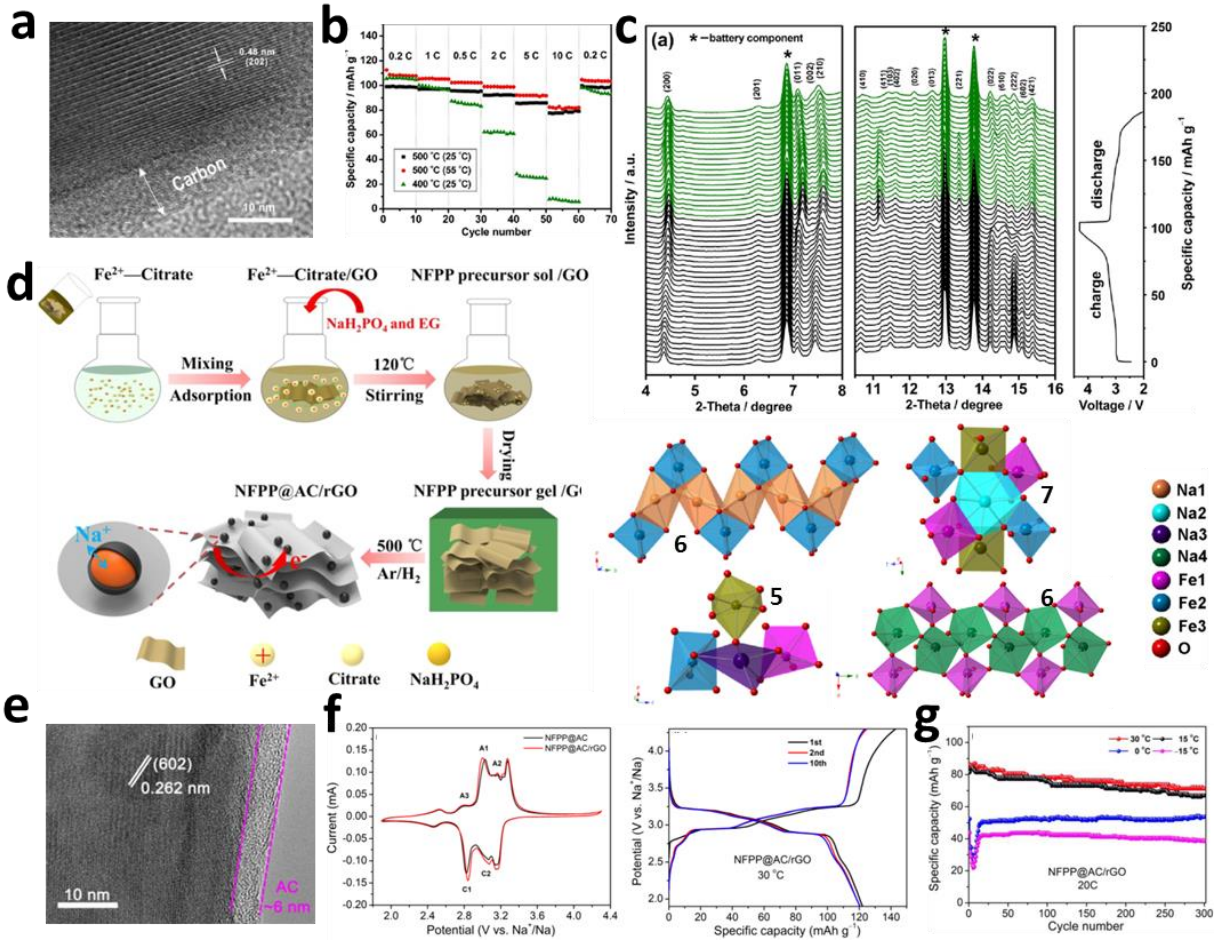

Fig. 13. a) TEM of the sol-gel prepared NFPP/C-500; b) The rate capability of the sol-gel prepared NFPP powders, heated at different temperatures; c) In-situ XRD patterns of NFPP/C-500 during the first charge-discharge cycle (Reprinted with permission from ref. [50], Copyright 2016, Elsevier); d) the scheme of the sol-gel procedure of NFPP@AC/rGO powder and e) its

HRTEM image; f, g) Rate/Cyclic performance of NFPP@AC/rGO and NFPP@AC obtained in $NaClO_4$/PC+FEC at different temperatures and current rates. (0.1 C, 1 C = 129 mAh g^{-1}) (Reprinted with permission from ref. [107], Copyright 2018, American Chemical Society).

Furthermore, Chen et al. [99] have successfully developed two types of $Na_4Fe_3(PO_4)_2(P_2O_7)$ powders with two different morphologies: i) nanoplate-like particles (NFPP-E), with the size of 150 nm (SSA is 3.52 m^2/g) and carbon content of 3.6 wt.% and ii) microporous $Na_4Fe_3(PO_4)_2P_2O_7$ particles (NFPP-C), with the particle size of 1 µm (SSA is 9.74 m^2/g) and carbon content of 4.1 wt.%, via a facile one-step sol-gel method, Fig. 14,a,b. They have used Na acetate and ammonium phosphate (mixed with glucose and stearic acid in water to give transparent solution A) as the source of sodium and phosphates and iron (II) acetate (mixed with cetyltrimethylammonium bromide and ethylenediaminetetraacetic acid for NFPP-E or citric acid monohydrate for NFPP-C to give transparent solution B) as the source of iron. The evaporation of A+B mixture to the gel formation, followed by the heating at 500 ^oC in Ar, results in the high phase purity powder (4 wt.% of maricite $NaFePO_4$ is still identified in both samples) and with the uniform carbon layer (4 nm for NFPP-E and 3 nm for NFPP-C).

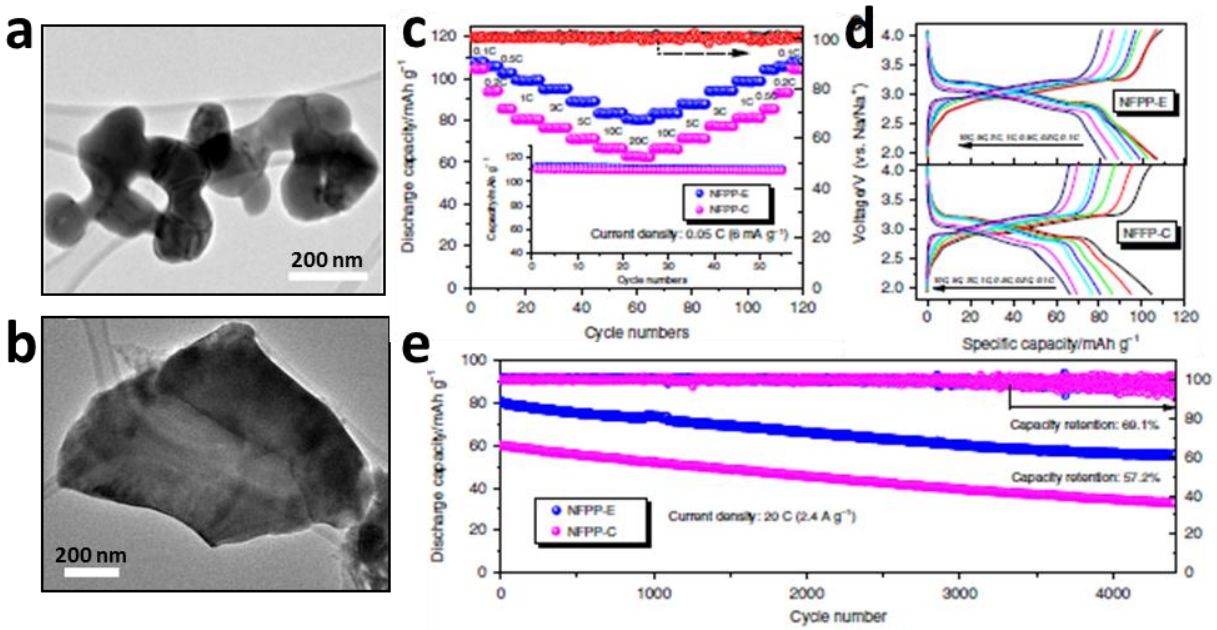

Fig. 14 SEM images of a) nanoplate-like $Na_4Fe_3(PO_4)_2P_2O_7$ (NFPP-E) and b) microporous $Na_4Fe_3(PO_4)_2P_2O_7$ (NFPP-C) particles; c, d) The comparison of cyclic performance of NFPP-E and NFPP-C, measured in $NaClO_4$/EC+PC+FEC at different current rates; e) Long-term cyclic stability of both NFPP-E and NFPP-C measured at 20 C (2400 mA g^{-1}) over more than 4000 cycles. (Reprinted with permission from ref. [99], Copyright 2019, Nature Communication).

Due to nanosized particles, the NFPP-E shows better high rate performance than NFPP-C. Its specific discharge capacity, measured at 20 C in $NaClO_4$/EC+PC+FEC electrolyte, amounts to 80.3 mAh g^{-1} (Fig. 14c,d). An outstanding cyclic stability of this material (100 % after 50 cycles at C/20 and 69.1 % after 4400 cycles of charging/discharging at 20 C) is obtained, without

morphological destruction and cracks' formation upon long-term cycling (Fig. 14e). While the specific capacity of NFPP-E, at lower scan rates (0.05 and 0.1 C), is in the range of other reported NFFP's prepared by solid-state reaction [47,97], its improvement is achieved at high rates such as 10 C and 20 C [50,107] . Its high sodium storage capability is also achieved at both low and high temperatures (- 20 ^{o} C and 50 ^{o} C), with outstanding cyclic stability (92.1 % and 91.4 % capacity retention at 0.5 C, respectively). The structural stability of NFPP, upon exposure to both air atmosphere (three-month period) and cycling in Na-containing electrolyte (volume changes of 4 %), is confirmed by in-situ XRD and in-situ XANES. The practical use of NFPP-E material is also tested in two full-cell SIB configurations such as polypyrolle (PPy)-coated Fe_3O_4//$NaClO_4$/EC+PC+FEC//NFPP-E// and hard carbon//$NaClO_4$/EC+PC+FEC//NFPP-E, which can deliver the initial discharge capacities of ~ 225 mAh g^{-1} and 170 mAh g^{-1} at 100 mA g^{-1}, with the capacity retention of ~ 77 % (after 500 cycles) and ~ 41 % (after 12 cycles), respectively.

3.2.4. Template and spray-drying methods

An adequate micro/nano structure of 3D polyanionic framework and its carbon coating, achieved by adjusting synthesis conditions through the solid-state reaction, sol-gel and combustion routes, is shown to provide the high rate capability of NFPP up to 20 C. The ultra-high rate capability (above 20 C) is not achieved by the sol-gel procedure itself. The reason could be in an insufficient purity of the synthesized NFPP since its formation is often accompanied by the appearance of some additional $NaFePO_4$ or $Na_2FeP_2O_7$ phases (they appear at least in traces, even under strictly controlled synthesis conditions) or electronic and ionic wiring. Still, the maricite is capable of showing the high electrochemical activity, when it is in the composite with NFPP, thus contributing to the high rate capability of the composite up to 100 C [119]. By demonstrating template [63] and ultra-spray method [102], these limitations have been overcome and the outstanding electrochemical properties of this material, (the rate capability up to 100 - 200 C and long-term cyclability up to 4000 - 6000 cycles) are achieved.

Pu et al. [63] have developed a novel template method to demonstrate ultra-high current capability of NFPP, evidenced by reaching the sodium storage capacity of 79 mAh g^{-1} at even 100 C (charge/discharge in 36 s). By introducing a nonionic triblock surfactant Pluronic-F127, as a template, and phenolic resinol into the mixture of reactants ($Na_4P_2O_7$, $NH_4H_2PO_4$ and $Fe(NO_3)_3 \cdot 9\ H_2O$), these authors prepared the pure uniform NFPP/C nanospheres (without traces of commonly identified maricite phase) with the average diameter of 29.3 nm (NFPP/HC sample with 14.3 wt. % C) and 56.8 nm (NFPP/LC sample with 9.4 wt.% C), coated by thin carbon layer (3 nm and 1.8 nm, respectively), Fig. 15 a. The carbon content and thickness can be adjusted by varying the phenolic resinol amount. Both produced NFPP/LC and NFPP/HC nanospheres reach almost theoretical capacity (~ 128.5 mAh g^{-1}) in $NaClO_4$/EC-DEC+FEC at a current rate of 0.2 C (Fig. 15b). The specific capacity of NFPP/HC retains its high value at higher current rates (about 123, 120, 116, 114, 111, 108, 106, 91 and 79 mAh g^{-1} at 0.5, 1, 5, 10, 20, 30, 50, 80 and 100 C, respectively) and during cycling, where 63.5 % of the initial capacity is measured over 4000 cycles at 10 C (Fig. 15c,d). An ultra-high-power density of 24.1 kW kg^{-1}, at

the energy density of 146.6 Wh kg^{-1}, is obtained for Na//NFPP/HC battery cell (based on the total active masses of both cathode and Na anode). This remarkable performance of NFPP/C, Pu et al. [63] attribute to the ultra-small particles and 3D continuous carbon network structure which facilitate both ions and electronic transport through the nanospheres.

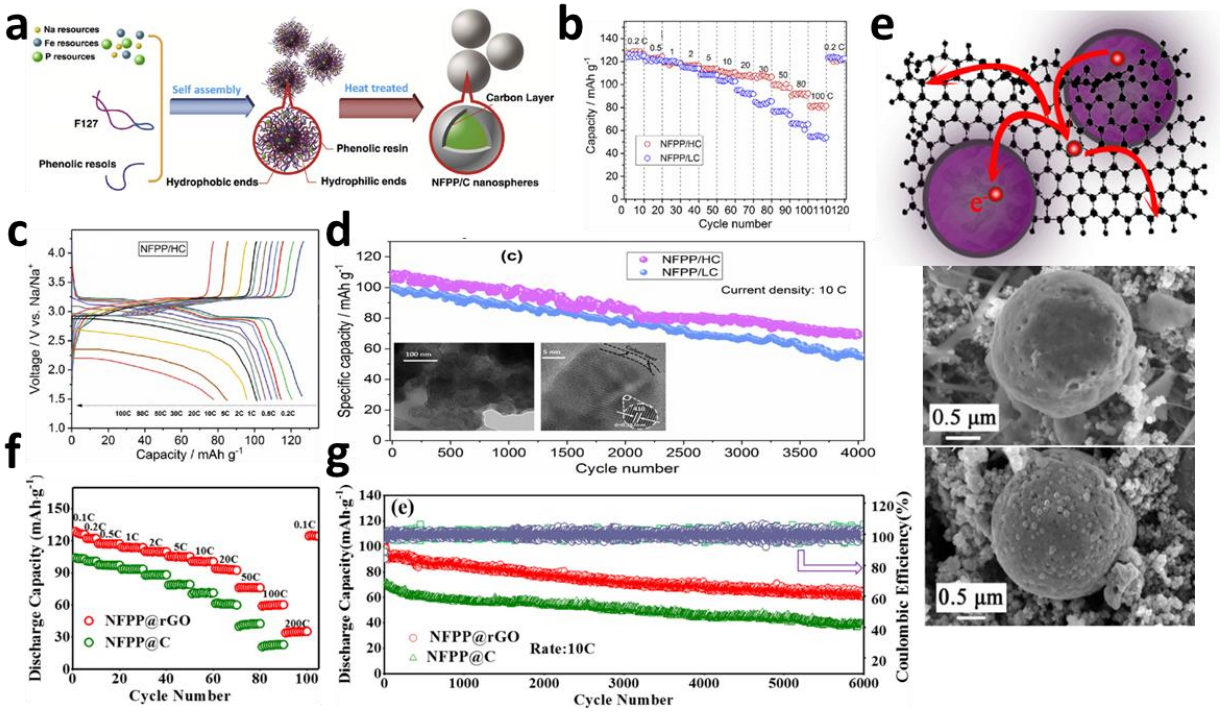

Fig. 15. a) Schematic design of the synthesis of NFPP/C nanospheres and their b-d) electrochemical performance in $NaClO_4$/EC-DEC+FEC at different current rates and during long-term cycling at 10 C; Reprinted with permission from ref. [63], Copyright 2019, Elsevier); e) Schematic design of NFPP nanoparticles and rGO sheets and f, g) their electrochemical performance at different current rates and during long-term cycling at 10 C (Reprinted with permission from ref. [102], Copyright 2019, Elsevier) (1 C = 129 mA g^{-1}).

By demonstrating the facile spray pyrolysis method, Yuan et al. [102] have synthesized NFPP nanoparticles (60 nm), homogenously enwrapped by 3D interconnected rGO network (NFPP@rGO), Fig. 15e, starting from aqueous solution of $NaH_2PO_4{\cdot}2\ H_2O$, $Fe(NO_3)_3 \cdot 9H_2O$ and $C_6H_8O_7 \cdot H_2O$. These particles are capable of providing not only the theoretical capacity, at low current rates (~ 128 mAh g^{-1} at 0.1 C), but also an impressive capacity value (~ 35 mAh g^{-1}) at a very high current rate of even 200 C (discharge process can be accomplished within 18 s). Furthermore, ~ 62 % of capacity retention upon over 6000 cycles at 10 C, is measured. Explicitly, the specific discharge capacity of NFPP@GO, containing 8.3 wt.% C (based on NFPP mass), measured in the $NaClO_4$/EC-DEC+FEC electrolyte, amounts to 128, 122, 117, 114, 110, 105, 101, 93, 76, and 60 mAh g^{-1}, at different C rates of 0.1, 0.2, 0.5, 1, 2, 5, 10, 20, 50 and 100 C, respectively. The material keeps 88% of the initial capacity after 1300 cycles at 1 C, thanks to the high fraction of the surface stored charge (i.e. intercalation pseudocapacitance). The maximum power density of the full Na//NFPP@rGO cell (~ 52.3 kW kg^{-1} corresponding to ~

70.9 Wh kg^{-1}) is substantially higher than the value of cells containing other reported iron-based mixed polyanionic cathodes. The beneficial role of 3D highly conductive graphene framework can be seen through the comparison of the sodium storage behavior between NFPP@rGO and NFPP@C composites (NFPP@C contains 7.8 wt.% C). The latter is also obtained by the spray-drying method, under the same synthesis conditions, where the only difference is seen in the replacement of rGO by an additional amount of citric acid. Poorer electrochemical performance of NFFP@C vs. NFPP@rGO (129 vs. 106 mAh g^{-1} at 0.1 C and 60 vs. 23 mAh g^{-1} at 100 C) originates from the: i) 6 nm amorphous carbon layer of NFPP@C versus 2 nm fine graphene layer of NFPP@rGO ii) lower specific surface area (8.38 m^2 g^{-1} vs. 28.68 m^2 g^{-1}) and iii) the larger aggregation of NFPP particles when compared to NFPP@C ones. It should be added that the higher specific surface area of NFPP@rGO vs. NFPP@C contributes to the higher fraction of pseudocapacitance, as evidenced by the shape of their curves at the end of discharge.

Recently, Cao et al [64] have also used the spray drying method to obtain $Na_4Fe_3(PO_4)_2P_2O_7$ nanoparticles (20 - 50 nm) growing on multi-walled carbon nanotubes (MCNTs). The NFPP@MCNTs sample shows slightly lower capacities in $NaClO_4$/EC+DEC+FEC than those measured for NFPP@rGO sample, which amount to 115.7, 103.3, 99.2, 96.7, 94, 90.5, 82.1 and 62.8 mAh g^{-1} at current rates of 0.1, 0.5, 1, 2, 5, 10 and 20 C. Besides, the specific capacities of the full cell CHC//$NaClO_4$/EC+DEC+FEC//NFPP@MCNTs (based on the mass of both anode and cathode materials) were found to be very high at different currents of 0.1, 0.5, 1, 2 and 5 C amounting to 69.3, 60.5, 51.8, 40.1 and 35.2 mAh g^{-1}, respectively.

Unlike NCPP, more diverse synthesis methods of NFPP have been developed which resulted in its high rate properties. However, the issue of the lower voltage remains a great challenge, and the future research should be focused on the improvement of the operating voltage of this material.

3.3 $Na_4Ni_3(PO_4)_2(P_2O_7)$ – NNPP

As we emphasized, NNPP is isostructural to NFPP and NCPP. Its crystal structure, determined by Sanz et al. [46,48], presents three-dimensional network of $[Ni_3P_2O_{13}]_\infty$ layers, composed of NiO_6 octahedra and (PO_4^{3-}) tetrahedra in the bc plane, which are bridged by $(P_2O_7)^{4-}$ dimers in a way that create the large channels along b-axis available for Na-ion diffusion. Four distinguishable Na sites are identified, where Na1 and Na4 are positioned in the large channels parallel to the b-axis. Also, Sanz et al. [120] determined the crystal structure of the $Na_4Ni_5(PO_4)_2(P_2O_7)_2$.

3.3.1. Solution combustion synthesis

The electrochemical behavior of NNPP has been examined since 2015 [106]. Generally, Ni-phosphate and pyrophosphate compounds have been widely known as high voltage cathodes for Li-ion battery applications, but the achievement of their high performance is difficult due to the intrinsic sluggish kinetics caused by the low electronic and Li-ion conductivity. In 2015, Islam et

al. [58] have predicted that Ni doping of NFPP leads to the increase of the cell voltage, while the high potential redox activity of NNPP in Na cell was experimentally evidenced somewhat later [96]. First, Senthilkumar et al. [106] revealed the Ni^{2+}/Ni^{3+} redox activity in NNPP, at ~ 0.35/0.17 V vs. Ag/AgCl, in an aqueous solution of NaOH. These authors have reported the combustion synthesis of $Na_4Ni_3(PO_4)_2(P_2O_7)$/C, using three different types of fuel such as glycine, urea and hexamine, for the sake of examining their effect on physicochemical/electrochemical properties of composite. By using $Na_4P_2O_7$, $NH_4H_2PO_4$ and $Ni(NO_3)_2 \cdot 6H_2O$ as reactants and the mentioned fuels, they have synthesized the pure $Na_4Ni_3(PO_4)_2(P_2O_7)$ phase (NNPP). This NNPP phase is obtained by heating at 600 ^{o}C (for 3 h in Ar atmosphere) and reveals its higher thermal stability compared to $Na_4Fe_3(PO_4)_2(P_2O_7)$. Authors have shown that the use of hexamine as a fuel reduces NNPP particle size to nano dimension (50 - 300 nm) and forms more voids/pores for an easier access of electrolyte ions, with respect to both urea and glycine. As a result, the higher current response of NNPP is obtained in the case of hexamine-assisted synthesis. Also, the presence of amorphous coated carbon (~ 2.7 wt.% C) reduces the particle size and increases electronic conductivity of the composite electrode.

3.3.2. Solid-state and sol-gel methods

Passerini et al. [96] were the first who demonstrated the high potential of NNPP (4.8 V vs. Na^+/Na) in the full Na-cell, using ionic liquid-based electrolyte (NaTFSI in $Py_{14}FSI$), which could provide better properties than typical carbonate-based electrolyte (1 M $NaPF_6$ in EC+DEC). High redox activity of NNPP/C is evidenced by three anodic (4.61, 4.67 and 5 V) and two cathodic (4.58 and 4.92 V) peaks, while the Ni redox activity in $Na_2NiP_2O_7$/C, under the same conditions, is not evidenced. When the submicrometric NNPP/C powder (~ 500 nm), obtained by citric-assisted solid state method + ball milling (using $Na_4P_2O_7$, $Ni(OCOCH_3)_2 \cdot 4H_2O$, $NH_4H_2PO_4$ as Na, Ni and P sources), is used as the cathode in two-electrode cell, along with metal Na as the negative electrode, it delivers the initial discharge capacity of 63 mAh g^{-1} and 40 mAh g^{-1} (@10 mA g^{-1}) in NaTFSI+$Py_{14}FSI$ (3 - 5.1 V) and $NaPF_6$/EC+DEC (3 - 4.9 V), respectively. This is still inferior to Fe- and Co-based analogues due to lower ionic conductivity of Ni-based mixed polyanionic compound. Also, the collapse of $[Ni_3P_2O_{13}]_\infty$ layers, occurring upon charge/discharge, causes its low sodium reversibility (1.3 Na^+ vs. 2.6 Na^+ in the first cycle) and consequently low coulombic efficiency. Based on ex-situ XRD, Na^+ ions are proposed to be extracted first from Na1 and Na2 sites (positions in the large channels constructed by P_2O_7 dimers) at lower potentials, thus resulting in the decrease of ***a*** parameter and the volume change of 1.6%. Afterwards, Na^+ ions, belonging to both Na3 and Na4 sites, are regarded to leave the structure, at the highest potential of 5 V vs. Na^+/Na, resulting in the rapid increase of the ***b*** parameter. Still, the total volume change during cycling is small and together with the high thermal stability, present advantage of this mixed polyanionic structure in terms of operating at high voltages.

Since the NNPP proved to be a high potential cathode material for SIBs, Passerini and collaborators [98] continue to study its electrochemical behavior trying to improve the electronic conductivity and prevent poor reversibility of sodium insertion. In this regard, composites of

NNPP with carbon and reduced graphene oxide have been prepared [98] by the sol-gel synthesis procedure (starting from $Ni(CH_3COO)_2 \cdot 4H_2O$, $(NH_2)HPO_4$ and $Na_4P_2O_7$ as reactants and graphene oxide and sucrose as the carbon source), followed by heating treatment at 700 ^{o}C under Ar for 24 h. The size of NNPP particles in these composites, which are covered by 7 nm carbon layer, is approximately 500 nm (for NNPP/rGO with 8.9 wt.% of C) and 600 nm (for NNPP-C with 8.45 wt.% of C), Fig.16a. Both composites undergo sodium multistep reaction path as evidenced by well-defined CV redox peaks in 1 M $NaPF_6$/EC+DMC solution, Fig. 16b. Their specific capacity is found to be higher than that for the pure sol-gel prepared sample and one prepared by solid-state reaction [96].

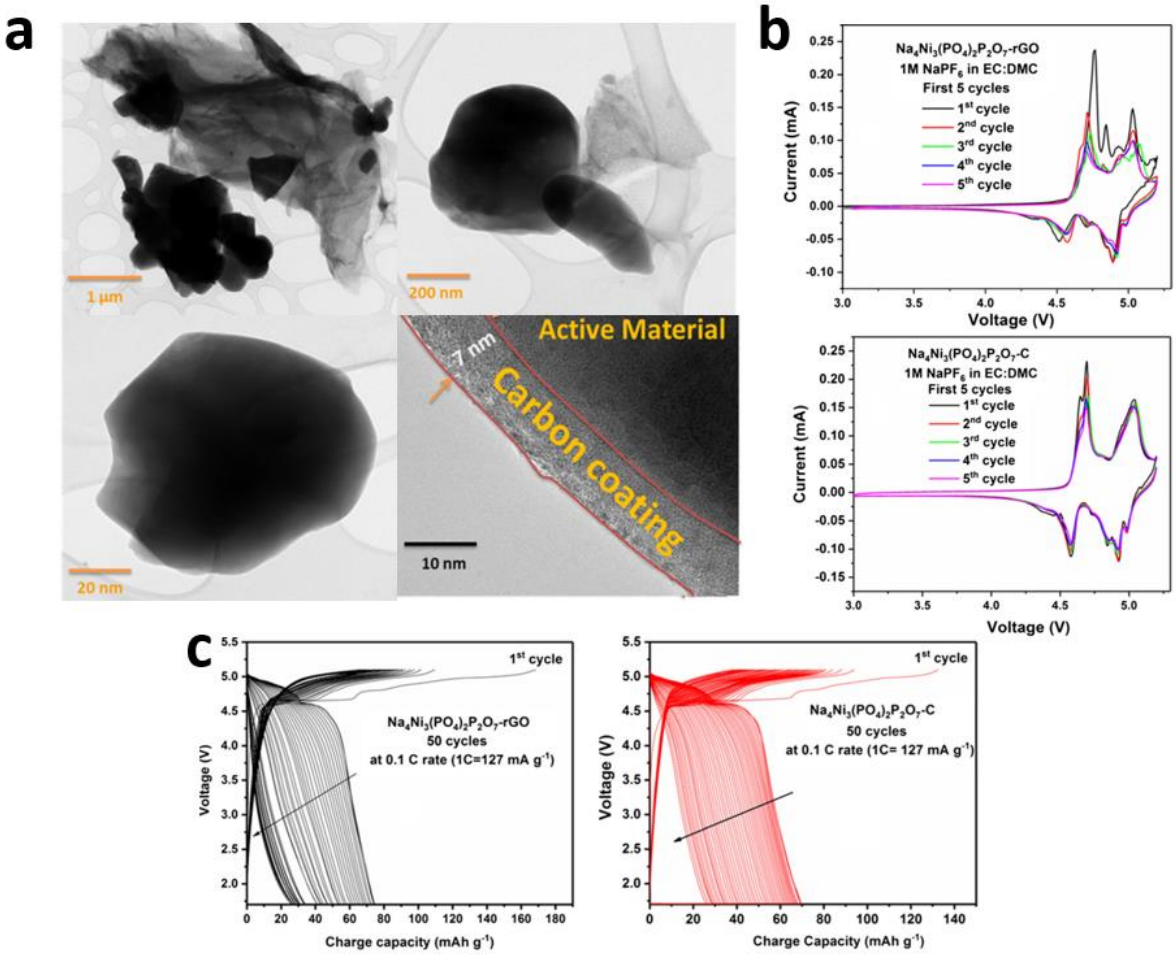

Fig. 16. a) TEM images of sol-gel prepared NNPP/rGO (top) and NNPP/C (bottom) composites and their b) CVs and c) Galvanostatic charge/discharge curves measured in $NaPF_6$ /EC+DMC, The current rate is 0.1 C (1 C = 127 mA g^{-1}) (Reprinted with permission from ref. [98], Copyright 2019, Springer).

The initial charge/discharge capacity, measured at 0.1 C (1 C = 127 mA g^{-1}) within the voltage range of 1.7 - 5.1 V, amounts to ~ 168/72 for NNPP-rGO and ~ 132/74 mA hg^{-1} for NNPP-C, Fig. 16c. However, the poor reversibility during cycling has been observed for both composites,

with only ~ 36 % of the capacity retention after 50 cycles due to the structural deformation upon third Na redox process (occurring at the highest voltage). It is attributed to the O_2 release from lattice at the fully charged state. Such assumptions have been confirmed through i) limited cycling of NNPP-C to insert/extract 1.3 Na^+, which leads to stable capacity of 51 mAh g^{-1} over 40 cycles at 0.1 C and ii) identification of structural changes after the first charge.

Further improvement of the performance of this high-voltage material, in terms of preventing structural changes upon cycling at high voltages (either through development of different strategies or new synthesis procedures), remains the challenge for the future research.

3.4 $Na_4Mn_3(PO_4)_2(P_2O_7)$ – NMPP

3.4.1. Solid-state method

Numerous Mn-based compounds have been synthesized and examined electrochemically, due to the abundance and high accessibility of manganese. Based on this, the cost of the material production would be cheaper than that for Ni, Co and Fe-based compounds. NMPP polyanionic compound has been firstly synthesized by Kim et al. [77] via a conventional mechanochemically-assisted solid-state reaction, using $Na_4P_2O_7$, $Mn_2C_2O_4 \cdot 2H_2O$ and $NH_4H_2PO_4$ as reactants and pyromellitic acid as a carbon source. Such synthesized NMPP/C powder (with the particle size of 200 - 500 nm), heated at 600 ^oC (first in the air to get NMPP phase and then in Ar for 2 h to coat NMPP particles by carbon) is found to be isostructural to NFPP and NCPP, but with larger lattice constants due to larger ionic radius of Mn^{2+} ion (0.83 Å) compared to Fe^{2+} (0.78 Å) or Co^{2+} (0.745 Å), which follows Vegard's law. Typically, 3D open polyanionic framework of orthorhombic NMPP crystal structure (Pn21a) is composed of $[Mn_3P_2O_{13}]_\infty$ layers along bc plane which are connected by P_2O_7 groups along the a-axis, with three crystallographically distinct edge and corner-shared Mn octahedra sites. $NaMnPO_4$ traces (< 4 wt.%) are also detected in the solid-state synthesized powder.

Kim et al. [77] demonstrated improved properties of NMPP compared to other manganese-based electrodes such as higher Mn^{2+}/Mn^{3+} redox potential of 3.84 V vs. Na^+/Na and larger energy density, amounting to 416 Wh kg^{-1} (on the materials' level), thus revealing that both sodium-ion mobility and cycling stability are not deteriorated by Jahn-Teller distortion (Mn^{3+}). Moreover, the typical Jahn-Teller distortion (Mn^{3+}) during NMPP cycling is found to open Na diffusion channels (the activation barrier of most Na diffusion pathways is considerable decreased). As a result, the solid-state synthesized NMPP reaches almost theoretical capacity (129.5 mAh g^{-1}) upon the first charge in $NaBF_4$/EC+PC solution at a rate of C/20, while the 85 % of this capacity (109 mAh g^{-1}) is measured after the first discharge. The capacity retention, after 100 cycles, is found to be 82 % at C/20 and 86 % at C/5, with the coulombic efficiency of 98.5 %. The material can deliver the discharge capacity of 121 mAh g^{-1} (93 % of its theoretical value) at elevated temperature of 60 ^oC (C/20), with the energy density of 416 Wh kg^{-1} (that is the energy density of Na/NFPP cell), while the corresponding energy density at a room temperature reaches 385 Wh kg^{-1}. (the energy density is based on the cathode level). At a higher current rate of 2 C, the

capacity of NMPPC amounts to ~ 83 mAh g^{-1} (25 ^{o}C) and ~ 112 mAh g^{-1} (60 ^{o}C), while the more than a half of the theoretical capacity is retained at 10 C (for both temperatures). The high rate capability and good cyclic performance of solid-state synthesized NMPP have been regarded as superior when compared to Mn-based compounds.

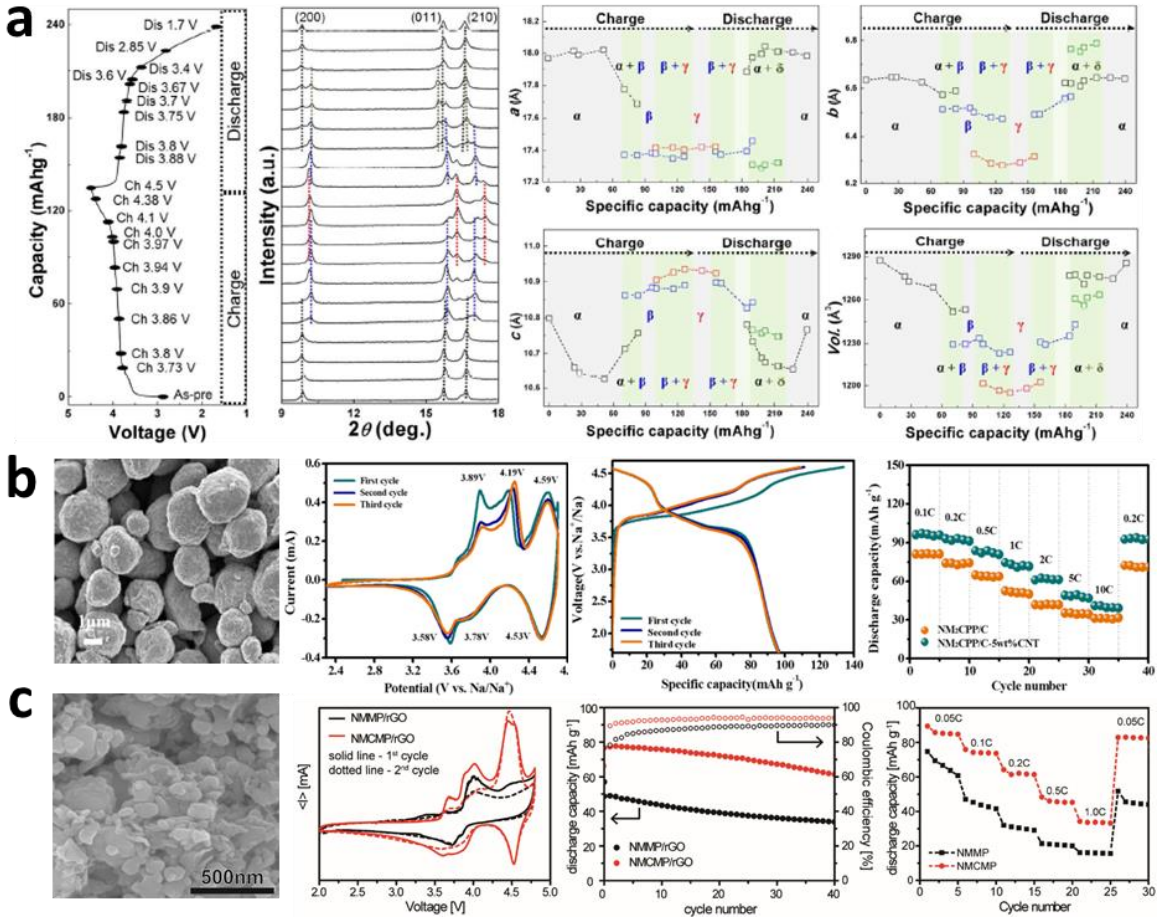

Fig. 17. a) Galvanostatic charge/discharge profile of solid-state prepared $Na_4Mn_3(PO4)_2P_2O_7$ at C/20 (1 C = 130 mA g^{-1}) and in-situ XRD patterns obtained during its charge/discharge (Reprinted with permission from ref. [77], Copyright 2015, The Royal Society of Chemistry); b) SEM, CVs (the scan rate is 0.05 mV s^{-1}), galvanostatic charge/discharge profile (the current rate is 0.1 C, 1 C = 128.7 mA g^{-1}) and rate performance of CNTs-decorated $Na_4Mn_2Co(PO_4)_2(P_2O_7)/C$ (NM_2CPP/C-5wt.% CNTs) measured in $NaClO_4$/EC+PC+FEC (Reprinted with permission from ref. [108], Copyright 2019, American Chemical Society); c) SEM, CVs (the scan rate is 0.025 mV s^{-1}), cyclic performance (the current rate is 0.1 C, 1C = 130 mA g^{-1}) and rate performance of $Na_4Mn_{2.4}Co_{0.6}(PO_4)_2P_2O_7$/rGO composite (NMCMP/rGO) measured in $NaPF_6$/EC+DEC (Reprinted with permission from ref. [121], Copyright 2019, Elsevier).

The NMPP experiences multi-phase reaction during the charge/discharge process (Fig. 17a), as evidenced by the existence of three anodic/cathodic peaks at 3.85/3.64 V, 3.89V/3.77V and 3.96/3.87 V vs. Na^+/Na in measured dQ/DV curve. After solid-solution behavior of NMPP in the

initial cycling (up to 3.86V vs Na^+/Na), where the one Na sodium is extracted from the structure (Na2 site), phase transition (α→β) is observed during further charging (up to 3.9 V vs Na^+/Na which corresponds to the extraction of approximately 1.6 Na ions), with the large difference in ***a*** and ***b*** parameters between α and β phase. Further deeper charging, above 4 V vs. Na^+/Na, leads to the appearance of new γ phase (Na-poor phase). These multi-phase changes result in 7 % of total volume change which is still higher than that for the NFPP (which is 4 %), but it is lower than those volume changes observed for other managanese-based electrodes such as O3-$NaNi_{0.5}Mn_{0.5}O_2$ (18 %), P2-$Na_xFe_{0.5}Mn_{0.5}O_2$ (11 %) and olivine $LiMnPO_4$ (10 %) [77]. On the discharge, the additional δ phase is identified as intermediate phase of β → α transition, most likely as the consequence of Na-vacancy ordering (Fig. 17a).

3.4.2. Spray-drying and solution combustion methods

Although improved properties of NMPP over other Mn-based electrodes are achieved [77], the reversible discharge capacity is still substantially below the theoretical limit (calculated for three Na ions), especially at higher currents. Because of that, further studies on NMPP have been focused on developing dual strategy for the improvement of the sodium storage behavior, including the partial Mn-Co substitution and carbon coating of NMPP particles [108,121] by selecting the highly conductive carbon nanotubes [108] and reduced graphene oxide [121]. Both ways can improve kinetics of the electrochemical reaction. Besides, the partial Mn substitution by Co results in smaller volume cell owing to smaller Co^{2+} radius (0.745 Å, high spin) than Mn^{2+} one (0.83 Å, high spin) and increased average redox potential of mixed-polyanion structure (from the average voltage of ~ 3.8 V for Co-free sample to ~ 4 V for Co-doped sample) [77,108].

Firstly, Tang et al. [108] have prepared CNT-decorated $Na_4Mn_2Co(PO_4)_2(P_2O_7)$/C microsphere structure (NM_2CPP/C-CNTs), through the typical spray-drying method, by mixing aqueous solutions of $Mn(NO_3)_2$, $Co(NO_3) \cdot 6\ H_2O$, citric acid (as both carbon source and chelating agent) and different concentration of CNTs (3.5 and 7 wt.%). The samples are heated at 350 ^{o}C for 3 h and 630 ^{o}C for 10 h in Ar. CNTs were found i) to control the morphology of mixed polyanionic compound, thus creating the microspherical network skeleton (composed of nanoparticles with an average size of 150 nm) instead of the large number of irregular micro pieces observed without CNT; ii) to increase the specific surface area (from 7.98 to 36.81 $m^2\ g^{-1}$) thus providing larger number of active sites for Na^+ ions, iii) to decrease the charge transfer resistance (i.e. to increase electron transport among NM_2CPP particles), iv) to increase sodium ion diffusion coefficient and v) consequently to increase specific capacity of composite. The optimal content of CNT in terms of the best electrochemical properties was found to be 5 wt.%. The initial discharge specific capacity of NM_2CPP/C-5wt.% CNTs in 1M $NaClO_4$/EC+PC+FEC amounts to 96.1 (71.65 % of the initial charge capacity), 93.5, 74.4 and 41 mAh g^{-1} at the current rates of 0.1, 0.5, 1 and 10 C (1 C = 128.7 mA g^{-1}), which is higher than that of NM_2CPP/C amounting to 81, 79.6, 52.5 and 31.2 mAh g^{-1}, respectively (Fig. 17b). The capacity retention after 100 cycles at 0.5 C is 78.1 % (NM_2CPP/C-5wt.% CNTs) and 35.1% (NM_2CPP/C), while NM_2CPP/C-5wt% CNTs retains 76.4 % of the initial capacity after 150 cycles at 1 C. Redox peaks of NM_2CPP/C-5 wt.% CNTs, positioned at 3.89/3.58, 4.19/3.78 and 4.59/.53 V vs. Na^+/Na (Fig. 17b), are shifted

towards higher potentials when compared to above indicated potentials of NMPP [77], due to Co-doping.

The energy density of Na//$NaClO_4$/EC+PC+FEC//NM_2CPP/C-5wt.% CNTs battery is estimated to be 371 Wh kg^{-1} (at 0.1 C, based on the materials' level), which is still close to the value of Na cell containing Co and CNTs-free NMPP sample as cathode [77] amounting to 385 Wh kg^{-1}, (although at two-fold lower current). From practical point of view, NM_2CPP/C-5wt.% CNT has the large potential, since the sodium-ion battery such as hard carbon//$NaClO_4$/EC+PC+FEC//NM_2CPP/C-5wt.% CNTs is capable of showing i) the high initial reversible capacity of 88.8, 74.8 and 57 mAh g^{-1} at 0.1, 1 and 5 C, respectively, ii) the working voltage of 3.85 V and iii) energy density of 249.9 Wh kg^{-1}, with the capacity retention of 75.1 % (at 0.5 C) after 100 cycles.

Next, Ryu et al. [121] have synthesized Co-substituted $Na_4Mn_2Co(PO_4)_2(P_2O_7)$/C ($Na_4Mn_{2.4}Co_{0.6}(PO_4)_2P_2O_7$) particles (100-200 nm) in the form of the composite with rGO sheet (denoted as NMCMP/rGO), Fig. 17c. NMCMP is first prepared through the solution combustion synthesis (using $Na_4P_2O_7$, $Mn(NO_3)_2 \cdot H_2O$, $Co(NO_3)_2 \cdot 6\ H_2O$ and $NH_4H_2PO_4$ as reactants) followed by heating at 600 ^{o}C (in Air for 6 h) and then it is dispersed with GO solution through the ball milling and heated at 600 ^{o}C for 2 h (in Ar) to get the reduced graphene oxide. Still, traces of impurity phases (less than 2 %) such as Mn_2O_3, and $Na_2MnP_5O_{15}$ are detected in NMCMP/rGO. The additional $NaMnPO_4$ phase is detected in NMMP/rGO with the total amount of impurities less than 5 %. Mn^{2+}/Mn^{3+} oxidation/reduction process can be evidenced within 3.6 - 4 V vs. Na^+/Na for both Co-free and Co-doped samples, while the additional redox process of Co^{2+}/Co^{3+} is recognized at ~ 4.5 V (vs. Na^+/Na) in CV of NMCMP/rGO (Fig. 17c), and is found to be faster than Mn redox process. Additionally, the partial Co substitution on Mn sites 1) reduces the degree of octahedral distortion; 2) facilitates the $Mn^{2+/3+}$ redox reaction; 3) facilitates the A → B phase transition during sodium deinsertion thus providing its completion and reversibility (this transition is incomplete in the Co absence since both A and B phases have been observed at 4.8 V vs. Na^+/Na); 4) suppresses the lattice distortion thus reducing the total volume change (5.7 % for Co-doped structure vs. 7.0 % for Co-free structure); 5) decreases the reaction resistance and 6) increases the sodium diffusion coefficient. As a result, the higher specific capacity and better cyclic stability of NMCMP/rGO vs. NMMP/rGO are obtained, as illustrated in Fig. 17c. The initial specific capacity of NMMP/rGO, measured in 1 M $NaPF_6$ in EC/DEC, amounts to 74.7, 47, 31.9, 21.3 and 16.1 mAh g^{-1} at 0.05, 0.1, 0.2, 0.5 and 1 C (1 C = 130 mA g^{-1}), while the corresponding values of NMCMP/rGO are found to be 89.4, 75.9, 64.2, 48.3 and 34.2 mAh g^{-1}, respectively. The capacity retention, after 40 cycles, is found to be 59.8 % (Co-free) and 76.8 % (with Co).

As in the case of NNPP, the future research concerning NMPP should be focused on developing different synthesis/strategies of this material, aimed at improving the specific capacity of this material and its cyclic performance.

4. The role of binder in the polyanionic electrode performance

Apart from the synthesis of active powder, which tailors the material properties, the electrode design can be critical for the electrochemical performance as well. Typically, the electrode is made of the active material, conductive additive and binder (attached to the Al current collector), in an appropriate ratio, that should ensure its uniform dispersion at particle level, proper electrochemical wiring and the mechanical stability upon long cycling (the prevention of the contact loss between active particles and current collector during cycling). Although less attention has been paid to the role of inactive components, the type and amount of binder could be pivotal in the final electrochemical properties, especially at higher loadings [122]. Design of the polymer binder has been attracting specific attention recently in the battery community. Some researchers are concentrated on finding alternative and sustainable solutions to replace the conventional poly(vinylidene difluoride) dissolved in N-methyl pyrrolidone, ($PVdF^{NMP}$), mostly focusing on the aqueous electrode processing route which uses cheaper and environmentally more friendly aqueous binders such as carboxymethyl cellulose (CMC), alginate, polyacrylic acid (PAA) and so on. These green alternative binders, enriched in COOH groups, offer advantages in terms of cost, toxicity and conductivity of the electrode (the use of toxic, flammable and expensive NMP would be avoided) [123], as well as simplicity and rapidness of its preparation. Moreover, they are able to provide better electrochemical properties of the electrode material, when compared to $PVdF^{NMP}$, especially for the materials possessing large volume changes during cycling such as silicon [124] Moreover, the carboxyl methylcellulose/styrene-butadiene rubber CMC/SRN has already been commercialized for graphite-based anode [122]. Still, the choice of the binder is strongly influenced by the type of the material.

Regarding polyanionic compounds, $PVdF^{NMP}$ is usually used as a binder while the focus is on development of synthesis strategies, aimed at improving electrochemical properties. Still, other binders such as CMC and PAA, dissolved in water (CMC_{aq} and PAA_{aq}), turned out to be better solution than conventional PVdF [65,125,126]. Namely, improved rate capability and cycling stability of Nasicon $Na_3V_2(PO_4)_2F_3$ (75 mAh g^{-1} for CMC vs. 18 mAh g^{-1} for PVdF at 70 C, with the retention of ~ 79 % vs. ~55 % over 3500 cycles at 30C in 1M $NaClO_4$/EC+PEC + 5wt% FEC, 1C = 128 mA g^{-1}) [126], $Na_3V_2O_{2X}(PO_4)_2F_{3-2x}$–rGO (108 mAh g^{-1} for CMC vs. 103 mAh g^{-1} at 0.1C for PVdF), with the retention of 98% over 250 cycles vs. 84% over 60 cycles at 0.1C in 1M $NaClO_4$/PC + 2wt% FEC, 1C = 130 mA g^{-1}) [125] and Na_2FePO_4F/C (66.8 mAh g^{-1} vs. 25.1 mAh g^{-1} at 4C, with the retention of ~ 92 % vs. ~81 % over 200 cycles at 1C in 1M $NaClO_4$/PC + 2 wt.% FEC, 1 C = 130 mA g^{-1}) [65] were achieved with the use of both CMC (10wt%) and PAA binders (10 wt%) instead of PVdF. These aqueous binders were found to i) accelerate the charge transfer process during cycling; ii) facilitate Na^+ ion diffusion, iii) improve the adhesion between active material and binder; iv) improve dispersity of active particles in electrode slurries and their integrity during cycling, when compared to PVdF binder.

Besides, the development of binder-free flexible electrodes has attracted attention in recent years [127]. Design of binder-free electrodes by directly growing on different carbonaceous substrates (carbon cloth, carbon paper, graphene, carbon nanofibers) has been considered as an efficient strategy in providing outstanding rate performance and ultralong cycling. This type of electrodes enables the integration of active material and current collector as a whole, thus avoiding the use of the binder. This way, the closer connection of active particles and current collector is achieved which reduces the contact resistance, thus facilitating the electron transfer. Thanks to the flexible nature of these electrodes, flexibility of battery device can be achieved [127,128]. Different binder-free polyanionic cathodes such as $NaVPO_4F$/C@carbon fibers [129], $Na_3V_2(PO_4)_3$@carbon nanofibers [130], $Na_3V_2(PO_4)_3$@carbon paper (NVP@CP) [131], $Na_3V_2(PO_4)3$@carbon cloth [132], $Na_2FeP_2O_7$ @ porous carbon cloth [133] $Na_3(VO)_2(PO_4)_2F$@graphene foam [134] were made through the different template free and template-assisted methods such as electrospinning method [127,130] and impregnation-carbonization techniques assisted by freeze-drying [131], sol-gel [132] and solvothermal process [134]. These electrodes deliver high-rate performance over long cycling (up to 3000 cycles).

Most electrodes of examined mixed polyanion cathode are prepared with $PVdF^{NMP}$ (5% or 10 wt%), as listed in Table S1, while CMC_{aq} is only used as a binder for the preparation of $Na_4Co_3(PO_4)_2P_2O_7$–MWCNT [67] and $Na_4Ni_3(PO_4)_2P_2O_7$ [98]. Actually, Kumar et al [67,98] have used CMC since they have previously shown that CMC improved sodium storage properties of sodium vanadium oxy-fluorophosphate [125]. Regarding the amount of PVDF, 5wt% was mostly used for the preparation of NCPP [68,69,109,110], while one study uses 10% of PVdF thus maintaining percent of conductive additive to 10%. Electrodes of other polyanonic compounds including NFPP, NMPP and NNPP [47,50,63,64,71,77,96,99,102,107,108,112,115–117,121] mostly contain 10 wt. % of PVdF, while the amount of conductive additive is 20 or 10 wt. %. By surveying the TableS1, in terms of used binder, additive and active material ratio, it is difficult to conclude, with certainty, whether the amount of binder influences the cycling stability, since different synthesis procedures and different electrolytes were also used. It can be assumed that 10% of PVdF, used in the electrode of hollow Al-doped $Na_4Co_3(PO_4)_2P_2O_7$ microspheres [111], is favorable for such a long cycling, over 8000 charge/discharge cycles, due to the stronger bonding effect needed to maintain the active material-support contact. Also, we can notice that the NFPP-based electrode containing 10 wt% of PVdF [112] shows higher capacity retention (97% over 100 cycles at C/20) than the electrode with 5 wt% of PVdF (90% over 50 cycles at 1 C) [114] in the common electrolyte (1M $NaClO_4$/PC+EC), while the similar procedure for preparation of the active powder was used. Still, it should be borne in mind that different current rates were used, which can have an impact on anode polarization and consequently on the capacity retention. On the other hand, no capacity fade observed over 3000 cycles for the $Na_4Fe_3(PO_4)_2(P_2O_7)$@$NaFePO_4$@C (NFPP@NFP@C-CC) [119], grown on a flexible carbon cloth (CC) substrate (Fig. 18a-d), without the use of any binders and additives. Among all examined mixed-polyanionic cathodes (Table S1), this electrode actually shows the best sodium-storage capacity (Fig. 18a-d). It is the consequence of avoiding the insulator

behavior of the binder, achieved through the sol-gel-based, dip-coating method. By growing the NFPP@NFP particles on the pretreated carbon cloth consisting of carbon fibers, the strong anchoring of active particles with the support can be achieved, thus enabling the easier electron transfer process between support and active material. This method, which implies in-situ preparation of flexible binder-free NFPP@NFP@C-CC cathode (with the capacity of 136 mAh g^{-1} @0.1C, 97 mAh g^{-1} @10 C and 68 mAh g^{-1} @100C) [119], was shown to be more effective than the method for the preparation of binder-free $Na_2FeP_2O_7$ electrode on porous carbon cloth [133] in terms of simplicity, control of chemical composition and sodium storage capability (95 mAh g^{-1}@0.1 C, 68 mAh g^{-1} @10 C .

To summarize, the binder influence on the electrochemical properties of common $Na_4M_3(PO_4)_2P_2O_7$ electrode is still not systematically studied. Numerous studies are still needed to evaluate the best optimal solutions as the most commercialization potential. The role of binder is especially critical issue for higher loadings, required for the commercial purpose. Of course, the selection of binder is in the strong correlation with both material properties and the type of the electrolyte.

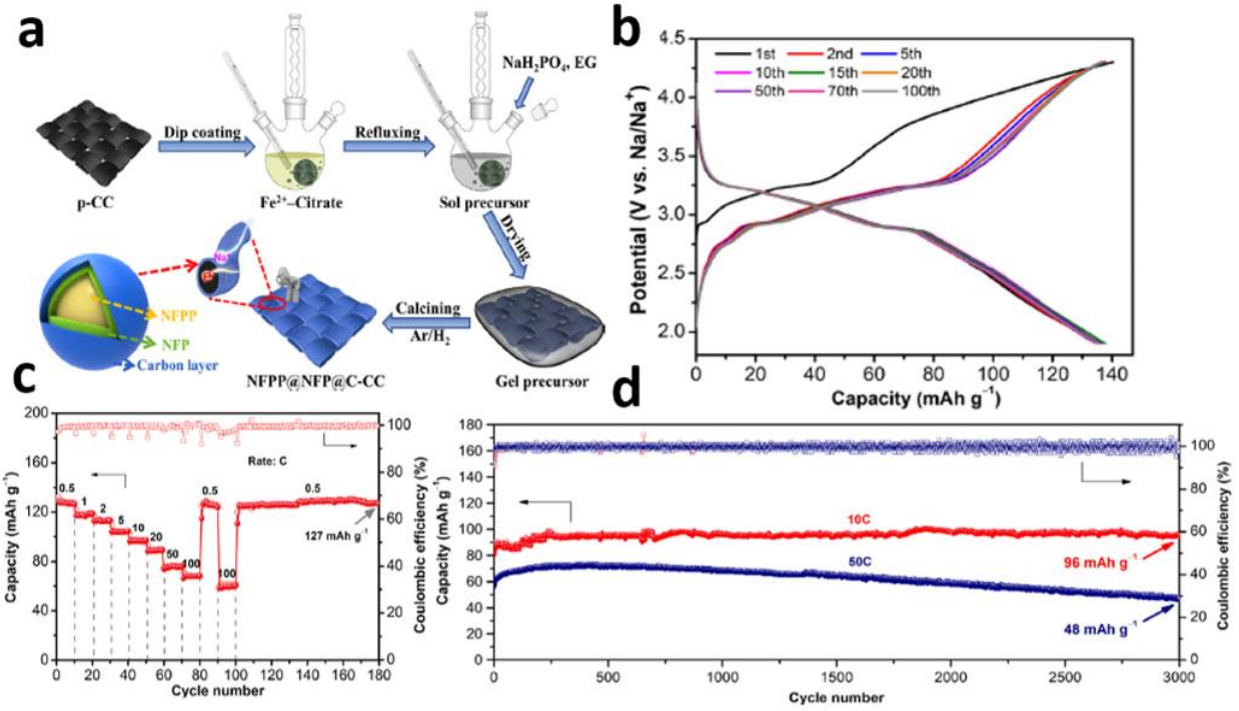

Fig. 18. a) Schematic illustration of the synthesis process of binder-free NFPP@NFP@C-CC electrode and its b) charge/discharge profiles at 0.1 C rate, c) Rate performance at different current rates and d) long-term cyclic stability at 10 C and 50 C for 3000 cycles obtained in a 1 M $NaClO_4$/PC+FEC, (1 C = 129 mA g^{-1}). (Reprinted with permission from ref. [119], Copyright 2019, Elsevier).

5. The influence of the electrolyte formulation on polyanionic electrode performance

Besides materials' properties, the nature of the electrolyte is the crucial in tailoring the interface suitable for high-performance sodium-ion batteries. Passerini et al. [25] have published recently a comprehensive review related to the progress, status and perspective of electrolytes for Na-ion rechargeable batteries. The most commonly used electrolytes are carbonate-based liquid electrolytes composed of typical salts ($NaClO_4$, $NaPF_6$, NaTFSI, NaFSI, $NaBF_4$) dissolved in cyclic carbonates such as propylene carbonate (PC) and ethylene carbonate (EC) or in their combination with any linear carbonates such as ethyl methyl carbonate (EMC), dimethyl carbonate (DMC) and diethyl carbonates (DEC). Besides, different ether-based, Ionic Liquids-based, aqueous, highly concentrated and solid-state electrolytes have been examined.

5.1. Nonaqueous organic electrolytes

An important aspect, regarding the role of the electrolyte in the final sodium storage performance of a certain electrode material, is not only related to the examined electrode interface, but also to the reactivity of Na metal electrode (acting as a reference and/or counter electrode) with the corresponding electrolyte. Sodium metal reacts with different organic carbonate electrolytes ($NaClO_4$/EC+DMC, $NaPF_6$/EC+DMC, $NaClO_4$/PC and $NaClO_4$/EC+DEC [112,135] to a varying extent, depending on the type of solvent. This process is more pronounced if the sodium half-cell is underwent to potentiodynamic cycling. However, the fluoroethylene carbonate (FEC) additive was found to be an effective solution for Na-ion batteries, which improves their performance, thus suppressing undesired electrolyte decomposition reactions at the Na metal (or hard-carbon electrode) [136,137]. Still, positive effect of FEC is not always observed [138,139]

Electrolytes which are used for the examination of polyanionic NMPP cathode are listed in Table S1. As can be seen, most common electrolyte salts such as $NaPF_6$ and $NaClO_4$ are dissolved in the solvent mixtures of PC+EC [77,97,112,114,140,141], EC+DMC [67,98,116,117], EC+DEC [68,69,96,109,110,121], PC+FEC [50,107,119] , EC+PC+FEC [99,108,141] or EC+DEC +FEC [63,64,102,111]. By examining the influence of two electrolytes (1 M $NaClO_4$/EC+PC and 1M $NaClO_4$/EC+DEC on the electrochemical performance of the common Na//NFPP half-cell, Jang et al [112] showed that 1M $NaClO_4$/EC+PC is a more suitable, thus providing the high reversible capacity of 122 mA h g^{-1} over 100 cycles, with a high coulombic efficiency of ~ 99%. Namely, EC+DEC-based electrolyte reacts with Na metal (as evidenced by the color change of separator soaked by this electrolyte) thus forming decomposition products (sodium alkyl carbonates and reactive organic radical species), identified by ^{13}C nuclear magnetic resonance (NMR) spectroscopy. The products diffuse towards NFPP cathode thus accelerating the electrolyte decomposition at higher potentials, which leads to the appearance of two additional plateaus in the charging curve of Na/NFPP cell (Fig. 10a). This results in the cell overcharging, thus reducing its coulombic efficiency and reversible capacity.

When any of the linear carbonates (DMC, EMC or DEC) is added to the solvent mixture of EC+PC (at the expense of the PC fraction), the sodium storage performance becomes disrupted [141], despite the fact that the addition of low viscous linear carbonates improves $NaClO_4$/EC+PC ionic conductivity (following the order DEC, EMC, DMC) and wettability of hydrophobic polyethylene (PE) separator (following the order DMC, EMC, DEC). Namely, these carbonate-containing electrolytes undergo decomposition by reacting with the Na anode, which is more pronounced during cycling. It is also confirmed by ^{13}C NMR spectroscopy of these electrolytes after their contact with the Na metal anode (without any applied potentials). Specifically, DMC undergoes irreversible decomposition at the Na metal anode thus forming dissolved by-products (sodium alkyl carbonate and $CH_3\cdot$ radical) which may diffuse to the NFPP cathode and further decompose at higher potentials during Na/NFPP charging (Fig. 19a). This contributes to an additional conveyed charge (Fig. 19b), which is not observed in the case of Li/NFPP cell. Mentioned by-products are also identified upon reaction of Na with EMC and DEC-based electrolytes, but the initial charge excess is not observed (Fig. 19c), due to the less pronounced reactivity when compared to DMC. It is evidenced by different color intensity of the separator, soaked by these linear carbonates-containing electrolytes. More importantly, the electrolyte decomposition byproducts were not identified when the FEC additive was added in any of DMC, EMC- and DEC-based electrolytes. FEC suppresses the reaction between Na and electrolyte effectively, thus forming stable electrode electrolyte interface (SEI) on the Na metal (Fig. 19d,e). As a result, the Na//$NaClO_4$/EC+PC+DMC+FEC//NFPP cell does not suffer overcharging c), while its coulombic efficiency is improved (from 91-98 % up to 99.3%). However, if compared to FEC-free cell, it displayed reduced capacity, due to formation of thick NaF resistive layer on the cathode surface, which acts as an additional barrier for Na ion diffusion. Since the amount of NaF, formed on the cathode upon cycling of the cell containing DEC+FEC-based electrolyte, is small, this film does not present diffusion barrier for Na ions in that cell. As a result, the capacity of the Na/EC+PC+DEC //NFPP cell is not reduced upon FEC addition into electrolyte. Its value is the highest among cells which use all three carbonates (DMC+FEC, EMC+FEC and DEC+FEC) as electrolytic components (90.5 mAh g^{-1} without noticeable capacity loss over 300 cycles, while the coulombic efficiency is 99.5 %).

Let's discuss obtained electrochemical performance from the aspect of the electrolyte composition. If we compare the experimental results, obtained by Jang's and Lee's groups [Fig. 5c in [112] and Fig. 2b in ref [141], the first overcharging of Na//1M$NaClO_4$/EC+DEC+PC//NFPP is not observed, while it happens in the of Na/1M $NaClO_4$/EC+DEC/NFPP cell. One can conclude that either PC slows down the reaction between DEC and Na metal, or such difference is simply governed by specific material properties. On the other hand, we can notice that the decomposition of DMC is not observed at Na metal [117], during cycling of half-cell using NFPP film and 1M $NaClO_4$/EC+DMC electrolyte, since the capacity is quite stable over 500 cycles. If we compare this behavior with Lee's results [141] on decomposing DMC component in the mixture of EC+PC and if we consider this difference from the aspect of the electrolyte, one can assume that PC accelerates DMC decomposition. However,

the other reason for such difference could lie in different NFPP electrode engineering applied in references [141] and [117]. Therefore, the main question which arises here is related to the role of PC and/or material properties on the decomposition rate of linear carbonates at the sodium metal surface. This issue remains the subject matter for further researches.

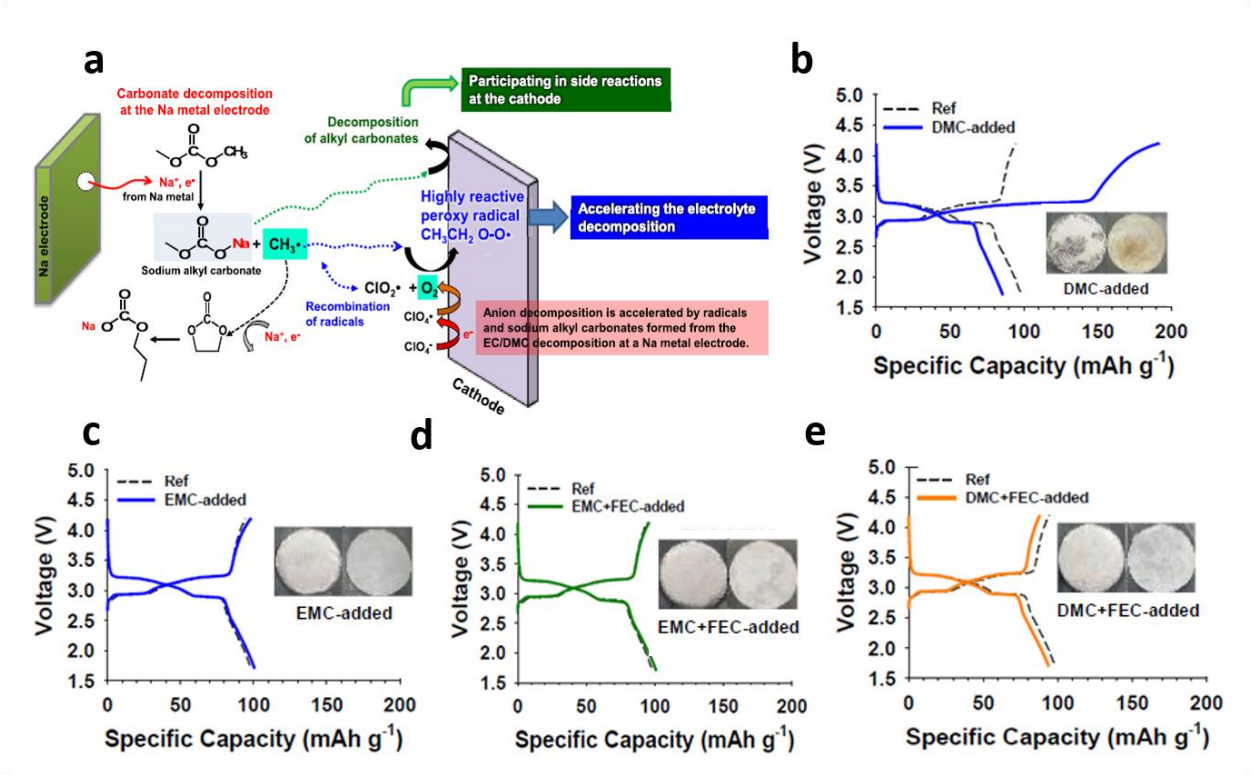

Fig. 19. a) Schematic illustration of the decomposition process of DMC-containing electrolyte at the Na metal anode (dissolved by-products diffuse to the NFPP cathode); the voltage profiles of NFPP, measured at C/20 C (1 C = 100 mA g^{-1}) and 30 ° C, in b) 0.5 M $NaClO_4$/EC+PC+DMC, c) 0.5 M $NaClO_4$/EC+PC+EMC, d) 0.5 M $NaClO_4$/EC+PC+EMC+FEC and e) 0.5 M $NaClO_4$/EC+PC+DMC+FEC. Insets shows the color change of the GFF separator before and after wetting with the corresponding electrolyte (Reprinted with permission from ref. [141], Copyright 2016, Elsevier).

The fact that the choice of the electrolyte determines the sodium storage performance of polyanionic cathode is clearly demonstrated by Kumar et al [67], who showed different CV behavior for the common NCPP electrode (containing CMC binder) if measured in 1 M $NaPF_6$ in EC:DMC and if measured in 1 M $NaClO_4$/PC+FEC. Since FEC addition in PC can be favorable for sodium storage performance [119], the reason for poorer performance of NCPP electrode [67], in 1 M $NaClO_4$/PC+FEC can be attributed to the "bad combination" of CMC and FEC binder [139]. Their synergy can cause an additional resistive layer on the Na metal thus increasing the cell polarization resistance. At the cathode side, the oxidation of Al in PC+FEC-

based electrolyte could be more intensive within the used potential interval (from 4 to 4.8 V vs. Na), since this electrolyte may start to decompose at 3.8 V vs. Na on the Al foil [136] (the interval stability up to 4.8 V is shown for Pt current collector). Additional reason could be in the Al corrosion due to increased pH value of the CMC-based slurry. Unlike $NaPF_6$-based electrolyte, $NaClO_4$-based electrolyte does not contain fluorine which can passivate the current collector [142].

Beside the most common, carbonate-based organic electrolytes, ionic liquids (ILs) and concentrated electrolytes with organic solvents are also used for examining mixed polyanionic cathode [140]. By comparing the electrochemical behavior of NNPP in NaTFSI-Py_{13}FSI with that in $NaPF_6$/EC+DEC (1:1), Passerini at al [96] found an improved sodium storage in ILs-based electrolyte (63 mAh g^{-1} vs. 40 mAh g^{-1}). Also, a wider potential window was provided with ILs- (3-5.1 V vs. Na^+/Na) than with standard, carbonated-based electrolyte (3-4.9 V vs. Na^+/Na), which is crucial for high-voltage material such as NNPP. Furthermore, the use of ultraconcentrated electrolyte (5 M) composed of sodium bis (fluorosulfonyl)imide in 1,2 dimethoxyethane (NaFSI-DME) shows good compatibility with NFPP, without corrosion of Al collector [140] . This highly concentrated electrolyte (conductivity of 0.584 S cm^{-1}) provides a high oxidation stability of Al collector (up to ~ 5 V vs. Na^+/Na), reversible Na plating/stripping and low decomposition rate at Na metal. As a result, the high and stable redox behavior of Na//NaFSI-DME//NFPP cell was observed during 300 charging/discharging cycles. By comparing the sodium storage performance of NFPP in 5 M NaFSI-DME with that in typical 1M $NaPF_6$/EC+PC electrolyte, the improved behavior in first case was observed. Actually, the slightly higher initial capacity (116.2 vs. 111.4 mAh g^{-1}) and more noticeable improvement of the capacity efficiency (99 % vs. 96 %) and capacity retention (~ 94 % vs. ~ 85%) upon 300 cycles, was observed in the case of concentrated NaFSI-DME electrolyte.

Although the conventional liquid-based electrolytes provide high-rate performance of metal-ion batteries, their use bears potential environmental risk mostly caused by flammable and volatile nature of the organic solvent. In this context, two types of safer and reliable alternative batteries, which use aqueous or solid-state electrolytes, have drawn attention.

5.2. Aqueous electrolytes

Apart from safety issues, aqueous electrolytes offer the higher ionic conductivity, lower price and simple manufacture process in comparison to the organic electrolyte. By comparing NFPP behavior in an organic solution (1 M $NaClO_4$ in EC:PC) and in 1 M Na_2SO_4 in H_2O [114], both higher capacity and better cyclic stability were observed in organic electrolyte. As we have already mentioned, the side reactions with water result in the capacity fade during cycling. So, the development of various strategies including particles coating procedures are needed to prevent the capacity fade and improve the capacity itself.

Generally, the main drawback and at the same time the main challenge with aqueous electrolyte is the lower voltage window limited by the electrolytic decomposition of water. By using highly

concentrated salts in appropriate solvents, the potential window of aqueous solution could be extended up to 4 V [143], which opened a new door for future research directions in the field of aqueous rechargeable batteries. Lee at al [115] showed that the use of highly concentrated $NaClO_4$ (17 M), instead of 1 M $NaClO_4$ aqueous solution, resulted in shifting of the OER onset potential towards more positive potentials (from 4 to 4.4 V vs. Na^+/Na) and HER onset potential toward more negative value (from 2.3 to 1.7 V vs. Na^+/Na). As a result, a wider potential region of 2.7 V was obtained in 17 M $NaClO_4$. By comparing the sodium performance of NFPP in different aqueous electrolytes, such as 17 M $NaClO_4$, 1 M $NaClO_4$ and 9.26 M $NaCF_3SO_3$ (in the form of full cell with $NaTi_2(PO_4)_3$), the capacity retention after 200 cycles was found to be improved significantly in concentrated aqueous solution (75, 18 and 63 % for 17 M $NaClO_4$, 1M $NaClO_4$ and 9.26 M $NaCF_3SO_3$, respectively). Besides, the coulombic efficiency of NFPP-based cell after 200 cycles is significantly higher in 17 M $NaClO_4$ (~99%) than in 1 M $NaClO_4$ (~68 %), while the similar values are obtained between 17 M $NaClO_4/H_2O$ and $NaCF_3SO_3/H_2O$.

Taking into account the possibility of broadening a potential window of aqueous electrolyte as well as the fact that the strategies for the high and stable capacitive performance are successfully developed for aqueous rechargeable batteries, further developments of this specific family of polyanionic compounds for aqueous rechargeable Na-ion batteries are worthy of investigations and remain a challenge.

5.3. Solid-state electrolytes

Solid-state electrolytes present potential solution to mitigate safety issues of conventional liquid electrolytes (mostly related to flammability and leakage of the electrolyte), thus allowing a high thermal stability, wider electrochemical stability window (> 5 V), longer life cycle and excellent mechanical/flexible properties. Besides, they simplify the cell-assembly process in terms of avoiding the separator wetting procedure by the electrolyte. On the other hand, there are big challenges regarding lower ionic conductivity, at a room temperature, when compared to liquid electrolytes, as well as the issues of controlling electrode/electrolyte interface and engineering processes [25]. Generally, solid-state electrolytes can be classified into conductive inorganic ceramic/glass-ceramic electrolytes, solid polymer electrolytes (SPEs) and their composite/hybrid versions. There are two types of inorganic solid electrolytes (ISEs): sulphide- (Na_3PS_4, Na_3SbS_4 $Na_2S–SiS_2$, $Na_2S–GeS_2$) and oxide-based organic electrolytes (β-Alumina electrolyte, Nasicon), while solid polymer electrolytes (SPEs) can be roughly divided into gel polymer and solvent-free solid polymer electrolytes [25,144].

β -Alumina electrolyte was the first fast ion conductor used in Na-S and Na-metal chloride batteries [144], while the main focus is currently on alternative sodium super ionic conductors such as NASICON with a general formula $Na_{1+2x+y+z}M_xM_yM_{2-x-y}Si_zR_{3-z}O_{12}$, where M is replaced by divalent, trivalent or tetravalent cations, while R can be Si or As [144].

Let’s consider some developments of polyanionic structures for solid-state batteries. The first works on the use of Nasicon ($Na_3Zr_2Si_2PO_{12}$) as the solid electrolyte for both room and mid-high

temperature sodium batteries were performed using polyanionic $Na_3V_2(PO_4)_3$ cathode [145,146]. The ionic conductivity of Nasicon $Na_3Zr_2Si_2PO_{12}$ was found to be ~ 9.4 x 10^{-4} S cm^{-1} at a room temperature [145], while its value at 200 ^{o} C amounted to ~ 1.5 x 10^{-3} S cm^{-1} [146]. The initial capacity of $Na_3V_2(PO_4)_3$ (NVP), in the form of symmetrical NVP/Nasicon/NVP battery cycled at a room temperature within 0.01-1.9 V, was 80 % of the discharge capacity (68 mAh g^{-1}@1.2 μA cm^{-2}) obtained for the symmetrical liquid NVP/$NaClO_4$-PC/NVP cell [145]. It was ~ 58% of NVP theoretical capacity (117 mAh g^{-1}). However, deep capacity decay was obtained within the first five cycles. The improved rate capability of this symmetrical solid-state sodium cell, was obtained under higher temperature of 200 ^{o} C [146]. Actually, when the NVP/$Na_3Zr_2Si_2PO_{12}$/cell operates at C/10 (97 uA cm^{-2}) under 200 ^{o} C, its initial capacity could reach ~ 85% of the NVP theoretical value. The capacity of ~ 50 mAh g^{-1} was evidenced at C/2, showing a gradual decline over 20 cycles. Afterwards, different polyanionic $Na_3V_2(PO_4)_3$, $NaTi_2(PO_4)_3$, $Na_3(VOPO_4)_2F$, $NaFePO_4$ cathodes were examined in the combination with both organic and polymer solid electrolytes [147–149]. Different solid polymer-based electrolytes are summarized in the paper of Qiao et al [149]. By combining NVP as the cathode with Na/C as metal anode and NaFSI-based solid polymer (PEO) as the electrolyte, Zhao et al. [150] constructed full solid-state cell which at 80 ^{o}C displays the high capacity (~111 mAh g^{-1} at 0.1 C and 92 mAh g^{-1} at 2 C where 1C is 117 mA g^{-1}) and ultrahigh capacity retention (92 % after 200 cycles and over 80% after 5000 cycles) for a relatively large mass loading of 6-8 mg cm^2 [150].

Generally, ISEs offer advantages over SPEs in terms of higher ionic conductivity (10^{-4} S cm^{-1} vs. 10^{-5} S cm^{-1}), higher cation transference number (~ 1 vs. ~ 0.2-0.4), higher resistance to the shocks and vibrations, and wider electrochemical potential window, while they are too hard and brittle unlike highly flexible and lightweight SPEs. Their hybridization in terms of making an ion-conducting ceramic/polymer composite is an effective way to afford advantages of both individual components. Kim al. [151] proposed the use of such NASICON-based composite hybrid solid electrolyte (HSE), composed of NASICON ceramic powder (70wt%), a poly (vinylidene fluoride–hexafluoropropylene) (PVdF HFP) and ether-based electrolyte such as 1 M sodium triflate ($NaCF_3SO_3$)/TEGDME liquid electrolyte, for sodium battery (C/$NaFePO_4$). The initial specific capacity of $NaFePO_4$ in this half-cell amounted to 131 mAh g^{-1} at a 0.2 C rate, while the full cell arrangement with carbon anode, displayed 120, 103 and 75.4 mAh g^{-1} at rates 0.2, 0.5 and 1 C, respectively. The average voltage of this full HC/HSE/$NaFePO_4$ cell was 2.6 V, while the capacity retention was found to be 96 % after 200 cycles.

Although various aforementioned polyanionic structures have been examined for solid-state batteries, according to the best of our knowledge, there is no attempt of examining interface between NMPP electrode and solid electrolyte interface. So, there is much space for studies of NMPP electrochemical properties, using various solid-state electrolytes, especially polymer-based ones which are successfully used for other polyanion compounds. Surely, it will define one of the future directions and, at the same time, present a great challenge in the field of the future energy storage.

6. Conclusions, challenges and opportunities for moving forward

6.1. Future issues

The sodiation/desodiation performance of $Na_4M_3(PO_4)_2(P_2O_7)$, experienced large advancement since 2013, especially $Na_4Fe_3(PO_4)_2(P_2O_7)$ one. Nevertheless, there are still lots of vague and unclarified issues, crucial for the "commercial design" of this material. Herein, we would like to summarize contradictions appearing in the literature and some unexplored segments, as the challenges for further research directed to the improvement sodium interfacial processes.

First, the issue of the full capacity upon deinsertion/insertion of Na^+ ions has not been entirely addressed. Different values of theoretical capacity have been reported, based on the transfer of three or four Na ions. Some authors regarded that the extraction of the fourth Na ion from $Na_4Co_3(PO_4)_2(P_2O_7)$ can only occur above 4.8 V vs. Na^+/Na, but the question remains whether it is followed by Co^{3+}-Co^{4+} transition or the lattice oxygen oxidation. Otherwise, the partial extraction of all four Na ions may occur during redox process within the 4.1-4.7 V voltage interval. Furthermore, Kim et al [47] highlighted that the theoretical capacity of $Na_4Fe_3(PO_4)_2P_2O_7$ should be 129 mA hg^{-1} (3 Na^+) instead of 170 mAh g^{-1} (4 Na^+), due to the pillar role of the remaining Na ion. This is in line with the three Fe ions in +2 oxidation state. Guided by Kim's studies, most authors have adopted theoretical capacity including three Na ion transfers, not only for Fe but also for Mn and Ni-based mixed phosphates. Regarding the structural characterization, we have also noticed some inconsistencies in the interpretation of Infrared and Raman spectra i.e. in the assignation of vibrational modes (as displayed in the section 2.1). Although the interpretation of Infrared spectra is difficult due to overlap of certain vibrational modes, we believe that an appropriate commitment can clarify some issues.

The next crucial issue is related to the determination of the Na^+ reaction path through the solid channel structure during charging/discharging procedure. The reported sequences of Na extraction are not unambiguous, which is probably the consequence of distinctive experimental and theoretical approaches. Further observations, relying on combined experimental and theoretical studies, still require more attention, in order to match the final outputs, or, at least, to explain causes of discrepancies. Nevertheless, there are general conclusions about the low activation barrier for diffusion of all Na ions through the polyanionic framework, especially for ions with a fewer coordination number, which are assumed to leave the solid skeleton first.

Let us also shed more light on the importance of the synthesis procedure and the lack of explanation concerning the synthesis conditions and their influence to the final composition of polanionic powder. Aqueous solutions of different salts such as oxalates, nitrates, acetates etc were generally used as the source of transition metals, while $Na_4P_2O_7$ or NaH_2PO_4 were mainly used as Na and P source. One can notice some differences between reactants acting as a phosphorous source. In some syntheses, both $Na_4P_2O_7$ and NaH_2PO_4 (or NaH_2PO_4) reactants, in the amount corresponding to the targeted stochiometric composition, were used as the source of

phosphorus (usually in the solid-state procedures), while some other procedures (for instance solution-based synthesis such as sol-gel one) used phosphate salts exclusively. The second case implies the thermal phosphate to pyrophosphate conversion. However, there is no general explanation as to why the phosphate decomposition is actually prevented under certain synthesis conditions and how $PO_4 \rightarrow P_2O_7$ thermal conversion can be adjusted/controlled to avoid the excess of phosphate or pyrophosphate phase. Formation of an additional phase ($NaFePO_4$, $Na_2FeP_2O_7$…), in numerous synthesis of $Na_4M_3(PO_4)_2(P_2O_7)$, is practically inevitable (Table S1). The amount of mixed polyanionic phase, in the synthesized sample, as well as the type and amount of the secondary phase strongly depend on the synthesis conditions. For instance, the NFPP can be prepared by the solid-state reaction method, but only with the assistance of ball-milling. Also, the quenching of the sample can increase the content of the desired phase in the sample, but it deteriorates its structural and electrochemical properties. Notably, the temperature strongly controls the chemical composition. Furthermore, the amount of sodium should be controlled since it may determine the phase composition. On the other hand, the template method offers the possibility of obtaining the pure NFPP phase with an impressive ultra-fast rate capability. To summarize, optimization/tailoring of synthesis conditions, aimed at getting pure phase, still requires more attention.

Lastly, the achievement of high sodium storage properties of polyanionic compounds, which is closely related to the previous discussion, is of the crucial importance. The NFPP was shown to be the mostly investigated polyanionic cathode material, with the best performance. Its sodium storage performance has been gradually improving (Table S1), as the synthesis methods evolved over time, from the simple toward more complex procedures. The high and stable capacity of this compound, obtained by the solid-state reaction method, can be achieved at a lower current rate (128 mAh g^{-1}, 1C=120 mA h g^{-1}), while its rate capability was limited to 1C (and barely to 10C when too low capacity was measured). The sol-gel synthesis procedure enables the rate capability to extend from 10 C to 50 C, whereas NFPP gradually improves columbic capacity with the progress of sol-gel procedure, thus delivering the value of 78 mA hg^{-1} at 10C [50], 85 mA hg^{-1} at 10 C, 78 mA h g^{-1} at 20 C [107] and ~ 80 mA hg^{-1} at 20 C [99] up to 97 at 10C [119]. Finally, the ultra-fast sodium storage properties (up to 200 C) have been achieved by the means of novel template [63] and ultra-spray methods [102], which provide the capacity of 79 mA hg^{-1} at 100 C or 35 mAh g^{-1} at 200C, along with the long-term cyclability over 4000-6000 cycles.

On the other hand, such outstanding rate properties still remain a great challenge for Co, Ni and Mn-based compounds. Namely, the capacity of these compounds is generally lower than that of NFPP, especially at high current rates and upon long-term cycling. One of the reasons is the occurrence of different sodiation/desodiation redox potentials, depending on the type of transition metal. Namely, the average sodium redox potentials of $Na_4M_3(PO_4)_2(P_2O_7)$ are found to be ~3.2V (Fe), ~3.8 V (Mn), ~4.5 V (Co), ~4.8 V (Ni). The lowest redox potential implies less change of free Gibs energy upon charging/discharging, which can lead to better structural stability. In addition to that, the sodiation/desodiation redox process of NFPP was found to be imperfect single-phase reaction, while the several biphasic transitions characterized the redox switching of Co, Ni, Mn-based compounds. Otherwise, the higher thermal stability of NCPP,

NNPP and NMPP than NFPP, could provide the high crystallinity, favorable for the prolonged cycling stability. Anyhow, the novel synthesis/strategies of high-voltage polyanionic compounds (Co, Ni and Mn), aimed at improving capacity/stability, need to be developed. A lack of developed synthesis methods of Co, Ni and Mn-based compounds can be identified as a critical issue in overcoming inferior properties. Unlike NFPP which is synthesized by versatile synthesis procedures, only few methods, for Co, Ni and Mn-based compounds, have been reported so far. Namely, the sol-gel and ultra-spray-pyrolysis are used for the synthesis of NCPP, while the NNPP have been developed by the sol-gel and solid-state methods. The discharge capacity of NCPP at lower currents is below the theoretical one, amounting to ~100 mA hg^{-1} at 0.2 C, where 1 C = 170 mAh g^{-1} (Table S1). Its maximum rate capability is found at 20 C, with the corresponding coulombic capacity of 80 mA h g^{-1}. If someone replaces the certain fraction of Co with Al, the modified material will deliver higher rate capability (73.4 mAh g^{-1} at 50C). Further, the NNPP in the form of composite with carbon, delivers even lower capacity, amounting to ~74 mAh g^{-1} at 0.1 C (1 C =127 mA g^{-1}), with a very poor cyclic stability. Its capacity at higher currents has not been reported, while the oxygen release upon redox reaction is the major obstacle that needs to be overcome in the future. The solid-state, spray drying and gel-combustion methods were used for the synthesis of NMPP, whereas the dual strategy, including carbon coating and Co doping, is shown as an effective way to improve kinetics of the electrochemical reaction. The theoretical capacity of this Mn-based compound is withdrawn at low currents rates of 1 C (1 C = 130 mAh g^{-1}), while the maximum reported current rate is 10 C with the corresponding capacity of 41 mA hg^{-1}. Regarding NMPP, a great progress is made in terms of improving its electrochemical properties with respect to other Mn-based compounds, without the negative impact of the Jahn-Teller Distortion. Although NMPP shows significantly lower capacity than NFPP, observation that the diffusion barrier for Na ion decreases upon P_2O_7 distortion, at the final stage of charging (for Na1-Na4 pathway from 560 meV to 306 meV), appears encouraging. The same distortion in NFPP crystal lattice causes the narrowing of its Na diffusion channels thus leading to the significant increase of the activation energy for Na motion (it became even higher than 500 eV) and pronounced polarization (at the highest potentials) in the charge/discharge curves.

One should bear in mind that Fe and Mn are the most attractive components, from the sustainable and economic point of view. Accordingly, the research on Mn-based compounds, aimed at reaching/overcoming Fe-based compounds, seems to be the most challenging and promising in the future. Besides, $Na_4M_3(PO_4)_2P_2O_7$ type of polyanionic compound is found to be functional as cathode material, in various full battery cell configurations with the hard carbon as anode material (section 6.3). The best capacity can reach the value of 100 mA h g^{-1} (based on the cathode mass). One can conclude that two-electrode cell arrangement still requires a lot of attention in terms of improving electrochemical performance, in order for this class of materials to penetrate the battery market.

In addition to the structure and synthesis, the choice of the electrolyte is of the vital importance for the capacity and especially its retention. As elaborated above, its nature influences the interface properties and various interfacial processes related to decomposition of solvent

components, additive and degradation of the active material as well, which further determine the sodium storage performance. By screening the table S1, one can notice that the performance of NFPP electrodes, which can withstand a large number of cycles in carbonate-based electrolytes (more than 3000 cycles) refers to the electrolyte containing FEC additive. Actually, when the material's properties are adjusted via synthesis to enable high-rate performance, it seems that the presence of FEC is favorable for long-term cyclic stability. However, it also depends on the type of binder and solvent mixture. For example, the positive effects of FEC to the performance are not evidenced with CMC binder (as explained above) [139] and with highly concentrated NaFSI-DME [140]. Regarding other types of this new class of polyanionic structures (NCPP, NNPP and NMPP), rational synthesis methods, strategies and electrolyte formulations should be further developed to adjust the interface for the advanced battery performance of these structures.

6.2. Effective strategies to improve the kinetics of polyanionic cathode

In the $Na_4M_3(PO_4)_2P_2O_7$) structure, the MO_6 octahedra are linked with $(PO_4)^{3-}$ groups to form layers in the bc plane, which are bridged along the a-axis by $(P_2O_7)^{4-}$ groups (Fig. 3), thus forming 3D diffusion channels. Such opened 3D framework allows diffusion of Na ions along all three directions, offering an advantage over other polyanions which enable the Na ion diffusion through 1D channel ($NaFePO_4$) or 2D channels (Na_2FePO_4F). To achieve the fast-redox reaction, the rapid transport of electrons, that encounter Na ions within the framework, should be provided as well. The anchoring of the $NaM_3(PO_4)_2P_2O_7$) nanoparticles with conductive matrix of large specific surface area (1D, 2D, and 3D) can result in creation of 3D interconnected porous conductive framework and enhancement of the contact electrode/electrolyte area. So, this is an effective strategy to facilitate both electron and ionic wiring of $NaM_3(PO_4)_2P_2O_7$ particles, and boost kinetics of the mixed polyanionic cathode. There are several strategic approaches:

i) Embedding of mixed polyanionic nanoparticles into 3D interconnected carbon network, which provides thin and uniform carbon layer (with a few nm) around active particles [50,63,77,96,97,99]. The carbon coating prevents the growth of $Na_4M_3(PO_4)_2P_2O_7$) particles during the synthesis procedure, thus providing reduced dimensions which shorten the path of electrons and ions. One can see, from the Table S1, that sub-micron/micron NCPP and NNPP particles (> 200 nm) are usually obtained. So, reduction of Co- and Ni-based polyanions materials to nano-dimensions (below 200 nm), through different approaches including carbon coating, should be one of the future directions towards improved properties. On the other hand, the reduced dimension of Fe- and Mn-based particles (especially NFPP), from 30 nm to 200 nm, have been synthesized. These nanodimensions of NFPP particles, coated by thin and homogeneous 2-3 nm carbon layer, provide an excellent performance [63]. Despite producing NMPP particles with the size of ~100 nm, achievement of the high rate performance and long capacity retention remains a challenge.

ii) Carbon nanotubes wrapping of micro/nano spheres and growth of active particles on multi-walled carbon nanotubes (MWCNTs) [64,67,108,111]. Tang at al [108,111] have prepared

carbon nanotube (CNT)-modified $Na_4Mn_2Co(PO_4)_2P_2O_7$ (NM_2CPP/C-CNTs) and Al-doped $Na_4Co_3(PO_4)_2P_2O_7$ (Al-NCPP/CNT) microspheres with hollow structure, by using spray drying methods. These hollow microspheres (composed of nanoparticles), with shell thickness of ~ 465 nm, can allow large reaction area and fast mass transfer, thus shortening Na^+ diffusion distance. Moreover, they are able to accommodate the large volume changes during charge/discharge which is crucial for long-term cycling. Benefits of highly conductive surface CNTs are indicated in the subsection 3.4.2. As a result, Al-NCPP/CNT hollow structure is capable of delivering not only the high capacity and rate capability, but also exceptional cycling stability over 8000 cycles (for the small electrode loadings of 1.3 mg cm^{-2}). When compared to other carbon-coated polyanionic hollow spheres (Na_2FePO_4F/C, Na_2MnPO_4F/C, $Na_3V_2(PO_4)_3$/C) [152–154], the Al-NCPP/CNT hollow structure possesses higher rate capability and longer cycling life. By growing NFPP particles on MWCNTs [64], the high rate capability and an excellent capacity retention of NFPP/MWCNTs composite was also achieved.

iii) 3D decorating of mixed-polyanions particles with conductive graphene network, which is able to prevent the aggregation of nanoparticles [102,121]. Namely, the encapsulation of mixed polyanion particles into 3D network of graphene sheets was found to enhance the electronic wiring and supply the electrode with many nanovoids for Na^+ diffusion. Such unique structure is able to accommodate large volume changes during cycling and deliver theoretical capacity, the outstanding rate capability and ultralong cycling life (up to 200 C and over 6000 cycles) [102].

iv) carbon coating of nanoparticles + embedding of polyanionic nanoparticles into cross-linked porous graphene network [98,107]. 3D porous conductive network, composed of in-situ formed amorphous carbon layer and cross-linked graphene sheets, restricts the aggregation of polyanionic nanoparticles, increase electrode/electrolyte contact area and improves electrons transport and dispersity of electrode particles. Such unique NPFC@AC-rGO structure [107] exhibits an excellent sodium storage performance, especially at the high rate of 20C and the low temperature of -15 ^{o}C.

Synergy of amorphous carbon with CNTs [108] and graphene sheets [107] in the mixed polyanionic composite, is considered to improve the electrochemical properties. Still, the sodium storage performance of published 3D hierarchical micro/nano phosphate structures (the capacity, rate capability and capacity retention) are inferior when compared to the performance of carbon-coated $Na_3V_2(PO_4)_3$ (NVP/C) [155]. Carbon framework of NVP/C consists of graphene-like coating layers and interconnected nanofibers. Therefore, there is still considerable room for further improvements of existing 3D conductive mixed polyanion structures. One approach should be directed to the carbon surface chemistry and its tailoring through the heteroatoms (N, S…) doping, which facilitates the charge transfer process.

6.3. Comparison with other polyanionic structures

Representative properties of different polyanionic-type materials are presented in the Table S2 (Supp.Data) in order to compare their electrochemical behavior with mixed-polyanionic

compound. Although the comparison between different polyanionic structures is inappropriate, since the electrochemical performance varies depending on the used synthesis method or the type of the electrolyte, some advantages/disadvantages can be derived, as listed in the paper of Jin et al. [87]. Besides operating voltage (Fig. 2), the main advantage of 3D mixed-polyanionic framework over other polyanionic structures, (with a common transition metal M) such as phosphates (olivine and maricite $NaMPO_4$), fluorophosphates (Na_2MPO_4F) and pyrophosphates ($Na_2MP_2O_7$), is in term of the rate capability. Although the capacity of mixed phosphate-pyrophosphate structure, at lower current rates, can be slightly lower or comparable with the capacity of individual phosphates and pyroposphates, its values are usually higher at higher currents (Table S2). Let's compare some binder-free polyanionic cathodes. We can see that the capacity of the binder-free NFPP@NFP@C-CC electrode in 1 M $NaClO_4$/PC+ 5%FEC (136 mAh g^{-1} at 0.1 C, 1 C = 129 mA g^{-1}) [119] is lower than the capacity of binder-free maricite $NaFePO_4$@C (NFP@C) in 1 M $NaClO_4$/PC+5%FEC [156], at slow current rates (145 mAh g^{-1} at 0.2 C, 1 C = 154 mA g^{-1}), while their values are comparable at high current rates (97 mAh g^{-1} at 10 C, 1 C = 129 mA g^{-1} and 84 at 10 C , 1 C = 154 mA g^{-1}, respectively). However, NFPP@NFP@C-CC can withstand current rates up to 100 C [119], while the maximal reported current rate of NFP@C is 50 C [156]. Furthermore, the NFPP@NFP@C-CC capacity, at all current rates, is higher than the capacity values measured for free-standing pyrophosphates, which amount to 95 mAh g^{-1} at 0.1 C and 68 mAh g^{-1} at 10 C (1 C = 97 mA g^{-1}). On the other hand, the improved capacity of NFPP@NFP@C-CC, at ultrahigh current rates ranging from 10-200 C (68 mAh g^{-1} at 100 C, 1 C = 129 mA g^{-1}), remains the challenge when compared to the free-standing $Na_3V_2(PO4)_3$@C-CC (NVP@C-CC) electrode [132] (96.8 mAh g^{-1} at 100 C or 69.9 mA h g^{-1} at 200 C, 1 C = 117 mA g^{-1}). Still, their capacities are comparable at lower current rates. The operating voltage of NFPP is slightly lower than that of NVP (3.2 V vs. 3.4 V), while the operating potential of NVP is lower than the potential of Mn, Co and Ni-based mixed polyanions.

If we compare $Na_4M_3(PO_4)_2P_2O_7$ (M= Fe) with vanadium based-fluorophosphate $Na_3(VO_{1-x}PO_4)2F_{1+2x}$ (mostly $Na_3V_2(PO_4)_2O_2F_3$, $Na_3V_2(PO_4)_2F_3$) [157,158], the lower operating potential will be observed for Fe and Mn-based polyanions, while Co and Ni-based mixed compounds would have a higher voltage. Besides, the $Na_4M_3(PO_4)_2P_2O_7$ matches fluorophosphates (based on material level in half-cell) in terms of the capacity and rate capability [157], but achievement of energy performance, as those of $Na_3V_2(PO_4)_2F_3$/C-based prototype cell is still a challenge [157–159]. Still, Fe-based mixed polyanionic material offers an advantage in terms of the price and toxicity, while the high cost and toxicity of both V- and Co- based phosphates present the obstacle. Besides, there are high requirements for the synthesis equipment of the vanadium-based fluorophosphates [87]. On the other hand, the difficult control of the NFPP synthesis conditions, which is strongly related to an insufficient understanding of the reaction processes, is recognized as one of the critical issues.

Furthermore, Na-based silicate polyanion materials are also considered as the potential cathodes for SIBs [87] due to the high theoretical capacity when extracting two Na ions per unit formula (276 mAh g^{-1} for Na_2FeSiO_4), thermal stability, low cost and high abundance of elements (the Na_2FeSiO_4 is the cheapest compound due to abundant Na-Fe-Si resources). However, these compounds have low electronic conductivity, which causes difficult extraction of the second Na ion (occurring above 4 V vs. Na^+/Na) [160]. When compared with silicates, mixed $Na_4M_3(PO_4)_2P_2O_7$ compounds possess lower theoretical capacity, but higher voltage, while the eco-aspect of $Na_4M_3(PO_4)_2P_2O_7$ depends on the metal (Fe and Mn provide cheap and eco-friendly material unlike Co and Ni). Although Na-silicates possess high theoretical capacity (based on two Na ions followed by two electron process of Fe^{2+}/Fe^{4+} redox pair), its utilization is usually limited due to difficult deinsertion of the second Na. Besides, it is a matter of the structural stability when two Na ions are extracted. In that case, advantage of the higher capacity over mixed polyanions would be annulled. On the other hand, mixed $Na_4M_3(PO_4)_2P_2O_7$ could offer not only higher operating potential but also higher cycling and rate capability (Table S1 and Table S2). Difficulties in obtaining a phase pure material is typical for both silicate and mixed polyanion materials.

6.4. Full cell configurations

Survey of constructed two-electrode full cells containing mixed polyanionic cathode and suitable anode is given in the Table S3. As we can see, different structures such as hard carbon (HC), $Li_4Ti_5O_{12}$, $NaTi_2(PO_4)_3$, (PPy)-coated Fe_3O_4 and CHC were employed as anodes thus providing cells with different operating voltages and capacities. Regarding mixed-polyanionic cathode materials, the most reported cells include NFPP and NCPP structures, while only one cell is reported for NMPP. This clearly indicates that practical development of this class of polyanionic materials as cathode are in the infancy thus leaving a lot of space for further progress and improvement. The comparison between listed full Na-ion cells is difficult since the electrochemical parameters are calculated differently (based on cathode mass, based on anode mass or based on both anode and cathode masses). However, several common issues can be noticed. First, the specific capacity of mixed-polyanionic cathode and its retention upon cycling, in full-cell arrangement, is lower than in the half-cell configuration, using Na anode (comparison with Table S1), thus indicating incomplete possible utilization of this compound. The reason lies in the insufficient sodium storage performance of anode materials to match cathode performance, compatibility issues between electrodes and/or two-electrode cell construction. Second, the first irreversible capacity loss is typical for all assembled Na-ion full cells (Table S3), which can be attributed mostly to the formation of SEI layer on the anode surface. This irreversible capacity loss is between 20 - 40 % ($Q_{discharge}/Q_{charge}$) depending on the cell and applied current, while it is significantly reduced (5 - 10 %) when the anode is previously cycled in Na-full cell, which results in good coulombic efficiency (expressed as the discharge to charge capacity ratio) during further cycling.

The irreversible capacity loss is also evidenced for some other full Na-ion cells containing polyanionic cathodes [65,125] . Deng at al [65] showed that the initial coulombic efficiency of the $Na_2FePO_4F^-$based cathode, calculated as the ratio of charge (deinsertion) and discharge (insertion) capacity, can be tailored by controlling the charging cut-off voltage (Q_{charge}/Q_{disch} increases with the increase of the cut-off anodic potential). However, they have demonstrated that the charging of the $Na/Na_2FePO_4F^-$based cathode up to higher voltage (2 - 4.5 V), followed by discharge-charge towards lower voltage (2 – 4 V), during subsequent cycling, can increase the initial coulombic efficiency (Q_{charge}/Q_{disch}) of the cathode (when compared to the constant cycling within lower or higher voltage interval) and improve cycling stability of the cell. However, this strategy is not effective for full HC/Na_2FePO_4F cell, where the constant cycling in the extended voltage interval (0 - 4.5 V) causes the best cycling performance. The mentioned cycle modes should also be checked for the mixed polyanionic cathode in order to see whether the initial columbic efficiency of the material (that actually means the increase of the irreversible capacity loss) and consequently the cyclic performance can be improved by the cycling at higher voltages (overcharging). It is difficult for this strategy to be successfully applied for the high-voltage NCPP and NNPP cathodes due to issues related to electrolyte decomposition, but it could be a good way for improving performance of NFPP and NMPP-based cells. By comparing charge discharge/curves of all reported HC/NFPP-based cells [64, 99, 107, 119], we can notice that the cell cycled up to 4 V [64,99] shows the best discharge/charge ratio (after initial irreversible change) when compared to the other cells, cycled up to 3.2 V.

Generally, relatively poor capacity retention of the full Na-ion cell with mixed-polyanionic cathode is observed. It is more pronounced when compared to the performance in the half-cell configurations with the same cathode (Table S1) or some other hybrid systems (composed of polyanionic anode and carbon cathode) [161]. Actually, the cyclic performance is limited to several hundreds of cycles, which is in the range with full cells containing other polyanionic structures as cathode such as $Na_3V_2(PO_4)_3$, $VOPO_4$ [162–165]. On the other hand, same mixed-polyanionic cathodes can withstand several thousands of cycles in half-cell configurations. Apart from the improvement, related to anode materials and configurations, better understanding of the electrode/electrolyte interface is needed as well. Comprehensive approach of morphological and structural changes (the local atomic environment, diffusion coefficients, Na diffusion pathways and barriers) during charging /discharging, along with the developments of synthesis strategies and electrolyte formulations, is necessary to break a long-term cycling barrier.

In spite of the mentioned weaknesses, one can notice advantages of the mixed-polyanionic-based cells when compared to other polyanionic cathodes. HC/ NCPP-based full cell [111] could provide higher operating voltage (~ 4.3 V) than other high-performance cells (~ 3.2 V) such as $HC/Na_3V_2(PO_4)_3$ [164,165] and $HC/Na_{3.5}V_2(PO_4)_2F_3$ [166]. However, further challenges should relate to the increase of capacity and its stability upon long-term cycling. The reduction of NCPP particles to nano-dimension, the anchoring of NCPP particles with some heteroatom-doped carbon and replacement of Co fraction with a certain ion could be effective future strategies,

which would improve energy of NCPP-based cell, reduce its toxicity and price, thus maintaining the high operating voltage. On the other hand, ion doping of NFPP and NMPP with a suitable cation or anion, capable of increasing voltage and electronic conductivity, would be a good direction for further improvement of energy performance of full Na-ion cell with NFPP and NMPP cathode.

Sodium phosphate polyanion materials were also used as electrodes of hybrid devices, preferably electrochemical capacitors. Hybrid capacitors, especially sodium-ion hybrid capacitors [100, 161], are extensively studied as potential devices which satisfy requirements of both high energy density and high-power density, at a low cost. Although $Na_4M_3(PO_4)_2P_2O_7$ type materials, have not been studied till now as the electrodes of hybrid capacitors, they should be treated as perspective ones, on the basis of following two examples with simpler phosphate polyanionic materials. First, Thangavel et al. [167] reported bio-inspired sodium ion hybrid capacitor, one electrode of which was polyanionic material $Na_3V_2(PO_4)_3$ and the second one was a cinnamon-derived highly porous carbon. In an organic electrolyte, this hybrid capacitor delivered energy density of 118 Wh kg^{-1} and a power density of 850 W kg^{-1}. It displayed also high cycling stability, the highest ever reported for sodium ion-based intercalation compounds. Second, Thangavel et al. [168] constructed a new type hybrid capacitor consisting of sodium super ionic conductor $NaTi_2(PO_4)_3$/graphene nanoshets composite as an intercalation electrode, and 2D graphene nanosheets as an adsorption electrode. This capacitor displayed energy density of 80 Wh kg^{-1} and a respectable specific power of 8 kW kg^{-1}. The capacity fade was only 0.13% per 1000 cycles, and 90% after 75 000 cycles.

To confirm good perspective of these materials, we may outline excellent electrochemical half-cell behavior of $Na_4M_3(PO_4)_2P_2O_7$/C composite described by Chen et al. [99], Yuan [102] and Ma [119].

6.5. Future considerations

Based on the total overview, the universal concept to obtain the high-performance mixed-polyanionic electrode (on the research level) is still difficult to derive due to interplay between key electrode and electrolyte components (material, binder and electrolyte) that control interface. Additional studies are needed in order to determine contribution of these individual components and their combining effect to the electrochemical activity of the $Na_4M_3(PO_4)_2(P_2O_7)$. In the strict relation to this, high-rate performance, high specific energy and excellent cycling stability with high safety, still remain the challenge, especially in the case of the structures with higher operating voltage, while many bottlenecks need to be solved. Specifically, future issues, which should be addressed, include following aspects/topics:

- Key fundamental questions, regarding the influence of the synthesis conditions/parameters to the final composition of $Na_4M_3(PO_4)_2(P_2O_7)$ phase, must be understood for each type of $Na_4M_3(PO_4)_2(P_2O_7)$. Namely, one has to deal with the following questions: i) How to adjust synthesis conditions to obtain completely pure polyanionic phase (identified as the bottleneck);

ii) what parameters are determining formation of this phase and whether it depends on the specific synthesis; ii) does the pure phase show the best performance or whether its synergy with secondary polyanionic phases is more appropriate solution. Although some NFPP electrodes [99,102,119] hold the promise in the sodium batteries, further development of rational synthesis methods and strategies to design various nanoarchitectures (including impregnation with different conductive matrices), with improved energy/power performance, are highly needed, especially for i) higher currents/loadings; ii) NCPP, NMMP and NNPP electrodes and iii) full-cell configurations.

- the influence of the binder to the electrochemical properties of the common $Na_4M_3(PO_4)_2(P_2O_7)$ electrode is not yet reported. The comparison of electrochemical properties of the common $Na_4M_3(PO_4)_2(P_2O_7)$ electrode, containing different binders, is necessary. Since PVDF is the most common binder for the electrodes, examined so far (Table S1), the future directions should be focused more on the aqueous alternative binders, especially if we keep in mind the fact that CMC can cause better performance of polyanionic NVP cathode than PVdF [125]. Since the best performance among all examined $Na_4M_3(PO_4)_2(P_2O_7)$ samples is achieved for binder-free electrode, this processing way should also be pushed for all types of this specific polyanionic family and compared with other binder-containing powder electrodes, not only in terms of the electrochemical performance, but also concerning cost, simplicity and environmental compatibility.

- the influence of the electrolyte to the mixed-polyanionic cathode is examined in few studies, but the research in this field needs to be intensified more. Since individual solvent components are decisive for the final performance of polyanionic electrode (especially in terms of the capacity retention) their role in different interface processes (the decomposition rates of carbonate-based components at the metal surface, FEC-induced processes, the synergistic process of binder and FEC…) should be specified and elaborated.

- Since few papers are related to the examination in an aqueous electrolyte, while the use of this polyanionic cathode with the solid-state electrolyte has not been reported yet, these fields remain completely open. Moreover, the examination of comparative electrochemical behavior of the $Na_4M_3(PO_4)_2(P_2O_7)$ cathode in nonaqueous and aqueous electrolytes would be an effective strategy to understand sodium insertion mechanism better.

- All future issues, outlined above, should be elaborated through the various physicochemical and electrochemical methods and understood from the theoretical aspect in order to explain structural/morphological/electrochemical relations more profoundly and anticipate some future steps. The special focus should be on the study of Na-ion sequence during charging/discharging, in order to overcome ambiguity and find out the reason for discrepancy between theory and experiment. This would result in more accurate conclusions on the sodium redox mechanism of polyanionic materials, as an important link for their high energy performance.

Acknowledgments:

A. G. would like to thank to the Ministry of Science of Montenegro for selecting her to receive the "Scholarship for Doctoral Research in Montenegro". A. G and V. G. gratefully acknowledge the financial support from Ministry of Science of Montenegro under the same project entitled "Ecological cathode materials for lithium/sodium ion batteries". This research is supported by the Science Fund of the Republic of Serbia, PROMIS, #6062667, HISUPERBAT (M.V. and M.M. gratefully acknowledge this financial support). M. V., M. M. and S.M. would also like to acknowledge for support Ministry of Education, Science and Technological Development of the Republic of Serbia, Contract number: 451-03-68/2020-14/200146"**.** The continuous support for research in the field of energy storage through the bilateral project Montenegro-Serbia with title "Development of ecological Li-ionic batteries" is also acknowledged by V.G. and M.V. R. D. acknowledges support from Slovenian research agency through ARRS-MS-BI-ZP bilateral project and P2-0393 core research program. S.M. is indebted to the Serbian Academy of Sciences and Arts for supporting the study through the project "Electrocatalysis in the contemporary process of energy conversion".

5. References:

[1] J.B. Goodenough, K.S. Park, The Li-ion rechargeable battery: A perspective, J. Am. Chem. Soc. 135 (2013) 1167–1176. doi:10.1021/ja3091438.
[2] M.S. Whittingham, Lithium batteries and cathode materials, Chem. Rev. 104 (2004) 4271–4301. doi:10.1021/cr020731c.
[3] J.B. Goodenough, Y. Kim, Challenges for rechargeable Li batteries, Chem. Mater. 22 (2010) 587–603. doi:10.1021/cm901452z.
[4] D. Bresser, K. Hosoi, D. Howell, H. Li, H. Zeisel, K. Amine, S. Passerini, Perspectives of automotive battery R&D in China, Germany, Japan, and the USA, J. Power Sources. 382 (2018) 176–178. doi:10.1016/j.jpowsour.2018.02.039.
[5] B. Dunn, H. Kamath, J.M. Tarascon, Electrical energy storage for the grid: A battery of choices, Science 334 (2011) 928–935. doi:10.1126/science.1212741.
[6] B. Scrosati, J. Garche, Lithium batteries: Status, prospects and future, J. Power Sources 195 (2010) 2419–2430. doi:10.1016/j.jpowsour.2009.11.048.
[7] M. Hu, X. Pang, Z. Zhou, Review Recent progress in high-voltage lithium ion batteries, J. Power Sources. 237 (2013) 229–242. doi:10.1016/j.jpowsour.2013.03.024.
[8] C.P. Grey, J.M. Tarascon, Sustainability and in situ monitoring in battery development, Nat. Mater. 16 (2017) 45–56. doi:10.1038/nmat4777.
[9] D. Larcher, J.M. Tarascon, Towards greener and more sustainable batteries for electrical energy storage, Nat Chem 7 (2015). 19-29. doi:10.1038/NCHEM.2085.
[10] D. Buchholz, A. Moretti, R. Kloepsch, S. Nowak, V. Siozios, M. Winter, S. Passerini, Toward Na-ion batteries - Synthesis and characterization of a novel high capacity na ion intercalation material, Chem. Mater. 25 (2013) 142–148. doi:10.1021/cm3029615.
[11] A. Ponrouch, J. Bitenc, R. Dominko, N. Lindahl, P. Johansson, M.R. Palacin, Multivalent rechargeable batteries, Energy Storage Mater. 20 (2019) 253–262.

doi:10.1016/j.ensm.2019.04.012.
[12] J. Bitenc, N. Lindahl, A. Vizintin, M.E. Abdelhamid, R. Dominko, P. Johansson, Concept and electrochemical mechanism of an Al metal anode – organic cathode battery, Energy Storage Mater. 24 (2020) 379–383. doi:10.1016/j.ensm.2019.07.033.
[13] D. Aurbach, Z. Lu, A. Schechter, Y. Gofer, H. Gizbar, R. Turgeman, Y. Cohen, M. Moshkovich, E. Levi, Prototype systems for rechargeable magnesium batteries, Nature 407 (2000) 724–727. doi: 10.1038/35037553.
[14] V. Verma, S. Kumar, W. Manalastas, R. Satish, M. Srinivasan, Progress in Rechargeable Aqueous Zinc- and Aluminum-Ion Battery Electrodes: Challenges and Outlook, Adv. Sustain. Syst. 3 (2019) 1800111. doi:10.1002/adsu.201800111.
[15] J. Ming, J. Guo, C. Xia, W. Wang, H.N. Alshareef, Zinc-ion batteries: Materials, mechanisms, and applications, Mater. Sci. Eng. R Rep. 135 (2019) 58–84. doi:10.1016/j.mser.2018.10.002.
[16] M. Vujković, B.Š. Paunković, I.Stojković-Simatović, M. Mitrić, C.A.C. Sequeira, S. Mentus, Versatile insertion capability of $Na_{1.2}V_3O_8$ nanobelts in aqueous electrolyte solutions, Electrochim. Acta. 147 (2014) 167–175. doi:10.1016/j.electacta.2014.08.137.
[17] M. Vujković, M. Mitrić, S. Mentus, High-rate intercalation capability of $NaTi_2(PO_4)_3$/C composite in aqueous lithium and sodium nitrate solutions, J. Power Sources. 288 (2015). doi:10.1016/j.jpowsour.2015.04.132.
[18] V. Pamoleras, P. Serras, I. Villaluenga, K.B. Hueso, J. Gonzáles, T. Rojo, Na-ion batteries ,recent advances and present challenges to become low cost energy storage systems, Energy Environ. Sci. 5 (2012) 5884–5901. doi:10.1039/c2ee02781j.
[19] M. Balogun, Y. Luo, W. Qiu, P. Liu, Y. Tong, Review article A review of carbon materials and their composites with alloy metals for sodium ion battery anodes, Carbon 98 (2016) 162–178. doi:10.1016/j.carbon.2015.09.091.
[20] C. Masquelier, L. Croguennec, Polyanionic (phosphates, silicates, sulfates) frameworks as Electrode Materials for rechargeable Li (or Na) Batteries,Chem. Rev. 113 (2013) 6552-6591. doi:10.1021/cr3001862.
[21] C. Vaalma, D. Buchholz, M. Weil, S. Passerini, A cost and resource analysis of sodium-ion batteries, Nat. Rev. Mater. 3 (2018) 18013. doiČ 10.1038/natrevmats.2018.13.
[22] L. Li, Y. Zheng, S. Zhang, J. Yang, Z. Shao, Z. Guo, Recent progress on sodium ion batteries: potential high-performance anodes, Energy Environ. Sci. 11 (2018) 2310 – 2340 . doi:10.1039/c8ee01023d.
[23] S. Kim, D. Seo, X. Ma, G. Ceder, K. Kang, Electrode Materials for Rechargeable Sodium-Ion Batteries : Potential Alternatives to Current Lithium-Ion Batteries, Adv. Energy Mater. 2 (2012) 710–721. doi:10.1002/aenm.201200026.
[24] H. Pan, Y. S. Hu, L. Chen, R Room-temperature stationary sodium-ion batteries for large-scale electric energy storage, Energy Environ. Sci. 6 (2013) 2338–2360. doi:10.1039/c3ee40847g.
[25] G. G. Eshetu, G.A. Elia, M. Armand, M. Forsyth, S. Komaba, T. Rojo, S. Passerini, Electrolytes and interphases in sodium-based rechargeable batteries: Recent advances and perspectives, Adv. Energy Mater. 10 (2020) 2000093. doi:10.1002/aenm.202000093.
[26] T. Perveen, M. Siddiq, N. Shahzad, R. Ihsan, A. Ahmad, M. I. Shahzad, Prospects in anode materials for sodium ion batteries - A review, Renew. Sustain. Energy Rev. 119 (2020) 109549. doi:10.1016/j.rser.2019.109549.
[27] M. Chen, Q. Liu, S. Wang, E. Wang, X. Guo, High-Abundance and Low-Cost Metal-

Based Cathode Materials for Sodium-Ion Batteries : Problems,Progress, and Key Technologies, 9 (2019) 1803609. doi:10.1002/aenm.201803609.
[28] Y. You, A. Manthiram, Progress in High-Voltage Cathode Materials for Rechargeable Sodium-Ion Batteries, Adv. Energy Mater. 8 (2017) 1701785. doi:10.1002/aenm.201701785.
[29] Y Y. Fang, J. Zhang, L. Xiao, X. Ai, Y. Cao, H. Yang, Phosphate framework electrode materials for sodium ion batteries, Adv. Sci. 4 (2017) 1600392.. doi:10.1002/advs.201600392.
[30] P. Barpanda, L. Lander, S. Nishimura, A. Yamada, Polyanionic insertion materials for sodium-ion batteries, Adv. Energy Mater. 8 (2018) 1703055. doi:10.1002/aenm.201703055.
[31] M. Vujković, S. Mentus, Potentiodynamic and galvanostatic testing of $NaFe_{0.95}V_{0.05}PO_4$/C composite in aqueous $NaNO_3$ solution, and the properties of aqueous $Na_{1.2}V_3O_8$/$NaNO_3$/$NaFe_{0.95}V_{0.05}PO_4$/C battery, J. Power Sources. 325 (2016) 185–193. doi:10.1016/j.jpowsour.2016.06.031.
[32] M. Vujković, S. Mentus, Fast sodiation/desodiation reactions of electrochemically delithiated olivine $LiFePO_4$ in aerated aqueous $NaNO_3$ solution, J. Power Sources. 247 (2014) 184–188. doi:10.1016/j.jpowsour.2013.08.062.
[33] A. K. Padhi, K.S. Nanjundaswamy, J.B. Goodenough, Phospho-olivines as Positive-Electrode Materials for Rechargeable Lithium Batteries, J. Electrochem. Soc. 144 (1997) 1188–1194. doi: 10.1149/1.1837571
[34] C. Masquelier, A.K. Padhi, K.S. Nanjundaswamy, J.B. Goodenough, New Cathode Materials for Rechargeable Lithium Batteries : The 3-D framework structures $Li_3Fe_2(XO_4)_3$ (X=P, As), J. Solid State Chem. 135 (1998) 228–234. doi 10.1006/jssc.1997.7629. doi: 10.1006/jssc.1997.7629.
[35] A. K. Padhi, K.S. Nanjunclaswamy, C. Masquelier, S. Okada, J.B. Goodenough, Effect of structure on the Fe^{3+}/Fe^{2+} redox couple in iron phosphates, J. Electrochem. Soc. 144 (1997) 1609–1613. doi: 10.1149/1.1837649.
[36] Y. Niu, Y. Zhang, M. Xu, A review on pyrophosphate framework cathode materials for sodium-ion batteries, J. Mater. Chem. A 7 (2019) 15006-15025. doi:10.1039/C9TA04274A.
[37] D. V. Anishchenko, M. V. Zakharkin, V.A. Nikitina, K.J. Stevenson, E. V. Antipov, Phase boundary propagation kinetics predominately limit the rate capability of NASICON-type $Na_{3+x}Mn_xV_{2-x}(PO_4)_3$ ($0 \le x \le 1$) materials, Electrochim. Acta. 354 (2020) 136761. doi:10.1016/j.electacta.2020.136761.
[38] M. V. Zakharkin, O.A. Drozhzhin, S. V. Ryazantsev, D. Chernyshov, M.A. Kirsanova, I. V. Mikheev, E.M. Pazhetnov, E. V. Antipov, K.J. Stevenson, Electrochemical properties and evolution of the phase transformation behavior in the NASICON-type $Na_{3+x}Mn_xV_{2-x}(PO_4)_3$ ($0 \le x \le 1$) cathodes for Na-ion batteries, J. Power Sources. 470 (2020) 228231. doi:10.1016/j.jpowsour.2020.228231.
[39] A.J. Fernández-Ropero, D. Saurel, B. Acebedo, T. Rojo, M. Casas-Cabanas, Electrochemical characterization of $NaFePO_4$ as positive electrode in aqueous sodium-ion batteries, J. Power Sources. 291 (2015) 40–45. doi:10.1016/j.jpowsour.2015.05.006.
[40] N. V. Kosova, V.R. Podugolnikov, E.T. Devyatkina, A.B. Slobodyuk, Structure and electrochemistry of $NaFePO_4$ and Na_2FePO_4F cathode materials prepared via mechanochemical route, Mater. Res. Bull. 60 (2014) 849–857.

doi:10.1016/j.materresbull.2014.09.081.
[41] I. V. Tereshchenko, D.A. Aksyonov, O.A. Drozhzhin, I.A. Presniakov, A. V. Sobolev, A. Zhugayevych, D. Striukov, K.J. Stevenson, E. Antipov, A.M. Abakumov, The Role of Semilabile Oxygen Atoms for Intercalation Chemistry of the Metal-Ion Battery Polyanion Cathodes, J. Am. Chem. Soc. 140 (2018) 3994–4003. doi:10.1021/jacs.7b12644.
[42] M. Milović, D. Jugović, N. Cvjetićanin, D. Uskoković, A.S. Milošević, Z.S. Popović, F.R. Vukajlović, Crystal structure analysis and first principle investigation of F doping in $LiFePO_4$, J. Power Sources. 241 (2013) 70–79. doi:10.1016/j.jpowsour.2013.04.109.
[43] D. Jugović, M. Mitrić, M. Milović, N. Cvjetićanin, B. Jokić, A. Umićević, D. Uskoković, The influence of fluorine doping on the structural and electrical properties of the $LiFePO_4$ powder, Ceram. Int. 43 (2017) 3224–3230. doi:10.1016/j.ceramint.2016.11.149.
[44] G. Longoni, J.E. Wang, Y.H. Jung, D.K. Kim, C.M. Mari, R. Ruffo, The $Na_2FeP_2O_7$-carbon nanotubes composite as high rate cathode material for sodium ion batteries, J. Power Sources. 302 (2016) 61–69. doi:10.1016/j.jpowsour.2015.10.033.
[45] D. Jugović, M. Mitrić, M. Milović, V.N. Ivanovski, S. Škapin, B. Dojčinović, D. Uskoković, Structural and electrochemical properties of the $Li_2FeP_2O_7$/C composite prepared using soluble methylcellulose, J. Alloys Compd. 786 (2019) 912–919. doi:10.1016/j.jallcom.2019.01.392.
[46] F. Sanz, C. Parada, J.M. Rojo, C. Ruíz-Valero, Synthesis, structural characterization, magnetic properties, and ionic conductivity of $Na_4M^{II}_3(PO_4)_2(P_2O_7)$ (M^{II} = Mn, Co, Ni), Chem. Mater. 13 (2001) 1334–1340. doi: 10.1021/cm001210d.
[47] H. Kim, I. Park, D.H. Seo, S. Lee, S.W. Kim, W.J. Kwon, Y. U. Park, C.S. Kim, S. Jeon, K. Kang, New Iron-Based Mixed-Polyanion Cathodes for Lithium and Sodium Rechargeable Batteries: Combined First Principles Calculations and Experimental Study, J. Am. Chem. Soc. 134 (2012) 10369–10372. doi:10.1021/ja3038646.
[48] F. Sanz, C. Parada, U. Amador, M.A. Monge, C. Ruíz-Valero, $Na_4Co_3(PO_4)_2P_2O_7$, a new sodium cobalt phosphate containing a three-dimensional system of large intersecting tunnels, J. Solid State Chem. 123 (1996) 129–139. doi: 10.1006/jssc.1996.0161.
[49] B. Senthilkumar, C. Murugesan, L. Sharma, S. Lochab, An overview of mixed polyanionic cathode materials for sodium-ion batteries, Small Methods 3 (2019) 1800253. doi:10.1002/smtd.201800253.
[50] X. Wu, G. Zhong, Y. Yang, Sol-gel synthesis of $Na_4Fe_3(PO_4)_2(P_2O_7)$/C nanocomposite for sodium ion batteries and new insights into microstructural evolution during sodium extraction, J. Power Sources. 327 (2016) 666–674. doi:10.1016/j.jpowsour.2016.07.061.
[51] A. Gutierrez, N.A. Benedek, A. Manthiram, Crystal-chemical guide for understanding redox energy variations of $M^{2+/3+}$ couples in polyanion cathodes for lithium-ion batteries, Chem. Mater. 25 (2013) 4010–4016. doi:10.1021/cm401949n.
[52] P. Barpanda, G. Liu, C.D. Ling, M. Tamaru, M. Avdeev, S.C. Chung, Y. Yamada, A. Yamada, $Na_2FeP_2O_7$: A safe cathode for rechargeable sodium-ion batteries, Chem. Mater. 25 (2013) 3480–3487. doi:10.1021/cm401657c.
[53] P. Barpanda, T. Ye, S. Nishimura, S. Chung, Y. Yamada, M. Okubo, H. Zhou, A. Yamada, Electrochemistry Communications, Sodium iron pyrophosphate : A novel 3.0 V iron-based cathode for sodium-ion batteries, Electrochem. Commun. 24 (2012) 116–119. doi:10.1016/j.elecom.2012.08.028.
[54] M. Casas-Cabanas, V.V. Roddatis, D. Saurel, P. Kubiak, J. Carretero-González, V. Palomares, P. Serras, T. Rojo, Crystal chemistry of Na insertion/deinsertion in FePO4-

NaFePO4, J. Mater. Chem. 22 (2012) 17421–17423. doi:10.1039/c2jm33639a.
[55] N. V Kosova, D.O. Rezepova, O.A. Podgornova, A.B. Slobodyuk, S.A. Petrov, M. Avdeev, A comparative study of structure, air sensitivity and electrochemistry of sodium iron pyrophosphates $Na_{2-x}Fe_{1+x/2}P_2O_7$ (x = 0; 0.44), Electrochim. Acta 235 (2017) 42–55. doi:10.1016/j.electacta.2017.03.058.
[56] H. Kim, R.A. Shakoor, C. Park, S.Y. Lim, J.S. Kim, Y.N. Jo, W. Cho, K. Miyasaka, R. Kahraman, Y. Jung, J.W. Choi, $Na_2FeP_2O_7$ as a promising iron-based pyrophosphate cathode for sodium rechargeable batteries: A combined experimental and theoretical study, Adv. Funct. Mater. 23 (2013) 1147–1155. doi:10.1002/adfm.201201589.
[57] J. Clark, B. Parpanda, A. Yamada, M. S. Islam, Sodium- ion battery cathodes $Na_2FeP_2O_7$ and $Na_2MnP_2O_7$, J. Mater. Chem. A, 2 (2014) 11807-11812. doi:10.1039/c4ta02383h.
[58] S.M. Wood, C. Eames, E. Kendrick, M.S. Islam, Sodium Ion Diffusion and Voltage Trends in Phosphates $Na_4M_3(PO_4)_2P_2O_7$ (M = Fe, Mn, Co, Ni) for Possible High-Rate Cathodes, J. Phys. Chem. C. 119 (2015) 15935–15941. doi:10.1021/acs.jpcc.5b04648.
[59] S.P. Ong, V.L. Chevrier, G. Hautier, A. Jain, C. Moore, S. Kim, X. Ma, G. Ceder, Voltage, stability and diffusion barrier differences between sodium-ion and lithium-ion intercalation materials, Energy Environ. Sci. 4 (2011) 3680–3688. doi:10.1039/c1ee01782a.
[60] B.B.V. Chowdary, S. Chandana, B. Chaitanya, First-Principles Study of Olivine-Type $NaMnPO_4$ As Positive Electrode Materials for Rechargeable Sodium Ion Batteries., Int. J. Adv. Res. 5 (2017) 1298–1303. doi:10.21474/ijar01/3637.
[61] R. Triphati, S.M. Wood, M.S. Islam, L.F.Nazar, Na-Ion Mobility in Layered Na_2FePO_4F and Olivine $Na[Fe,Mn]PO_4$, Energy Environ. Sci. 6 (2013) 2257-2264. doi: 10.1039/C3EE40914G.
[62] K.M. Bui, V.A. Dinh, S. Okada, T. Ohno, Hybrid functional study of the NASICON-type $Na_3V_2(PO_4)_3$: crystal and electronic structures, and polaron-Na vacancy complex diffusion, Phys. Chem. Chem. Phys. 17 (2015) 30433–30439. doi:10.1039/c5cp05323d.
[63] X. Pu, H. Wang, T. Yuan, S. Cao, S. Liu, L. Xu, H. Yang, X. Ai, Z. Chen, Y. Cao, $Na_4Fe_3(PO_4)_2(P_2O_7)$/C nanospheres as low-cost, high-performance cathode material for sodium-ion batteries, Energy Storage Mater. 22 (2019) 330–336. doi:10.1016/j.ensm.2019.02.017.
[64] Y. Cao, X. Xia, Y. Liu, N. Wang, J. Zhang, D. Zhao, Y. Xia, Scalable synthesizing nanospherical $Na_4Fe_3(PO_4)_2(P_2O_7)$ growing on MCNTs as a high-performance cathode material for sodium-ion batteries, J. Power Sources. 461 (2020) 228130. doi:10.1016/j.jpowsour.2020.228130.
[65] X. Deng, W. Shi, J. Sunarso, M. Liu, Z. Shao, A Green Route to a Na2FePO4F-Based Cathode for Sodium Ion Batteries of High Rate and Long Cycling Life, ACS Appl. Mater. Interfaces. 9 (2017) 16280–16287. doi:10.1021/acsami.7b03933.
[66] N. Böckenfeld, A. Balducci, Determination of sodium ion diffusion coefficients in sodium vanadium phosphate, J. Solid State Electrochem. 18 (2014) 959–964. doi:10.1007/s10008-013-2342-6.
[67] P.R. Kumar, R. Essehli, H.B. Yahia, R. Amin, I. Belharouak, Electrochemical studies of a high voltage $Na_4Co_3(PO_4)_2P_2O_7$-MWCNT composite through a selected stable electrolyte, RSC Adv. 10 (2020) 15983–15989. doi:10.1039/d0ra02349c.
[68] M. Nose, H. Nakayama, K. Nobuhara, H. Yamaguchi, S. Nakanishi, $Na_4Co_3(PO_4)_2P_2O_7$: A novel storage material for sodium-ion batteries, J. Power Sources 234 (2013) 175–179.

doi:10.1016/j.jpowsour.2013.01.162.
[69] M. Nose, S. Shiotani, H. Nakayama, K. Nobuhara, S. Nakanishi, H. Iba, $Na_4Co_{2.4}Mn_{0.3}Ni_{0.3}(PO_4)_2P_2O_7$: High potential and high capacity electrode material for sodium-ion batteries, Electrochem. Commun. 34 (2013) 266–269. doi:10.1016/j.elecom.2013.07.004.
[70] H. Moriwake, A. Kuwabara, C.A.J. Fisher, M. Nose, H. Nakayama, S. Nakanishi, H. Iba, Y. Ikuhara, Crystal and electronic structure changes during the charge-discharge process of $Na_4Co_3(PO_4)_2P_2O_7$, J. Power Sources. 326 (2016) 220–225. doi:10.1016/j.jpowsour.2016.07.006.
[71] H. Kim, I. Park, S. Lee, H. Kim, K.Y. Park, Y.U. Park, H. Kim, J. Kim, H.D. Lim, W.S. Yoon, K. Kang, Understanding the electrochemical mechanism of the new iron-based mixed-phosphate $Na_4Fe_3(PO_4)_2(P_2O_7)$ in a Na rechargeable battery, Chem. Mater. 25 (2013) 3614–3622. doi:10.1021/cm4013816.
[72] S.M. Oh, S.T. Myung, J. Hassoun, B. Scrosati, Y.K. Sun, Reversible $NaFePO_4$ electrode for sodium secondary batteries, Electrochem. Commun. 22 (2012) 149–152. doi:10.1016/j.elecom.2012.06.014.
[73] J. Kim, D.H. Seo, H. Kim, I. Park, J.K. Yoo, S.K. Jung, Y.U. Park, W.A. Goddard III, K. Kang, Unexpected discovery of low-cost maricite $NaFePO_4$ as a high-performance electrode for Na-ion batteries, Energy Environ. Sci. 8 (2015) 540–545. doi:10.1039/c4ee03215b.
[74] S. Li, J. Guo, Z. Ye, X. Zhao, S. Wu, J.X. Mi, C.Z. Wang, Z. Gong, M.J. McDonald, Z. Zhu, K.M. Ho, Y. Yang, A Zero-Strain Na_2FeSiO_4 as Novel Cathode Material for Sodium-Ion Batteries, ACS Appl. Mater. Interfaces. 8 (2016) 17233–17238. doi:10.1021/acsami.6b03969.
[75] K. Saravanan, C.W. Mason, A. Rudola, K.H. Wong, P. Balaya, The first report on excellent cycling stability and superior rate capability of $Na_3V_2(PO_4)_3$ for sodium ion batteries, Adv. Energy Mater. 3 (2013) 444–450. doi:10.1002/aenm.201200803.
[76] Y. Kawabe, N. Yabuuchi, M. Kajiyama, N. Fukuhara, T. Inamasu, R. Okuyama, I. Nakai, S. Komaba, Synthesis and electrode performance of carbon coated Na_2FePO_4F for rechargeable Na batteries, Electrochem. Commun. 13 (2011) 1225–1228. doi:10.1016/j.elecom.2011.08.038.
[77] H. Kim, G. Yoon, I. Park, K.Y. Park, B. Lee, J. Kim, Y.U. Park, S.K. Jung, H.D. Lim, D. Ahn, S. Lee, K. Kang, Anomalous Jahn-Teller behavior in a manganese-based mixed-phosphate cathode for sodium ion batteries, Energy Environ. Sci. 8 (2015) 3325–3335. doi:10.1039/c5ee01876e.
[78] V. Priyanka, G. Savithiri, R. Subadevi, M. Sivakumar, An emerging electrochemically active maricite $NaMnPO_4$ as cathode material at elevated temperature for sodium-ion batteries, Appl. Nanosci. 10 (2020) 3945–3951. doi:10.1007/s13204-020-01506-8.
[79] C.S. Park, H. Kim, R.A. Shakoor, E. Yang, S.Y. Lim, R. Kahraman, Y. Jung, J.W. Choi, Anomalous manganese activation of a pyrophosphate cathode in sodium ion batteries: A combined experimental and theoretical study, J. Am. Chem. Soc. 135 (2013) 2787–2792. doi:10.1021/ja312044k.
[80] X. Lin, X. Hou, X. Wu, S. Wang, M. Gao, Y. Yang, Exploiting Na_2MnPO_4F as a high-capacity and well-reversible cathode material for Na-ion batteries, RSC Adv. 4 (2014) 40985–40993. doi:10.1039/c4ra05336b.
[81] M. Law, V. Ramar, P. Balaya, Na_2MnSiO_4 as an attractive high capacity cathode material

for sodium-ion battery, J. Power Sources. 359 (2017) 277–284. doi:10.1016/j.jpowsour.2017.05.069.
[82] A. Gutierrez, S. Kim, T.T. Fister, C.S. Johnson, Microwave-Assisted Synthesis of $NaCoPO_4$ Red-Phase and Initial Characterization as High Voltage Cathode for Sodium-Ion Batteries, ACS Appl. Mater. Interfaces. 9 (2017) 4391–4396. doi:10.1021/acsami.6b14341.
[83] P. Barpanda, J. Lu, T. Ye, M. Kajiyama, S.C. Chung, N. Yabuuchi, S. Komaba, A. Yamada, A layer-structured $Na_2CoP_2O_7$ pyrophosphate cathode for sodium-ion batteries, RSC Adv. 3 (2013) 3857–3860. doi:10.1039/c3ra23026k.
[84] J.C. Treacher, S.M. Wood, M.S. Islam, E. Kendrick, Na_2CoSiO_4 as a cathode material for sodium-ion batteries: Structure, electrochemistry and diffusion pathways, Phys. Chem. Chem. Phys. 18 (2016) 32744–32752. doi:10.1039/c6cp06777h.
[85] K. Kubota, K. Yokoh, N. Yanuuchi, S. Komaba, Na_2CoPO_4F as a High-voltage Batteries, Na-ion batteries, Electrochemistry 82 (2014) 909–911. doi: 10.5796/electrochemistry.82.909
[86] S. Chakraborty, A. Banerjee, T. Watcharatharapong, R.B. Araujo, R. Ahuja, Current computational trends in polyanionic cathode materials for Li and Na batteries, J. Phys. Condens. Matter Top. 30 (2018) 283003. doi: 10.1088/1361-648X/aac62d
[87] T. Jin, H. Li, K. Zhu, P.F. Wang, P. Liu, L. Jiao, Polyanion-tipe cathode materials for sodium-ion batteries, Chem. Soc. Rev. 49 (2020) 2342-2377. doi:10.1039/C9CS00846B.
[88] J.Y. Sun, S.T. Myung, Y.K. Sun, Sodium-ion batteries: present and future, Chem. Soc. Rev. 46 (2017) 3529-3614. doi:10.1039/c6cs00776g.
[89] Y. Fang, L. Xiao, Z. Chen, X. Ai, Y. Cao, H. Yang, Recent Advances in Sodium – Ion Battery Materials, Electrochem. Energy Rev. 1 (2018) 294–323. doi:10.1007/s41918-018-0008-x.
[90] X. Pu, H. Wang, D. Zhao, H. Yang, X. Ai, S. Cao, Z. Chen, Y. Cao, Recent Progress in Rechargeable Sodium-Ion Batteries : toward High-Power Applications, Small. 15 (2019) 1805427. doi:10.1002/smll.201805427.
[91] D. Bin, F. Wang, A.G. Tamirat, L. Suo, Y. Wang, C. Wang, Y. Xia, Progress in Aqueous Rechargeable Sodium-Ion Batteries, Advaned Energy Mater. 8 (2018) 1703008. doi:10.1002/aenm.201703008.
[92] S. Guo, J. Li, Q. Xu, Z. Ma, H. Xue, Recent achievements on polyanion-type compounds for sodium-ion batteries : Syntheses , crystal chemistry and electrochemical performance, J. Power Sources. 361 (2017) 285–299. doi:10.1016/j.jpowsour.2017.07.002.
[93] Q. Ni, Y. Bai, F. Wu, C. Wu, Polyanion-Type Electrode Materials for Sodium-Ion Batteries, Adv. Sci. 4 (2017) 1600275. doi:10.1002/advs.201600275.
[94] R. Liu, Z. Liang, Z. Gong, Y. Yang, Research Progress in Multielectron Reactions in Polyanionic Materials for Sodium-Ion Batteries, Small. 3 (2018) 1800221 doi:10.1002/smtd.201800221.
[95] M. Zarrabeitia, M. Jáuregui, N. Sharma, J.C. Pramudita, M. Casas-Cabanas, $Na_4Co_3(PO_4)_2P_2O_7$ through Correlative Operando X-ray Diffraction and Electrochemical Impedance Spectroscopy, Chem. Mater. 31 (2019) 5152–5159. doi:10.1021/acs.chemmater.9b01054.
[96] H. Zhang, I. Hasa, D. Buchholz, B. Qin, D. Geiger, S. Jeong, U. Kaiser, S. Passerini, Exploring the Ni redox activity in polyanionic compounds as conceivable high potential cathodes for Na rechargeable batteries, NPG Asia Mater. 9 (2017) e370-8.

doi:10.1038/am.2017.41.
[97] N. V. Kosova, V.A. Belotserkovsky, Sodium and mixed sodium/lithium iron ortho-pyrophosphates: Synthesis, structure and electrochemical properties, Electrochim. Acta. 278 (2018) 182–195. doi:10.1016/j.electacta.2018.05.034.
[98] P.R. Kumar, H.B. Yahia, I. Belharouak, M.T. Sougrati, S. Passerini, R. Amin, R. Essehli, Electrochemical investigations of high-voltage $Na_4Ni_3(PO_4)_2P_2O_7$ cathode for sodium-ion batteries, J. Solid State Electrochem. 24 (2020) 17–24. doi:10.1007/s10008-019-04448-6.
[99] M. Chen, W. Hua, J. Xiao, D. Cortie, W. Chen, E. Wang, Z. Hu, Q. Gu, X. Wang, S. Indris, S.L. Chou, S.X. Dou, NASICON-type air-stable and all-climate cathode for sodium-ion batteries with low cost and high-power density, Nat. Commun. 10 (2019) 1–11. doi:10.1038/s41467-019-09170-5.
[100] L.N. Zhao, T. Zhang, H.L. Zhao, Y.L. Hou, Polyanion-type electrode materials for advanced sodium-ion batteries, Mater. Today Nano. 10 (2020) 100072. doi:10.1016/j.mtnano.2020.100072.
[101] R. Essehli, B. El Bali, S. Benmokhtar, H. Fuess, I. Svoboda, S. Obbade, Synthesis, crystal structure and infrared spectroscopy of a new non-centrosymmetric mixed-anion phosphate $Na_4Mg_3(PO_4)_2(P_2O_7)$, J. Alloys Compd. 493 (2010) 654–660. doi:10.1016/j.jallcom.2009.12.181.
[102] T. Yuan, Y. Wang, J. Zhang, X. Pu, X. Ai, Z. Chen, H. Yang, Y. Cao, 3D graphene decorated $Na_4Fe_3(PO_4)_2(P_2O_7)$ microspheres as low-cost and high-performance cathode materials for sodium-ion batteries, Nano Energy. 56 (2019) 160–168. doi:10.1016/j.nanoen.2018.11.011.
[103] N. V. Kosova, O.A. Podgornova, E.T. Devyatkina, V.R. Podugolnikov, S.A. Petrov, Effect of Fe^{2+} substitution on the structure and electrochemistry of $LiCoPO_4$ prepared by mechanochemically assisted carbothermal reduction, J. Mater. Chem. A. 2 (2014) 20697–20705. doi:10.1039/c4ta04221b.
[104] H. Zhou, S. Upreti, N.A. Chernova, G. Hautier, G. Ceder, M.S. Whittingham, Iron and manganese pyrophosphates as cathodes for lithium-ion batteries, Chem. Mater. 23 (2011) 293–300. doi:10.1021/cm102922q.
[105] N. V. Kosova, A.M. Tsapina, A.B. Slobodyuk, S.A. Petrov, Structure and electrochemical properties of mixed transition-metal pyrophosphates $Li_2Fe_{1-y}Mn_yP_2O_7$ ($0 \le y \le 1$), Electrochim. Acta. 174 (2015) 1278–1289. doi:10.1016/j.electacta.2015.06.070.
[106] B. Senthilkumar, G. Ananya, P. Ashok, S. Ramaprabhu, Synthesis of Carbon coated Nano-$Na_4Ni_3(PO_4)_2P_2O_7$ as a Novel Cathode Material for Hybrid Supercapacitors, Electrochim. Acta. 169 (2015) 447–455. doi:10.1016/j.electacta.2015.04.088.
[107] X. Ma, X. Wu, P. Shen, Rational Design of $Na_4Fe_3(PO_4)_2(P_2O_7)$ Nanoparticles Embedded in Graphene: Toward Fast Sodium Storage Through the Pseudocapacitive Effect, ACS Appl. Energy Mater. 1 (2018) 6268–6278. doi:10.1021/acsaem.8b01275.
[108] L. Tang, X. Liu, Z. Li, X. Pu, J. Zhang, Q. Xu, H. Liu, Y.G. Wang, Y. Xia, CNT-Decorated $Na_4Mn_2Co(PO_4)_2P_2O_7$ Microspheres as a Novel High-Voltage Cathode Material for Sodium-Ion Batteries, ACS Appl. Mater. Interfaces. 11 (2019) 27813–27822. doi:10.1021/acsami.9b07595.
[109] M. Nose, K. Nobuhara, S. Shiotani, H. Nakayama, S. Nakanishi, H. Iba, Electrochemical Li^+ insertion capabilities of $Na_{4-x}Co_3(PO_4)_2P_2O_7$ and its application to novel hybrid-ion batteries, RSC Adv. 4 (2014) 9044–9047. doi:10.1039/c3ra45836a.
[110] S. Nakanishi, M. Nose, H. Nakayama, H. Iba, Study of New Active Materials for

Rechargeable Sodium-Ion Batteries, Adv. Sci. Technol. 93 (2014) 137–145. doi:10.4028/www.scientific.net/ast.93.137.
[111] X. Liu, L. Tang, Z. Li, J. Zhang, Q. Xu, H. Liu, Y. Wang, Y. Xia, Y. Cao, X. Ai, An Al-doped high voltage cathode of $Na_4Co_3(PO_4)_2P_2O_7$ enabling highly stable 4 V full sodium-ion batteries, J. Mater. Chem. A. 7 (2019) 18940–18949. doi:10.1039/c9ta04450g.
[112] J.Y. Jang, H. Kim, Y. Lee, K.T. Lee, K. Kang, N.S. Choi, Cyclic carbonate based-electrolytes enhancing the electrochemical performance of $Na_4Fe_3(PO_4)_2(P_2O_7)$ cathodes for sodium-ion batteries, Electrochem. Commun. 44 (2014) 74–77. doi:10.1016/j.elecom.2014.05.003.
[113] N. V Kosova, A.A. Shindrov, Effect of Mixed Li^+/Na^+-ion Electrolyte on electrochemical perforamce of $Na_4Fe_3(PO_4)_2(P_2O_7)$ in hybrid batteries, Batteries 5 (2019) 39. doi: 10.3390/batteries5020039.
[114] A.J. Fernández-Ropero, M. Zarrabeitia, M. Reynaud, T. Rojo, M. Casas-Cabanas, Toward Safe and Sustainable Batteries: $Na_4Fe_3(PO_4)_2(P_2O_7)$ as a Low-Cost Cathode for Rechargeable Aqueous Na-Ion Batteries, J. Phys. Chem. C. 122 (2018) 133–142. doi:10.1021/acs.jpcc.7b09803.
[115] M.H. Lee, S.J. Kim, D. Chang, J. Kim, S. Moon, K. Oh, K.Y. Park, W.M. Seong, H. Park, G. Kwon, B. Lee, K. Kang, Toward a low-cost high-voltage sodium aqueous rechargeable battery, Mater. Today. 29 (2019) 26–36. doi:10.1016/j.mattod.2019.02.004.
[116] S. Baskar, R. Angalakuthi, C. Murugesan, S.B. Krupanidhi, P. Barpanda, Exploration of Iron-Based Mixed Polyanion Cathode Material for Thin-Film Sodium-Ion Batteries, ECS Trans. 85 (2018) 227–234. doi:10.1149/08513.0227ecst.
[117] B. Senthilkumar, A. Rambabu, C. Murugesan, S.B. Krupanidhi, P. Barpanda, Iron-Based Mixed Phosphate $Na_4Fe_3(PO_4)_2(P_2O_7)$ Thin Films for Sodium-Ion Microbatteries, ACS Omega. 5 (2020) 7219–7224. doi:10.1021/acsomega.9b03835.
[118] K. Sada, C. Murugesan, S. Baskar, P. Barpanda, Potassium Intercalation into Sodium Metal Oxide and Polyanionic Hosts: Few Case Studies, ECS Trans. 85 (2018) 207–214. 10.1149/08513.0207ecst.
[119] X. Ma, Z. Pan, X. Wu, P.K.Shen, $Na_4Fe_3(PO_4)_2(P_2O_7)$@$NaFePO_4$@C core-double-shell architectures on carbon cloth: A high-rate, ultrastable, and flexible cathode for sodium ion batteries, Chem. Eng. J. 365 (2019) 132–141. doi:10.1016/j.cej.2019.01.173.
[120] F. Sanz, C. Parada, J.M. Rojo, C. Ruiz-Valero, Crystal structure, magnetic properties, and ionic conductivity of a new mixed-anion phosphate $Na_4Ni_5(PO_4)_2(P_2O_7)_2$, Chem. Mater. 11 (1999) 2673–2679. doi:10.1021/cm981105s.
[121] S. Ryu, J.E. Wang, J.H. Kim, R. Ruffo, Y.H. Jung, D.K. Kim, A study on cobalt substitution in sodium manganese mixed-anion phosphates as positive electrode materials for Na-ion batteries, J. Power Sources. 444 (2019) 227274. doi:10.1016/j.jpowsour.2019.227274.
[122] F. Zou, A. Manthiram, A Review of the Design of Advanced Binders for High-Performance Batteries, Adv. Energy Mater. 10 (2020) 1–28. doi:10.1002/aenm.202002508.
[123] D. Bresser, D. Buchholz, A. Moretti, A. Varzi, S. Passerini, Alternative binders for sustainable electrochemical energy storage-the transition to aqueous electrode processing and bio-derived polymers, Energy Environ. Sci. 11 (2018) 3096–3127. doi:10.1039/c8ee00640g.
[124] I. Kovalenko, B. Zdyrko, A. Magasinski, B. Hertzberg, Z. Milicev, R. Burtovyy, I.

Luzinov, G. Yushin, A major constituent of brown algae for use in high-capacity Li-ion batteries, Science 334 (2011) 75–79. doi:10.1126/science.1209150.
[125] P.R. Kumar, Y.H. Jung, S.A. Ahad, D.K. Kim, A high rate and stable electrode consisting of a $Na_3V_2O_{2X}(PO_4)_2F_{3-2X}$-rGO composite with a cellulose binder for sodium-ion batteries, RSC Adv. 7 (2017) 21820–21826. doi:10.1039/c7ra01047h.
[126] J. Zhao, X. Yang, Y. Yao, Y. Gao, Y. Sui, B. Zou, H. Ehrenberg, G. Chen, F. Du, Moving to Aqueous Binder: A Valid Approach to Achieving High-Rate Capability and Long-Term Durability for Sodium-Ion Battery, Adv. Sci. 5 (2018) 1700768. doi:10.1002/advs.201700768.
[127] T. Jin, Q. Han, L. Jiao, Binder-Free Electrodes for Advanced Sodium-Ion Batteries, Adv. Mater. 32 (2020) 1806304. doi:10.1002/adma.201806304.
[128] H. Li, M. Xu, Z. Zhang, Y. Lai, J. Ma, Engineering of Polyanion Type Cathode Materials for Sodium-Ion Batteries: Toward Higher Energy/Power Density, Adv. Funct. Mater. 30 (2020) 2000473. doi:10.1002/adfm.202000473.
[129] T. Jin, Y. Liu, Y. Li, K. Cao, X. Wang, L. Jiao, Electrospun NaVPO4F/C Nanofibers as Self-Standing Cathode Material for Ultralong Cycle Life Na-Ion Batteries, Adv. Energy Mater. 7 (2017) 1700087. doi:10.1002/aenm.201700087.
[130] Q. Ni, Y. Bai, Y. Li, L. Ling, L. Li, G. Chen, Z. Wang, H. Ren, F. Wu, C. Wu, 3D Electronic Channels Wrapped Large-Sized $Na_3V_{2(}PO_4)_3$ as Flexible Electrode for Sodium-Ion Batteries, Small. 14 (2018) 1702864. doi:10.1002/smll.201702864.
[131] K. Kretschmer, B. Sun, J. Zhang, X. Xie, H. Liu, G. Wang, 3D Interconnected Carbon Fiber Network-Enabled Ultralong Life $Na_3V_2(PO_4)_3$@Carbon Paper Cathode for Sodium-Ion Batteries, Small. 13 (2017) 1603318. doi:10.1002/smll.201603318.
[132] D. Guo, J. Qin, Z. Yin, J. Bai, Y.K. Sun, M. Cao, Achieving high mass loading of $Na_3V_2(PO_4)_3$@carbon on carbon cloth by constructing three-dimensional network between carbon fibers for ultralong cycle-life and ultrahigh rate sodium-ion batteries, Nano Energy. 45 (2018) 136–147. doi:10.1016/j.nanoen.2017.12.038.
[133] H.J. Song, D.S. Kim, J.C. Kim, S.H. Hong, D.W. Kim, An approach to flexible Na-ion batteries with exceptional rate capability and long lifespan using $Na_2FeP_2O_7$ nanoparticles on porous carbon cloth, J. Mater. Chem. A. 5 (2017) 5502–5510. doi:10.1039/c7ta00727b.
[134] D. Chao, C.H.M. Lai, P. Liang, Q. Wei, Y.S. Wang, C.R. Zhu, G. Deng, V.V.T. Doan-Nguyen, J. Lin, L. Mai, H.J. Fan, B. Dunn, Z.X. Shen, Sodium Vanadium Fluorophosphates (NVOPF) Array Cathode Designed for High-Rate Full Sodium Ion Storage Device, Adv. Energy Mater. 8 (2018) 1–8. doi:10.1002/aenm.201800058.
[135] K. Pfeifer, S. Arnold, J. Becherer, C. Das, J. Maibach, H. Ehrenberg, S. Dsoke, Can Metallic Sodium Electrodes Affect the Electrochemistry of Sodium-Ion Batteries? Reactivity Issues and Perspectives, ChemSusChem. 12 (2019) 3312–3319. doi:10.1002/cssc.201901056.
[136] S. Komaba, T. Ishikawa, N. Yabuuchi, W. Murata, A. Ito, Y. Ohsawa, Fluorinated ethylene carbonate as electrolyte additive for rechargeable Na batteries, ACS Appl. Mater. Interfaces. 3 (2011) 4165–4168. doi:10.1021/am200973k.
[137] S. Komaba, W. Murata, T. Ishikawa, N. Yabuuchi, T. Ozeki, T. Nakayama, A. Ogata, K. Gotoh, K. Fujiwara, Electrochemical Na insertion and solid electrolyte interphase for hard-carbon electrodes and application to Na-ion batteries, Adv. Funct. Mater. 21 (2011) 3859–3867. doi:10.1002/adfm.201100854.
[138] L. Wu, D. Buchholz, D. Bresser, L. Gomes Chagas, S. Passerini, Anatase TiO2

nanoparticles for high power sodium-ion anodes, J. Power Sources. 251 (2014) 379–385. doi:10.1016/j.jpowsour.2013.11.083.
[139] M. Dahbi, T. Nakano, N. Yabuuchi, T. Ishikawa, K. Kubota, M. Fukunishi, S. Shibahara, J.Y. Son, Y.T. Cui, H. Oji, S. Komaba, Sodium carboxymethyl cellulose as a potential binder for hard-carbon negative electrodes in sodium-ion batteries, Electrochem. Commun. 44 (2014) 66–69. doi:10.1016/j.elecom.2014.04.014.
[140] J. Lee, Y. Lee, J. Lee, S.M. Lee, J.H. Choi, H. Kim, M.S. Kwon, K. Kang, K.T. Lee, N.S. Choi, Ultraconcentrated sodium Bis(fluorosulfonyl)imide-based electrolytes for High-Performance Sodium metal batteries, ACS Appl. Mater. Interfaces. 9 (2017) 3723–3732. doi:10.1021/acsami.6b14878.
[141] Y. Lee, J. Lee, H. Kim, K. Kang, N.S. Choi, Highly stable linear carbonate-containing electrolytes with fluoroethylene carbonate for high-performance cathodes in sodium-ion batteries, J. Power Sources. 320 (2016) 49–58. doi:10.1016/j.jpowsour.2016.04.070.
[142] V. Dall'Asta, D. Buchholz, L.G. Chagas, X. Dou, C. Ferrara, E. Quartarone, C. Tealdi, S. Passerini, Aqueous Processing of Na0.44MnO2 Cathode Material for the Development of Greener Na-Ion Batteries, ACS Appl. Mater. Interfaces. 9 (2017) 34891–34899. doi:10.1021/acsami.7b09464.
[143] C. Yang, J. Chen, T. Qing, X. Fan, W. Sun, A. von Cresce, M.S. Ding, O. Borodin, J. Vatamanu, M.A. Schroeder, N. Eidson, C. Wang, K. Xu, 4.0 V Aqueous Li-Ion Batteries, Joule. 1 (2017) 122–132. doi:10.1016/j.joule.2017.08.009.
[144] Y. Wang, S. Song, C. Xu, N. Hu, J. Molenda, L. Lu, Development of solid-state electrolytes for sodium-ion battery–A short review, Nano Mater. Sci. 1 (2019) 91–100. doi:10.1016/j.nanoms.2019.02.007.
[145] Y. Noguchi, E. Kobayashi, L.S. Plashnitsa, S. Okada, J.I. Yamaki, Fabrication and performances of all solid-state symmetric sodium battery based on NASICON-related compounds, Electrochim. Acta. 101 (2013) 59–65. doi:10.1016/j.electacta.2012.11.038.
[146] F. Lalère, J.B. Leriche, M. Courty, S. Boulineau, V. Viallet, C. Masquelier, V. Seznec, An all-solid state NASICON sodium battery operating at 200°C, J. Power Sources. 247 (2014) 975–980. doi:10.1016/j.jpowsour.2013.09.051.
[147] W. Zhou, Y. Li, S. Xin, J.B. Goodenough, Rechargeable Sodium All-Solid-State Battery, ACS Cent. Sci. 3 (2017) 52–57. doi:10.1021/acscentsci.6b00321.
[148] R. Asakura, D. Reber, L. Duchêne, S. Payandeh, A. Remhof, H. Hagemann, C. Battaglia, 4 V Room-Temperature All-Solid-State Sodium Battery Enabled By a Passivating Cathode/Hydroborate Solid Electrolyte Interface, Energy Environ. Sci. 13 (2020) 5048–5058. doi:10.1039/d0ee01569e.
[149] L. Qiao, X. Judez, T. Rojo, M. Armand, H. Zhang, Review—Polymer Electrolytes for Sodium Batteries, J. Electrochem. Soc. 167 (2020) 070534. doi:10.1149/1945-7111/ab7aa0.
[150] C. Zhao, L. Liu, Y. Lu, M. Wagemaker, L. Chen, Y.S. Hu, Revealing an Interconnected Interfacial Layer in Solid-State Polymer Sodium Batteries, Angew. Chemie - Int. Ed. 58 (2019) 17026–17032. doi:10.1002/anie.201909877.
[151] J.K. Kim, Y.J. Lim, H. Kim, G.B. Cho, Y. Kim, A hybrid solid electrolyte for flexible solid-state sodium batteries, Energy Environ. Sci. 8 (2015) 3589–3596. doi:10.1039/c5ee01941a.
[152] A. Langrock, Y. Xu, Y. Liu, S. Ehrman, A. Manivannan, C. Wang, Carbon coated hollow Na_2FePO_4F spheres for Na-ion battery cathodes, J. Power Sources. 223 (2013) 62–67.

doi:10.1016/j.jpowsour.2012.09.059.
[153] L. Wu, Y. Hu, X. Zhang, J. Liu, X. Zhu, S. Zhong, Synthesis of carbon-coated Na_2MnPO_4F hollow spheres as a potential cathode material for Na-ion batteries, J. Power Sources. 374 (2018) 40–47. doi:10.1016/j.jpowsour.2017.11.029.
[154] J. Mao, C. Luo, T. Gao, X. Fan, C. Wang, Scalable synthesis of $Na_3V_2(PO_4)_3$/C porous hollow spheres as a cathode for Na-ion batteries, J. Mater. Chem. A. 3 (2015) 10378–10385. doi:10.1039/c5ta01007a.
[155] Y. Fang, L. Xiao, X. Ai, Y. Cao, H. Yang, Hierarchical Carbon Framework Wrapped Na3V2(PO4)3 as a Superior High-Rate and Extended Lifespan Cathode for Sodium-Ion Batteries, Adv. Mater. 27 (2015) 5895–5900. doi:10.1002/adma.201502018.
[156] Y. Liu, N. Zhang, F. Wang, X. Liu, L. Jiao, L.Z. Fan, Approaching the Downsizing Limit of Maricite $NaFePO_4$ toward High-Performance Cathode for Sodium-Ion Batteries, Adv. Funct. Mater. 28 (2018) 1–9. doi:10.1002/adfm.201801917.
[157] J.Z. Guo, P.F. Wang, X.L. Wu, X.H. Zhang, Q. Yan, H. Chen, J.P. Zhang, Y.G. Guo, High-Energy/Power and Low-Temperature Cathode for Sodium-Ion Batteries: In Situ XRD Study and Superior Full-Cell Performance, Adv. Mater. 29 (2017) 1–8. doi:10.1002/adma.201701968.
[158] T. Broux, F. Fauth, N. Hall, Y. Chatillon, M. Bianchini, T. Bamine, J.B. Leriche, E. Suard, D. Carlier, Y. Reynier, L. Simonin, C. Masquelier, L. Croguennec, High Rate Performance for Carbon-Coated $Na_3V_2(PO_4)_2F_3$ in Na-Ion Batteries, Small Methods. 3 (2019) 1–12. doi:10.1002/smtd.201800215.
[159] G. Yan, S. Mariyappan, G. Rousse, Q. Jacquet, M. Deschamps, R. David, B. Mirvaux, J.W. Freeland, J.M. Tarascon, Higher energy and safer sodium ion batteries via an electrochemically made disordered $Na_3V_2(PO_4)_2F_3$ material, Nat. Commun. 10 (2019). doi:10.1038/s41467-019-08359-y.
[160] B. Ali, A. ur-Rehman, F. Ghafoor, M.I. Shahzad, S.K. Shah, S.M. Abbas, Interconnected mesoporous Na_2FeSiO_4 nanospheres supported on carbon nanotubes as a highly stable and efficient cathode material for sodium-ion battery, J. Power Sources. 396 (2018) 467–475. doi:10.1016/j.jpowsour.2018.06.049.
[161] F. Li, Z. Zhou, Micro/Nanostructured Materials for Sodium Ion Batteries and Capacitors, Small. 14 (2018) 1–25. doi:10.1002/smll.201702961.
[162] H. Li, L. Peng, Y. Zhu, D. Chen, X. Zhang, G. Yu, An advanced high-energy sodium ion full battery based on nanostructured $Na_2Ti_3O_7$/$VOPO_4$ layered materials, Energy Environ. Sci. 9 (2016) 3399–3405. doi:10.1039/c6ee00794e.
[163] N. Wang, Z. Bai, Y. Qian, J. Yang, Double-Walled Sb@TiO2-xNanotubes as a Superior High-Rate and Ultralong-Lifespan Anode Material for Na-Ion and Li-Ion Batteries, Adv. Mater. 28 (2016) 4126–4133. doi:10.1002/adma.201505918.
[164] W. Ren, X. Yao, C. Niu, Z. Zheng, K. Zhao, Q. An, Q. Wei, M. Yan, L. Zhang, L. Mai, Cathodic polarization suppressed sodium-ion full cell with a 3.3 V high-voltage, Nano Energy. 28 (2016) 216–223. doi:10.1016/j.nanoen.2016.08.010.
[165] X. Liang, X. Ou, F. Zheng, Q. Pan, X. Xiong, R. Hu, C. Yang, M. Liu, Surface Modification of $Na_3V_2(PO_4)_3$ by Nitrogen and Sulfur Dual-Doped Carbon Layer with Advanced Sodium Storage Property, ACS Appl. Mater. Interfaces. 9 (2017) 13151–13162. doi:10.1021/acsami.7b00818.
[166] B. Zhang, R. Dugas, G. Rousse, P. Rozier, A.M. Abakumov, J.M. Tarascon, Insertion compounds and composites made by ball milling for advanced sodium-ion batteries, Nat.

Commun. 7 (2016) 1–9. doi:10.1038/ncomms10308.
[167] R. Thangavel, K. Kaliyappan, K. Kang, X. Sun, Y.S. Lee, Going beyond Lithium Hybrid Capacitors: Proposing a New High-Performing Sodium Hybrid Capacitor System for Next-Generation Hybrid Vehicles Made with Bio-Inspired Activated Carbon, Adv. Energy Mater. 6 (2016) 1–9. doi:10.1002/aenm.201502199.
[168] R. Thangavel, B. Moorthy, D.K. Kim, Y.S. Lee, Pushing the Energy Output and Cyclability of Sodium Hybrid Capacitors at High Power to New Limits, Adv. Energy Mater. 7 (2017) 1-10 doi:10.1002/aenm.201602654.

Figure 1

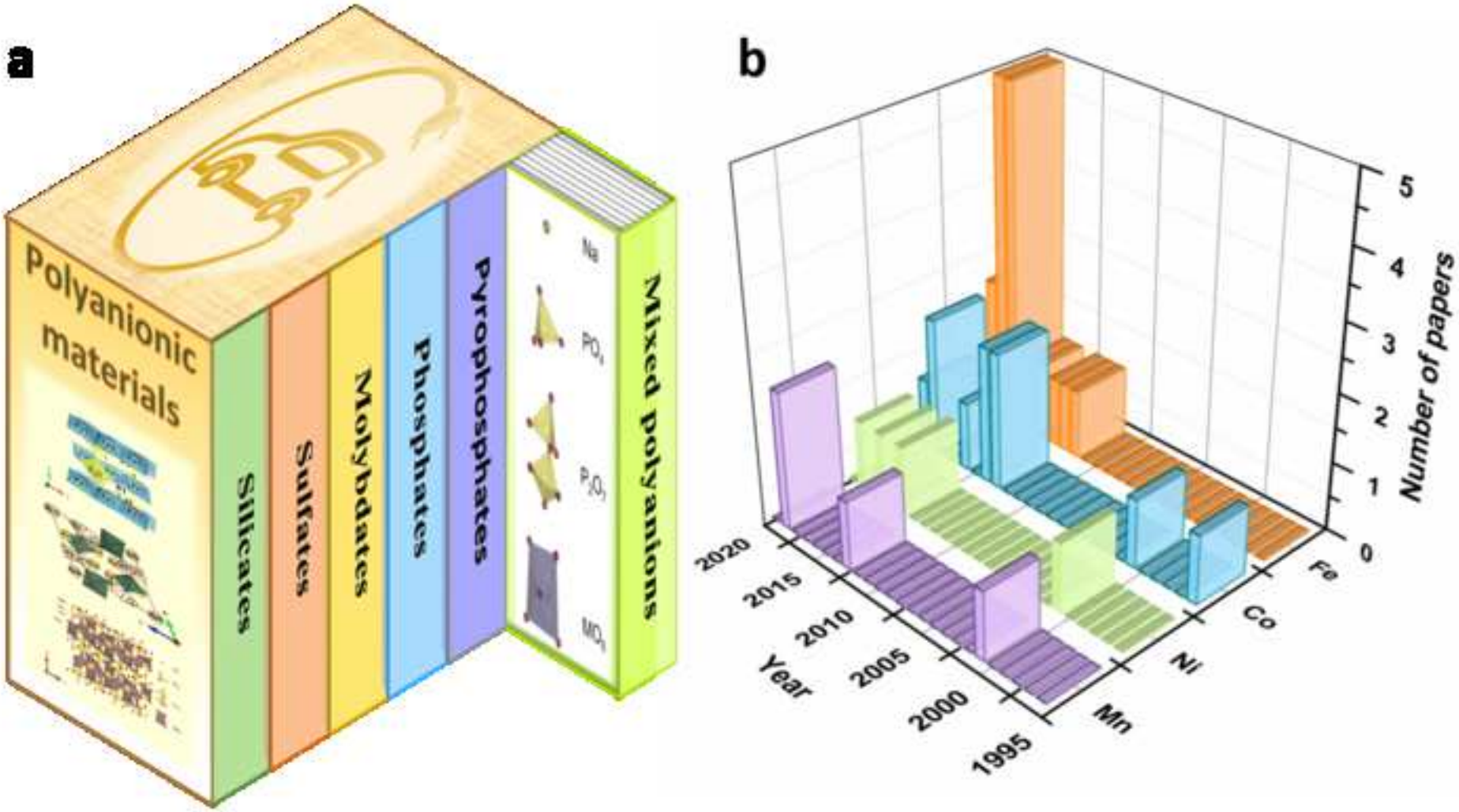

Figure 2

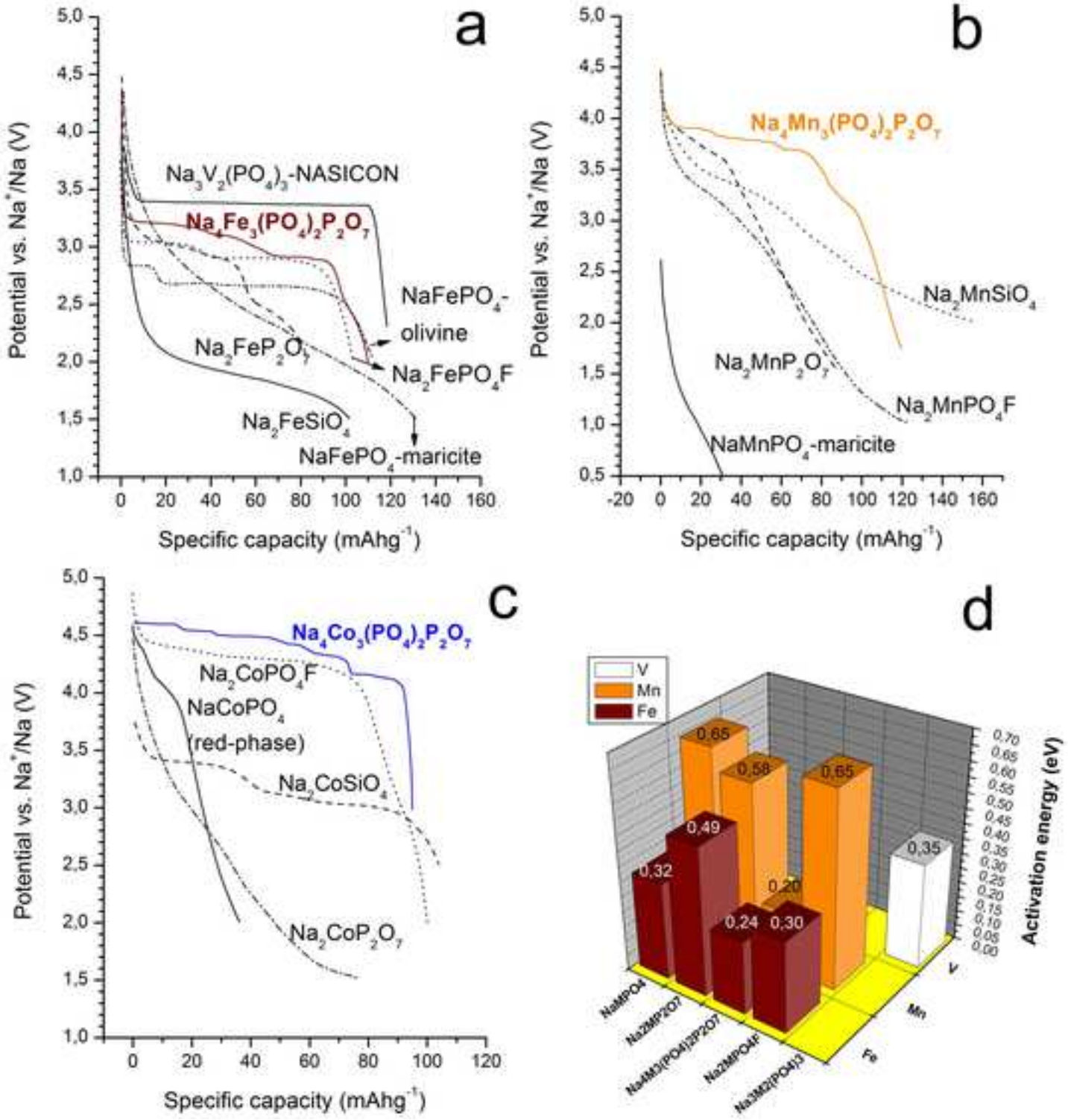

Figure 3

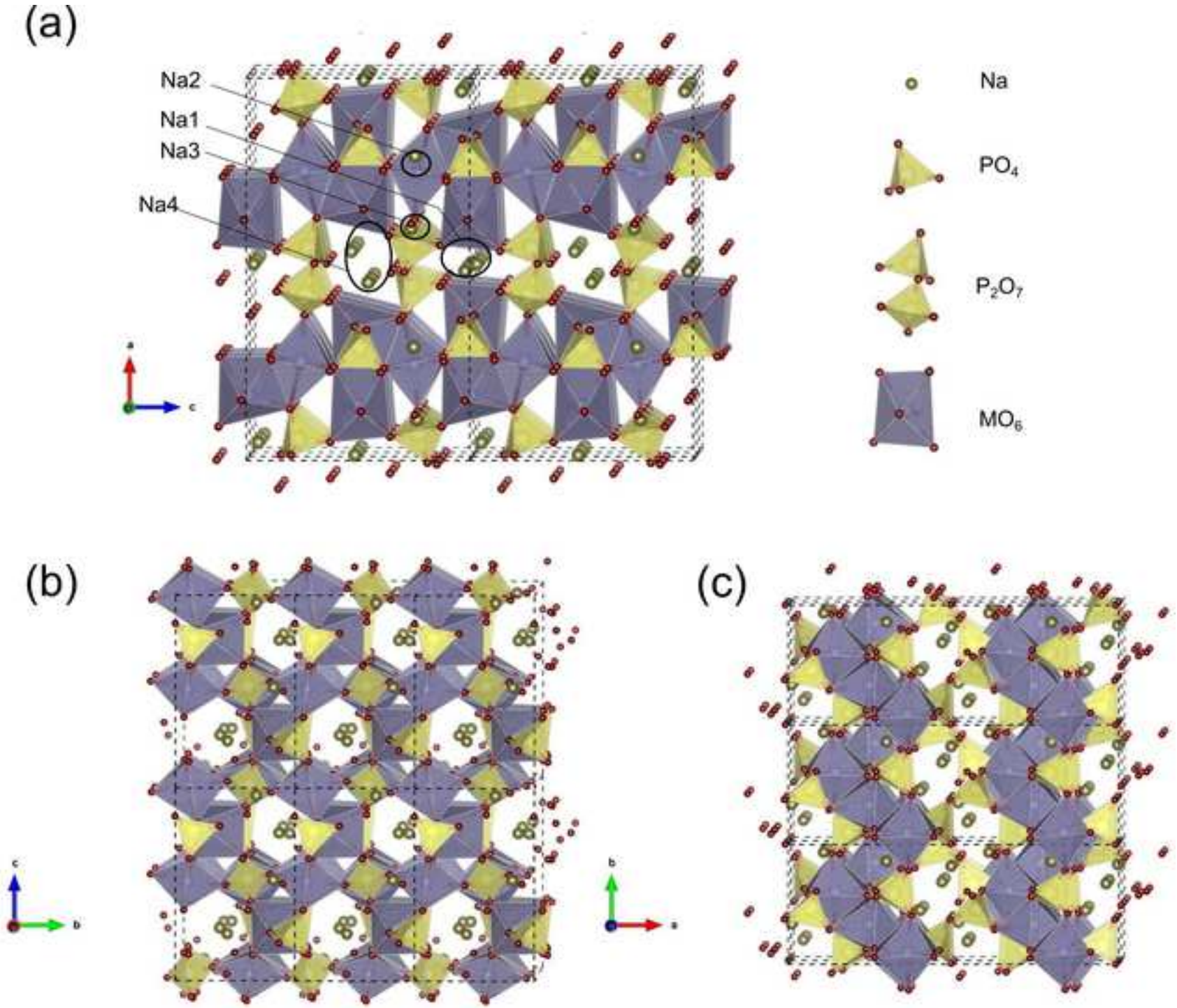

Figure 4

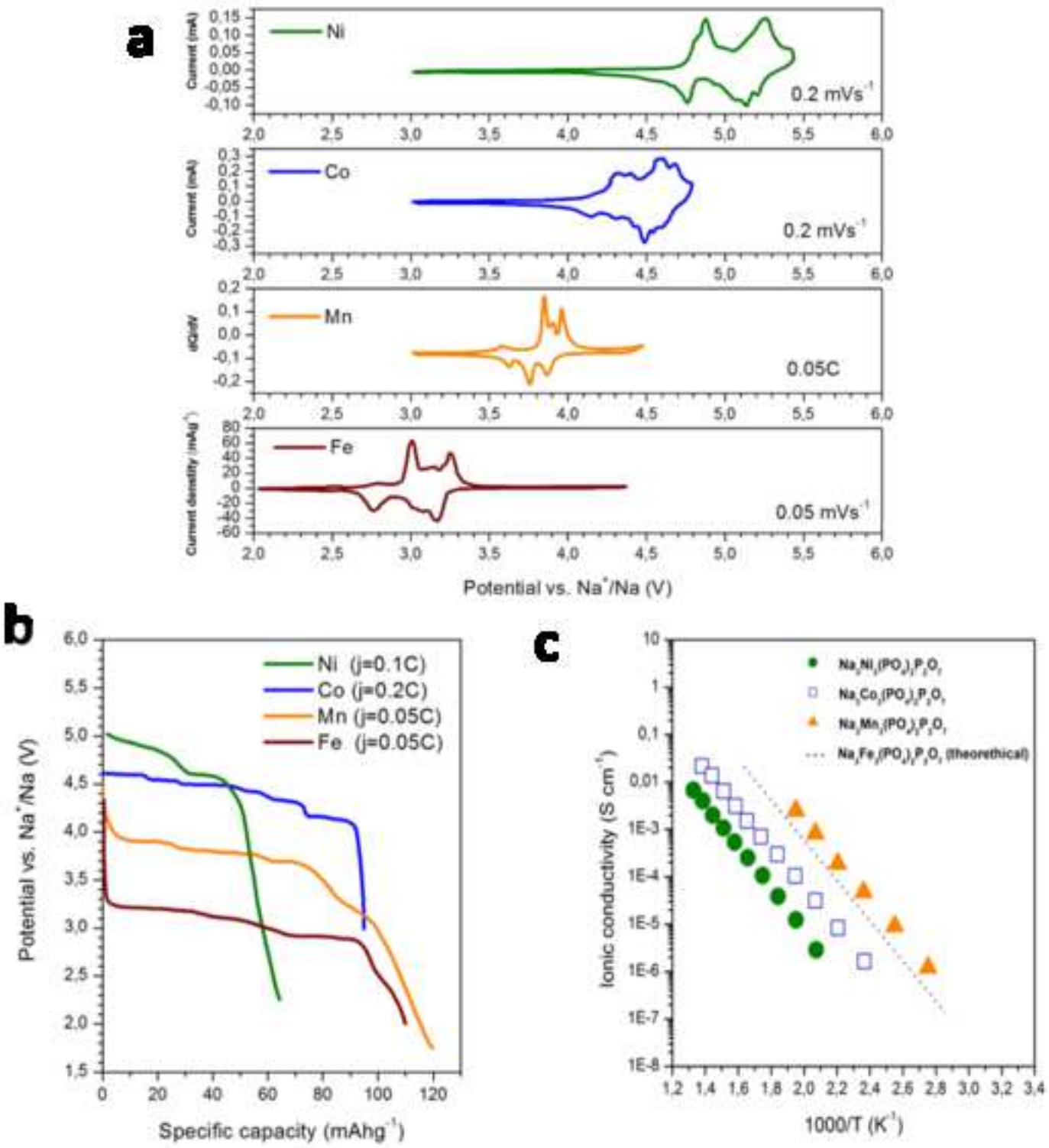

Figure 5

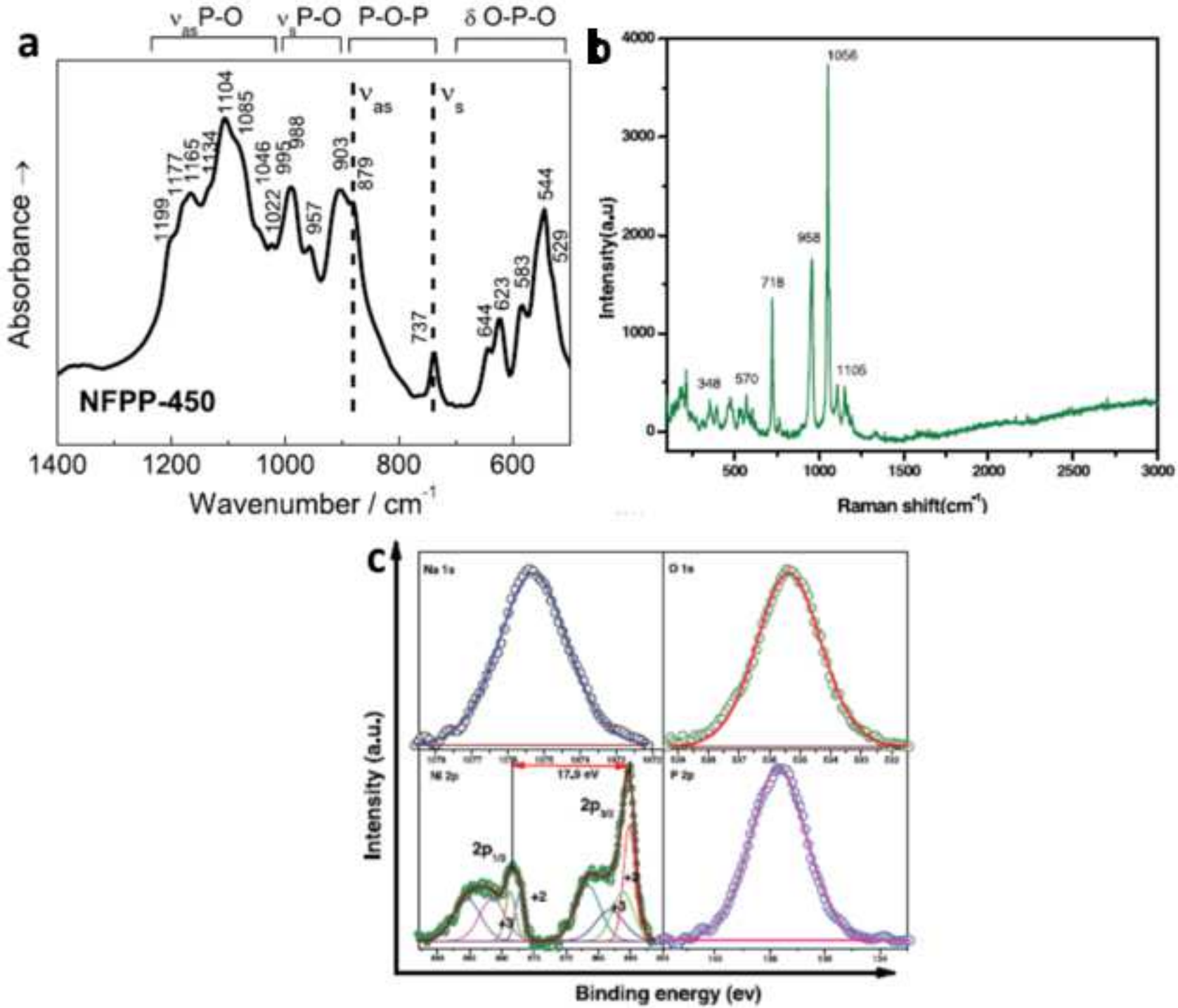

Figure 6

Click here to access/download;Figure;Fig.6..tif

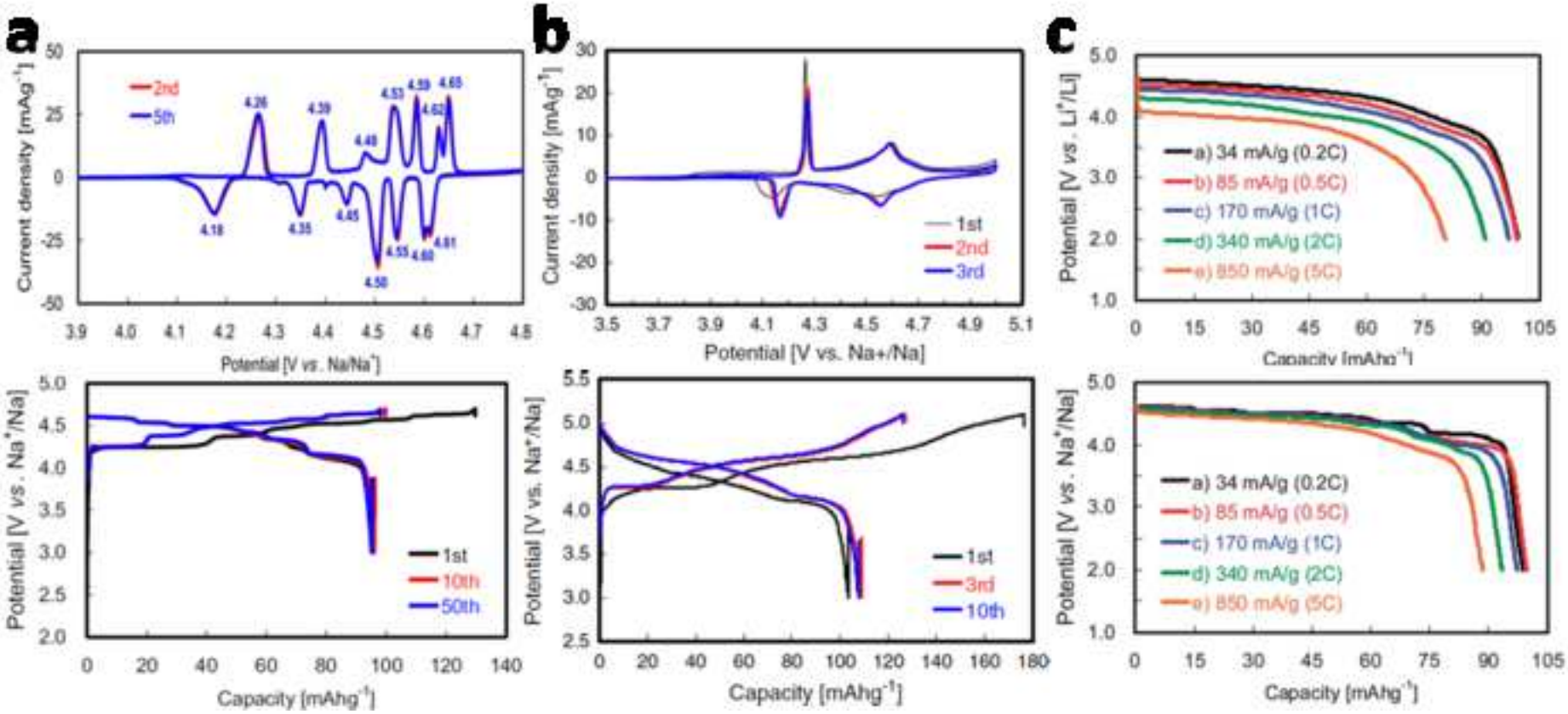

Figure 7

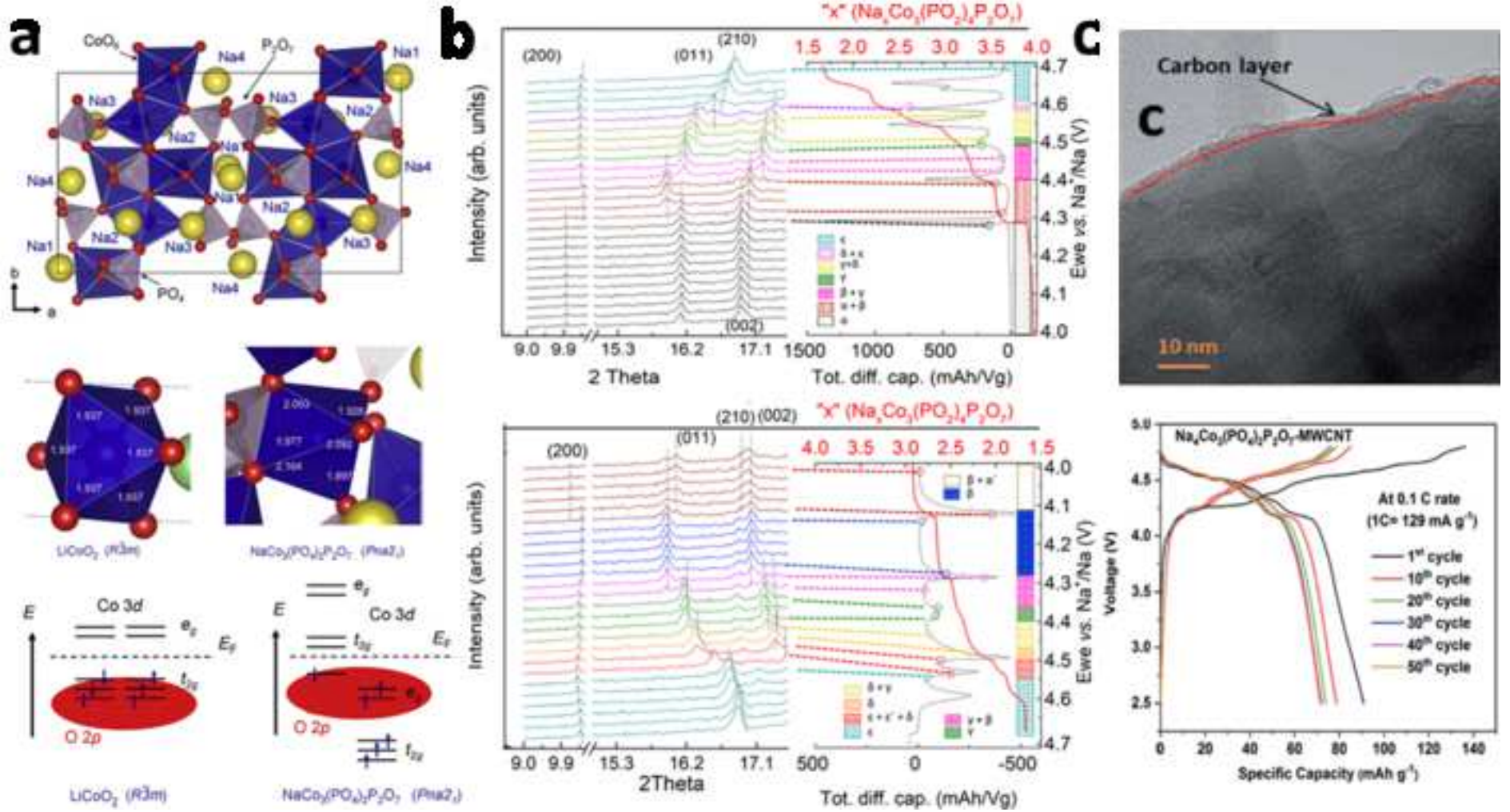

Figure 8

Click here to access/download;Figure;Fig.8..tif

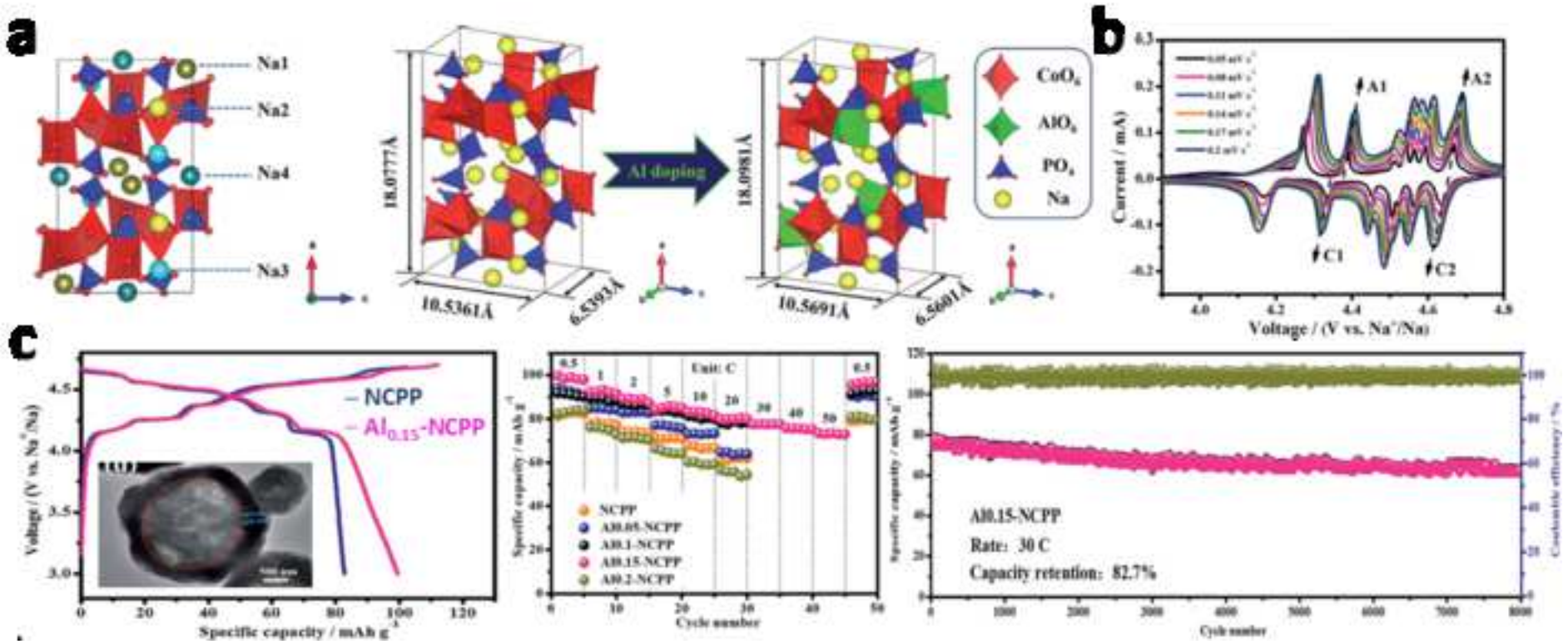

Figure 9

Click here to access/download;Figure;Fig.9..tif

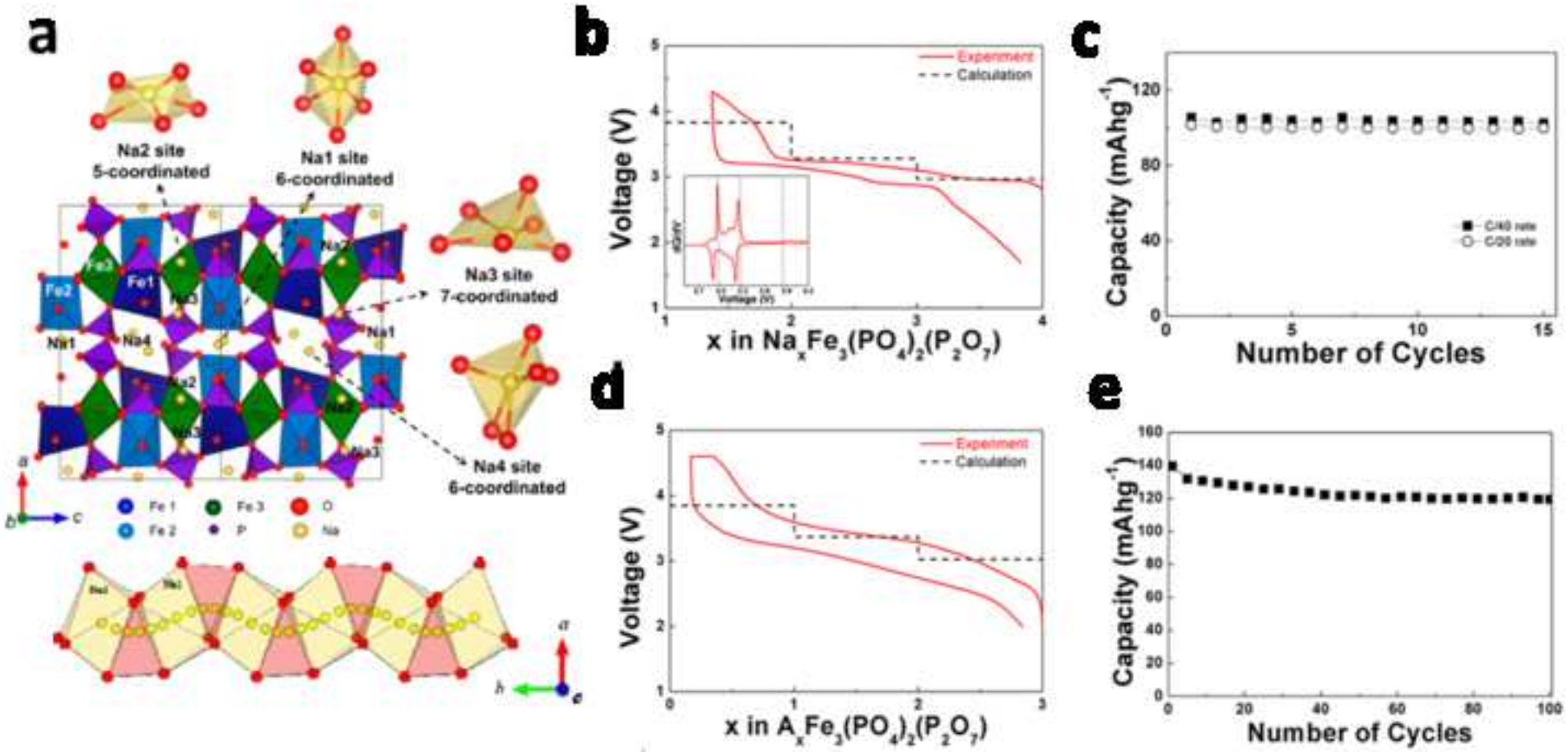

Figure 10

Click here to access/download;Figure;Fig.10..tif

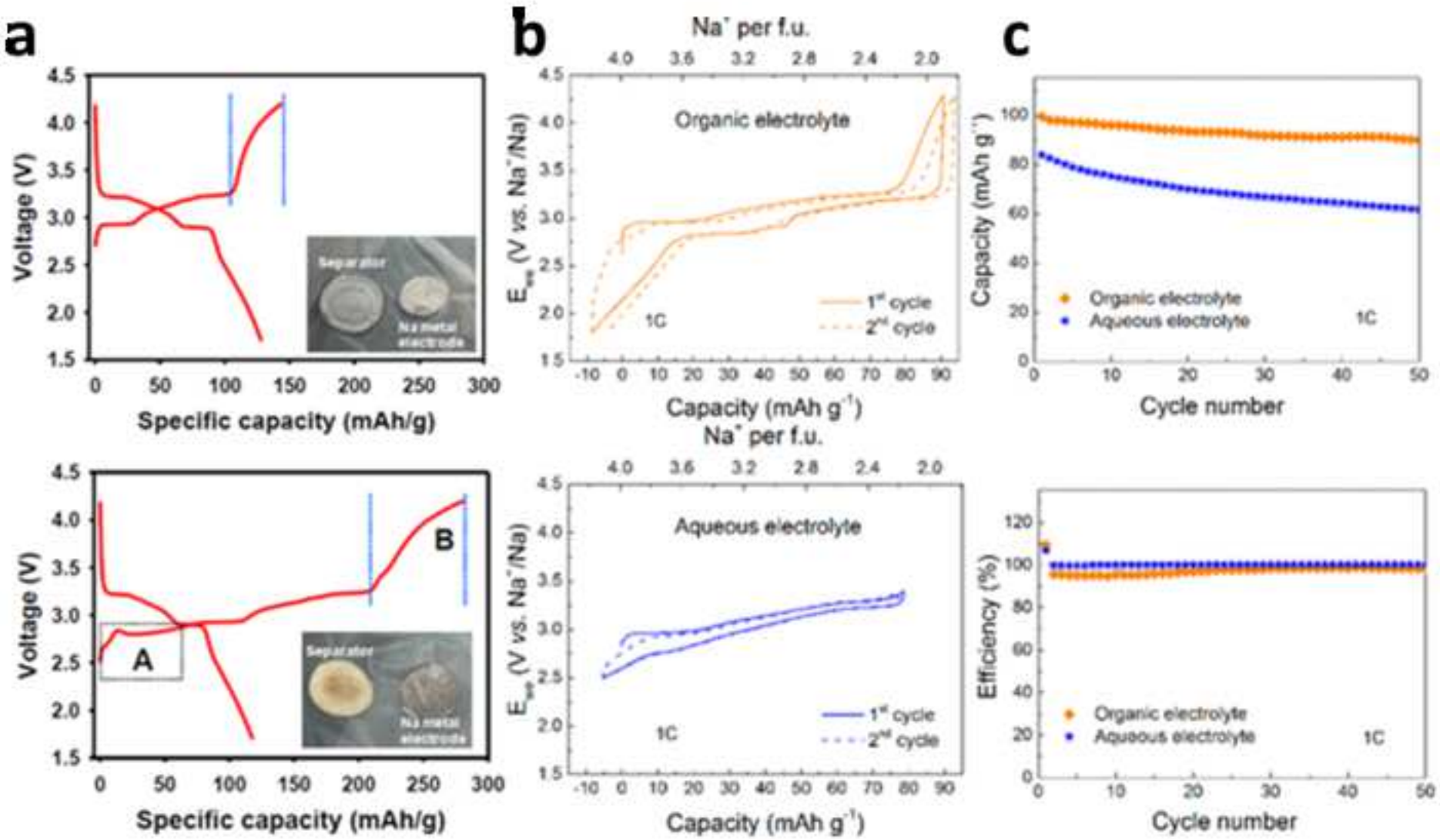

Figure 11

Click here to access/download;Figure;Fig.11..tif

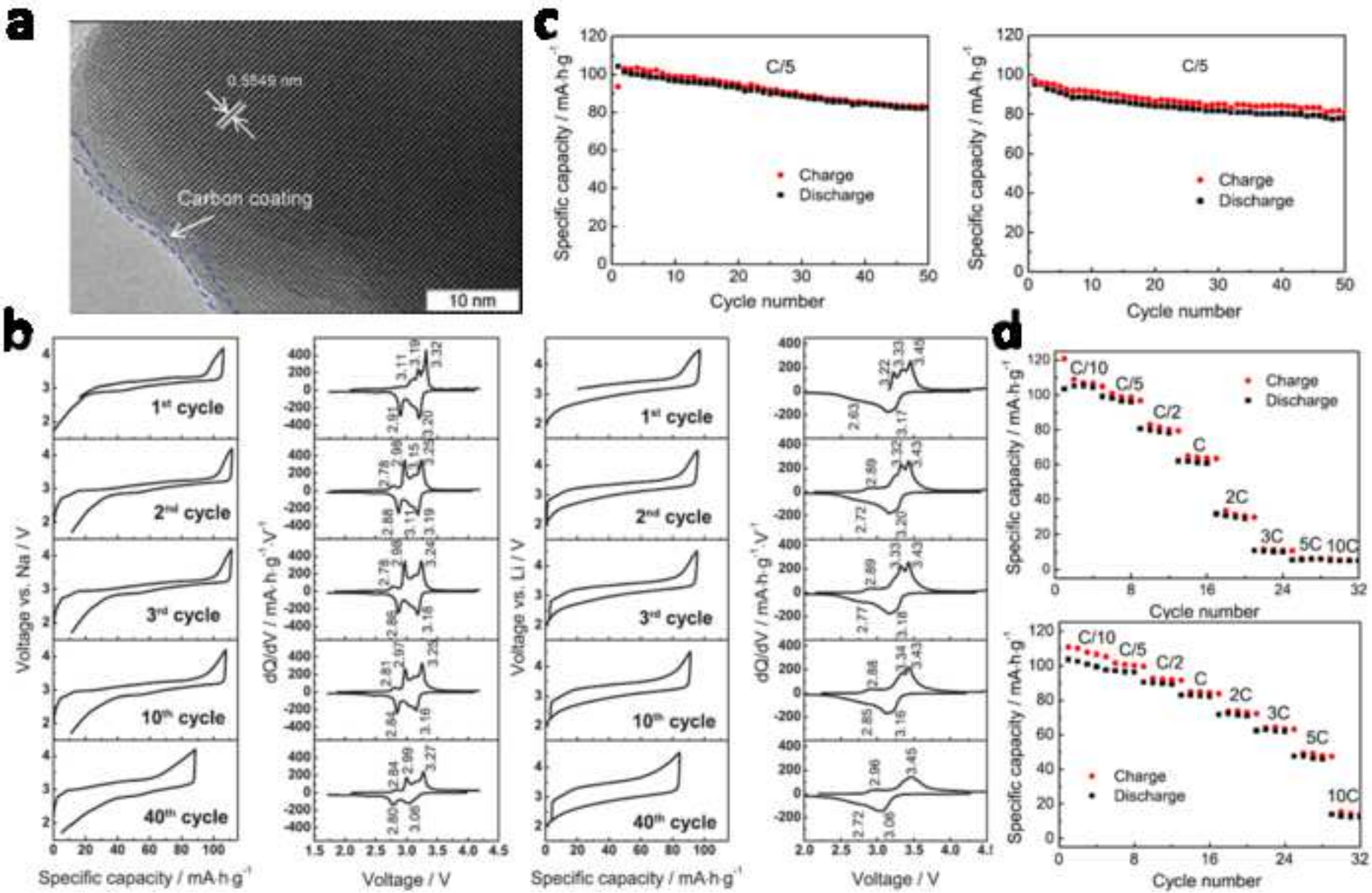

Figure 12

Click here to access/download;Figure;Fig.12..tif

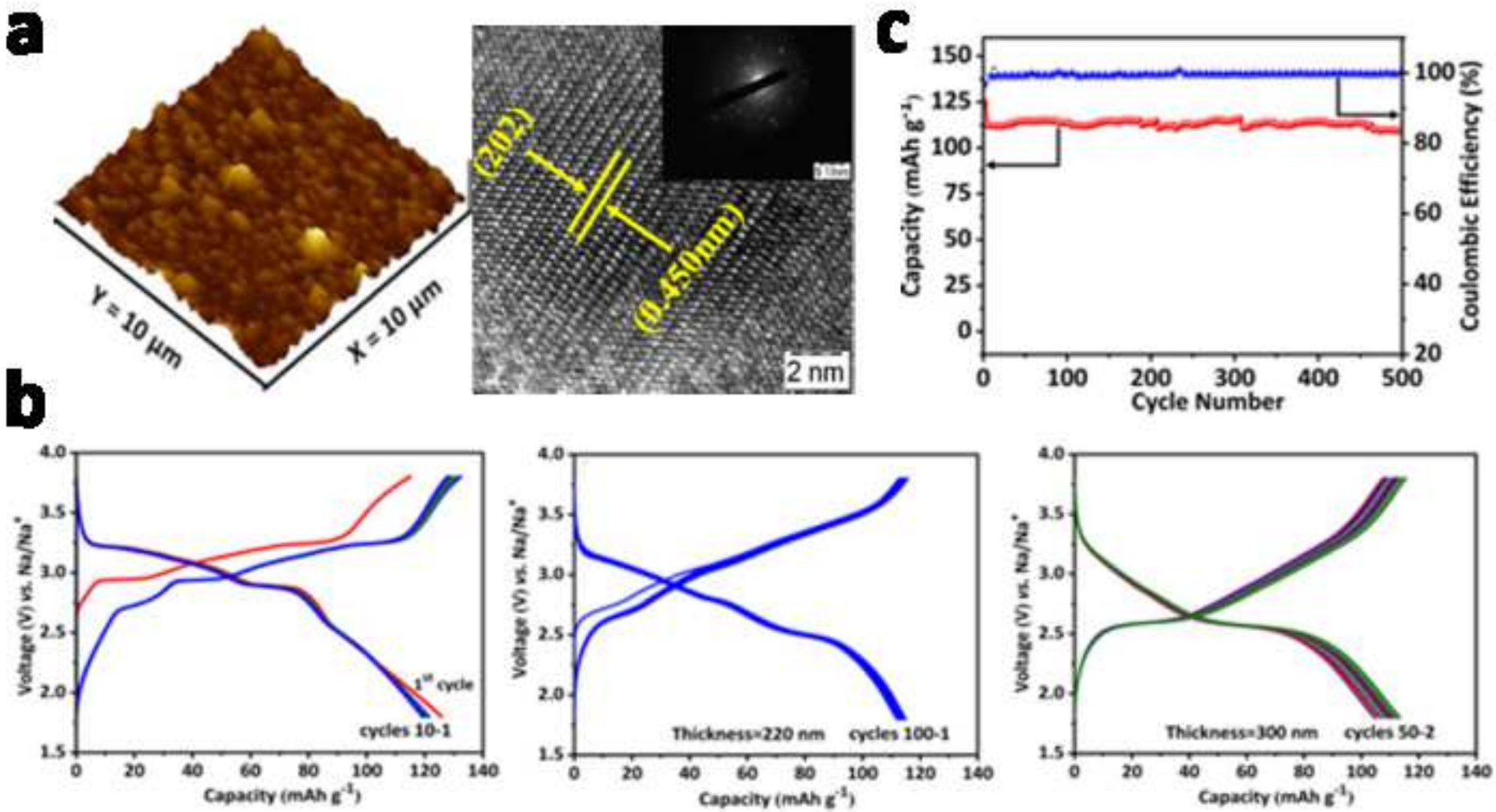

Figure 13

Click here to access/download;Figure;Fig.13..tif

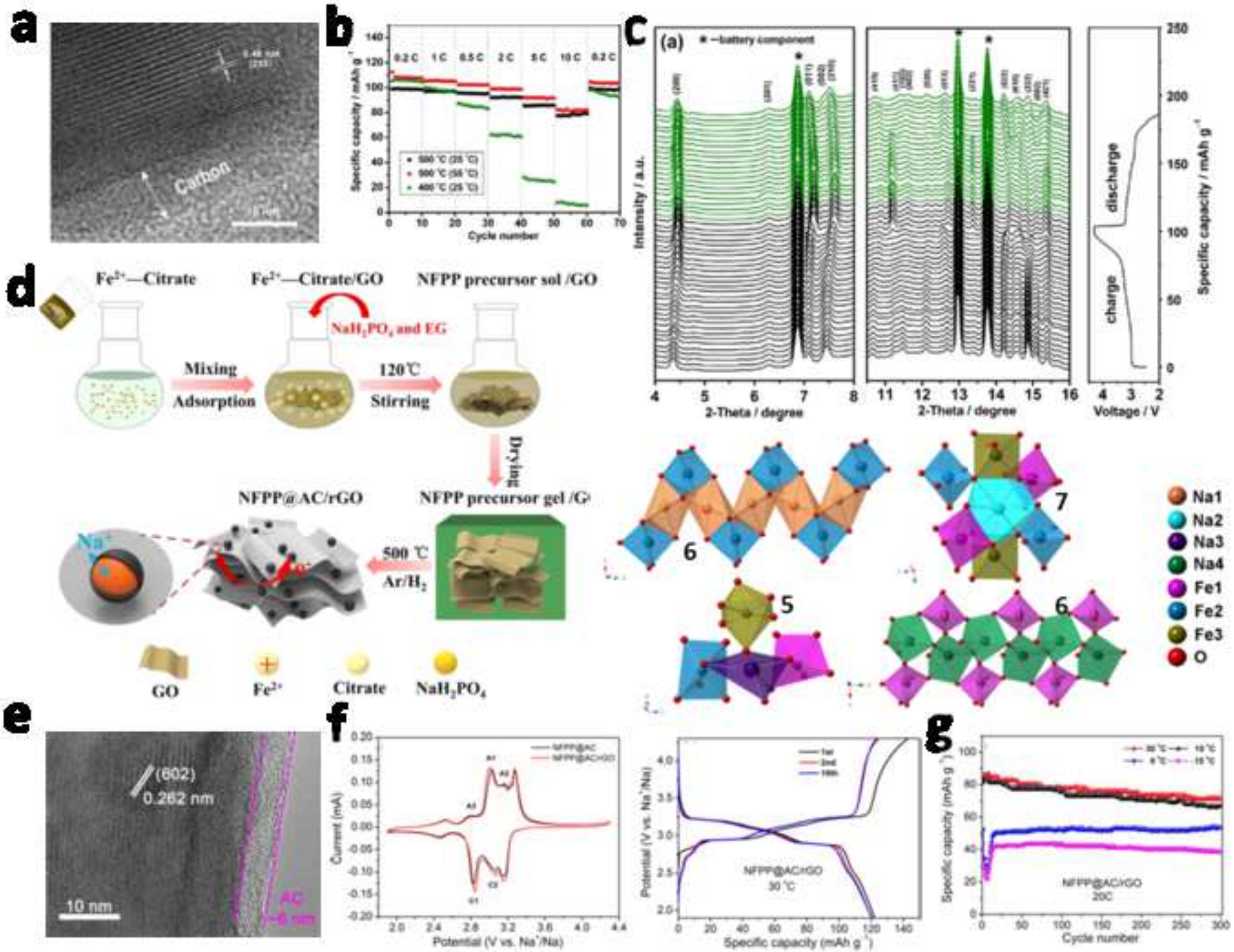

Figure 14

Click here to access/download;Figure;Fig.14..tif

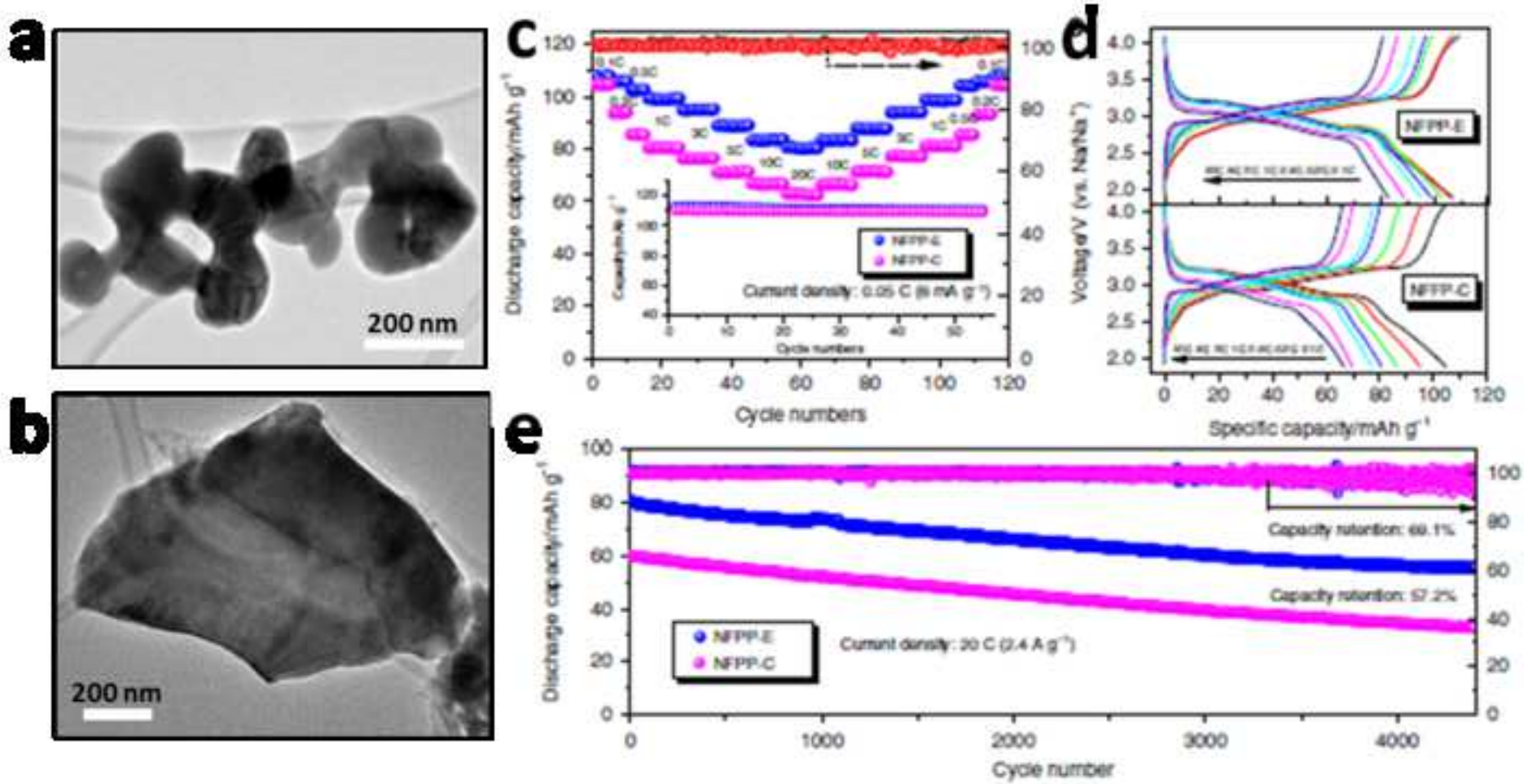

Figure 15

Click here to access/download;Figure;Fig.15..tif

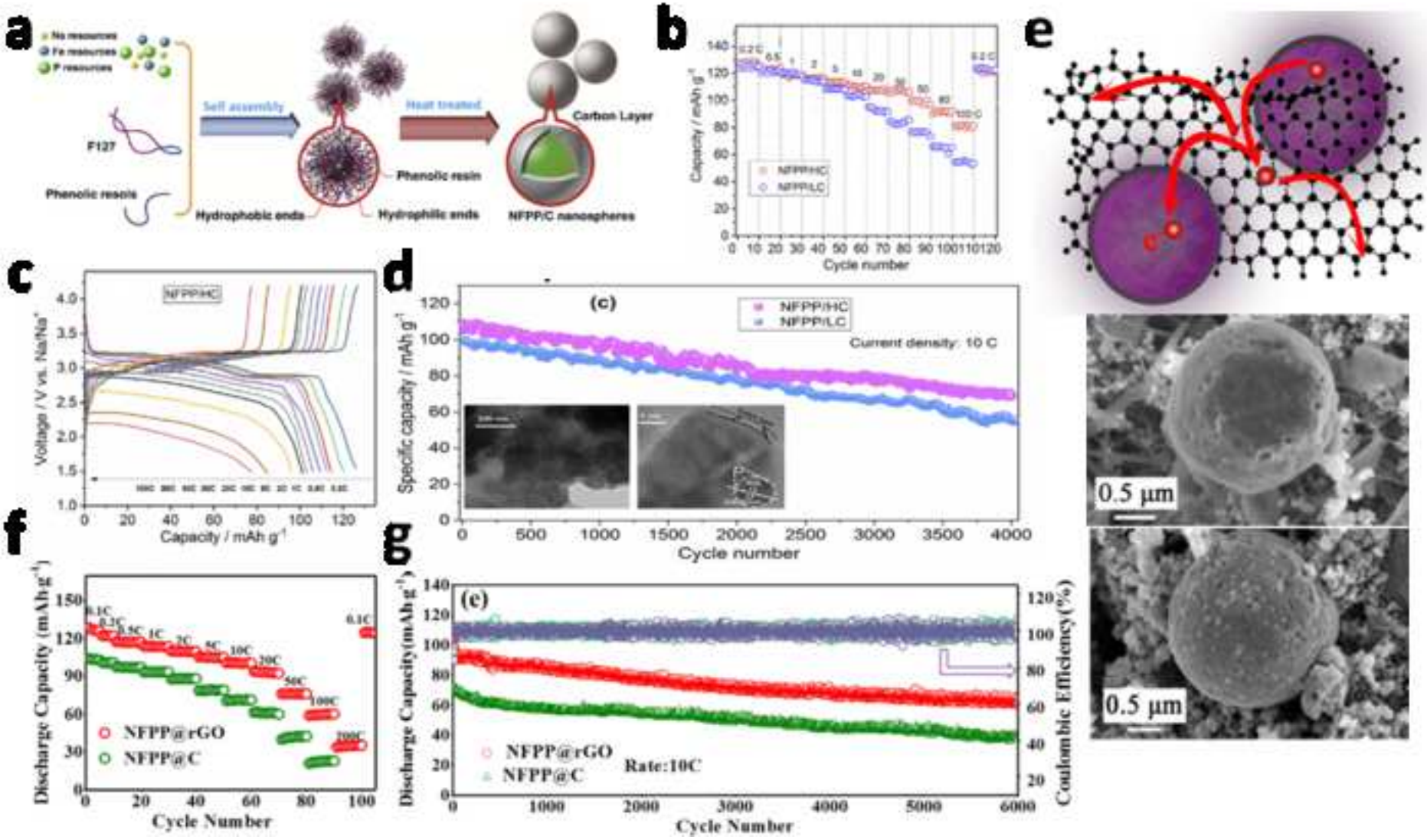

Figure 16

Click here to access/download;Figure;Fig.16..tif

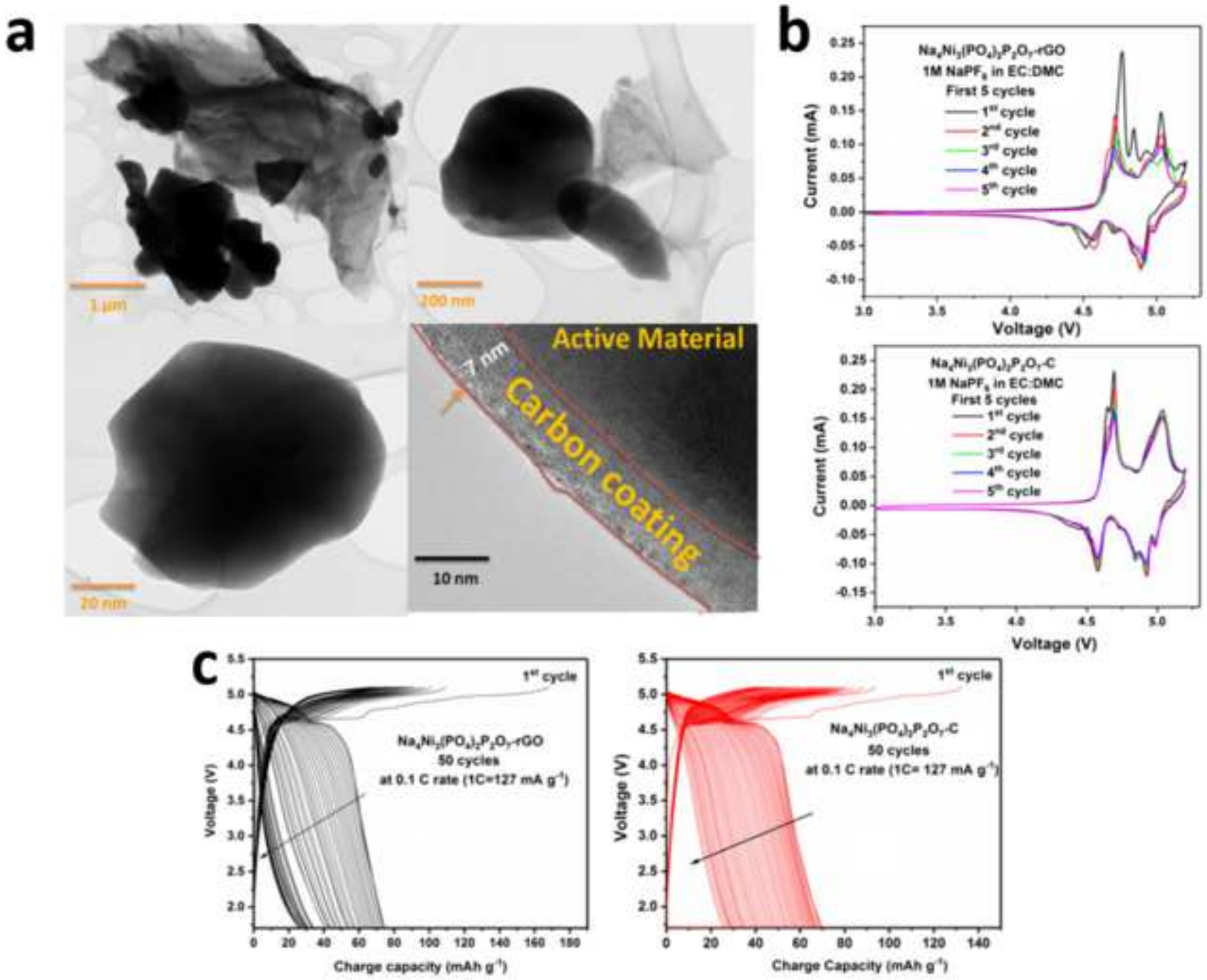

Figure 17

Click here to access/download;Figure;Fig.17..tif

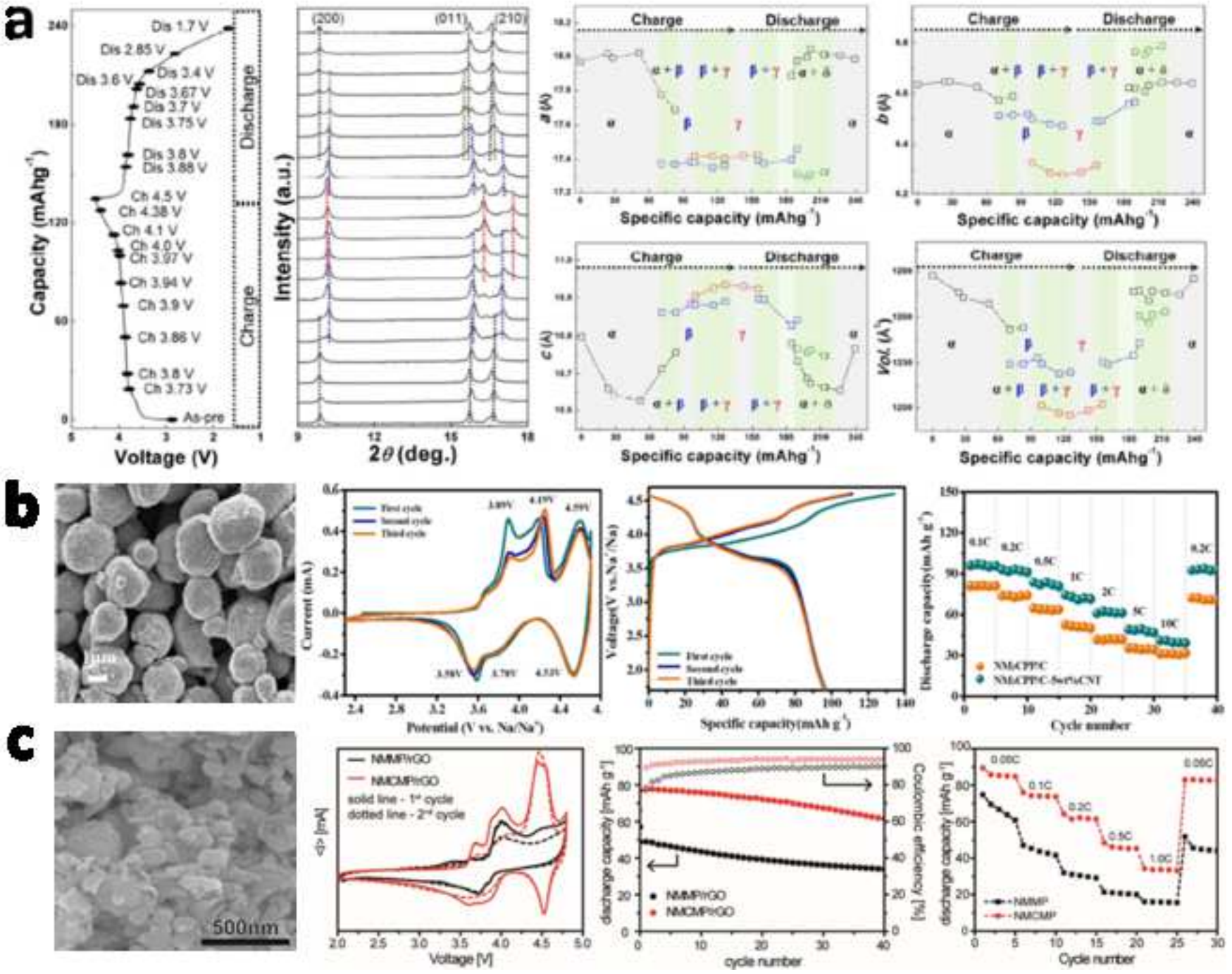

Figure 18

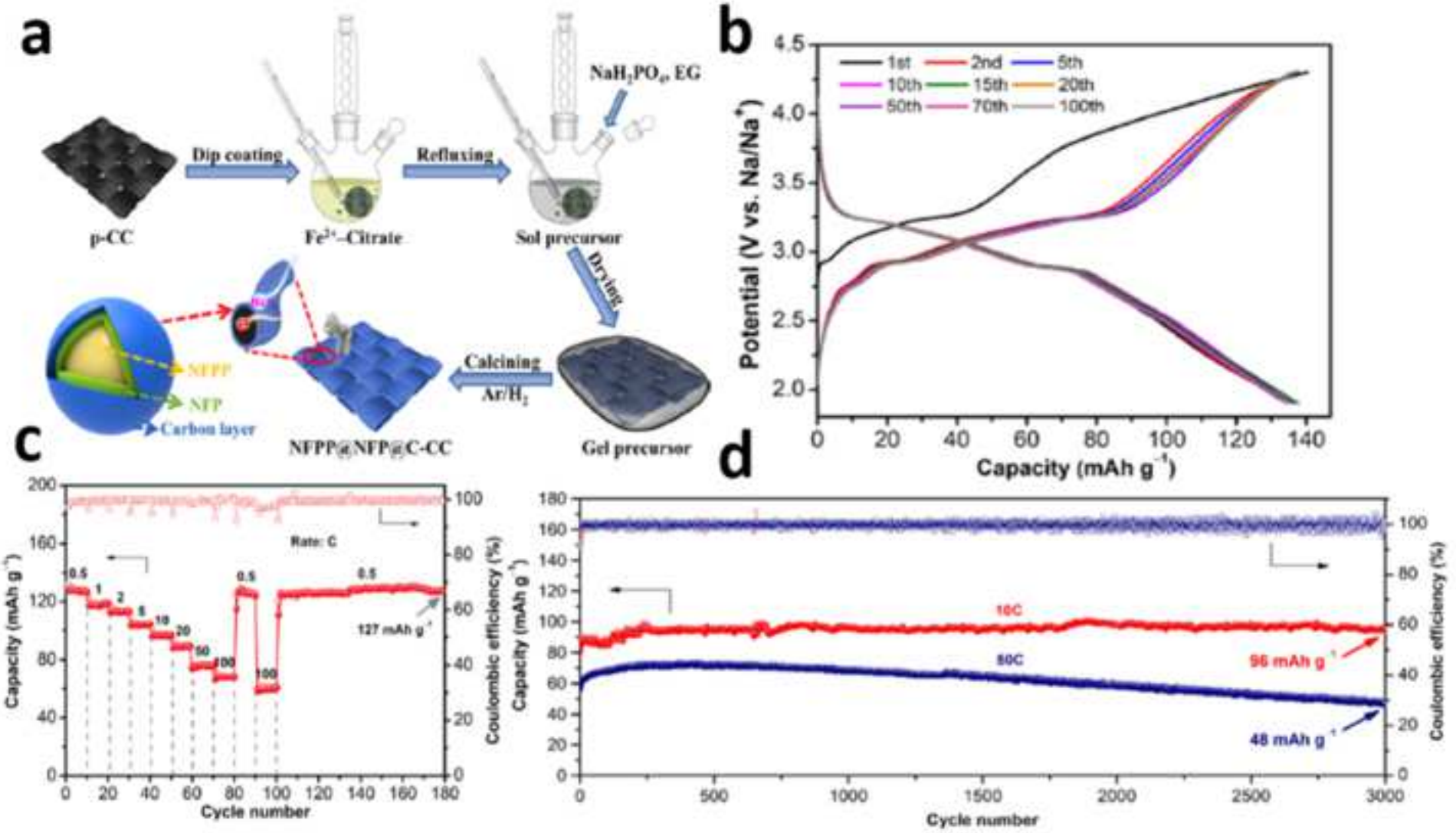

Figure 19

Click here to access/download;Figure;Fig.19..tif

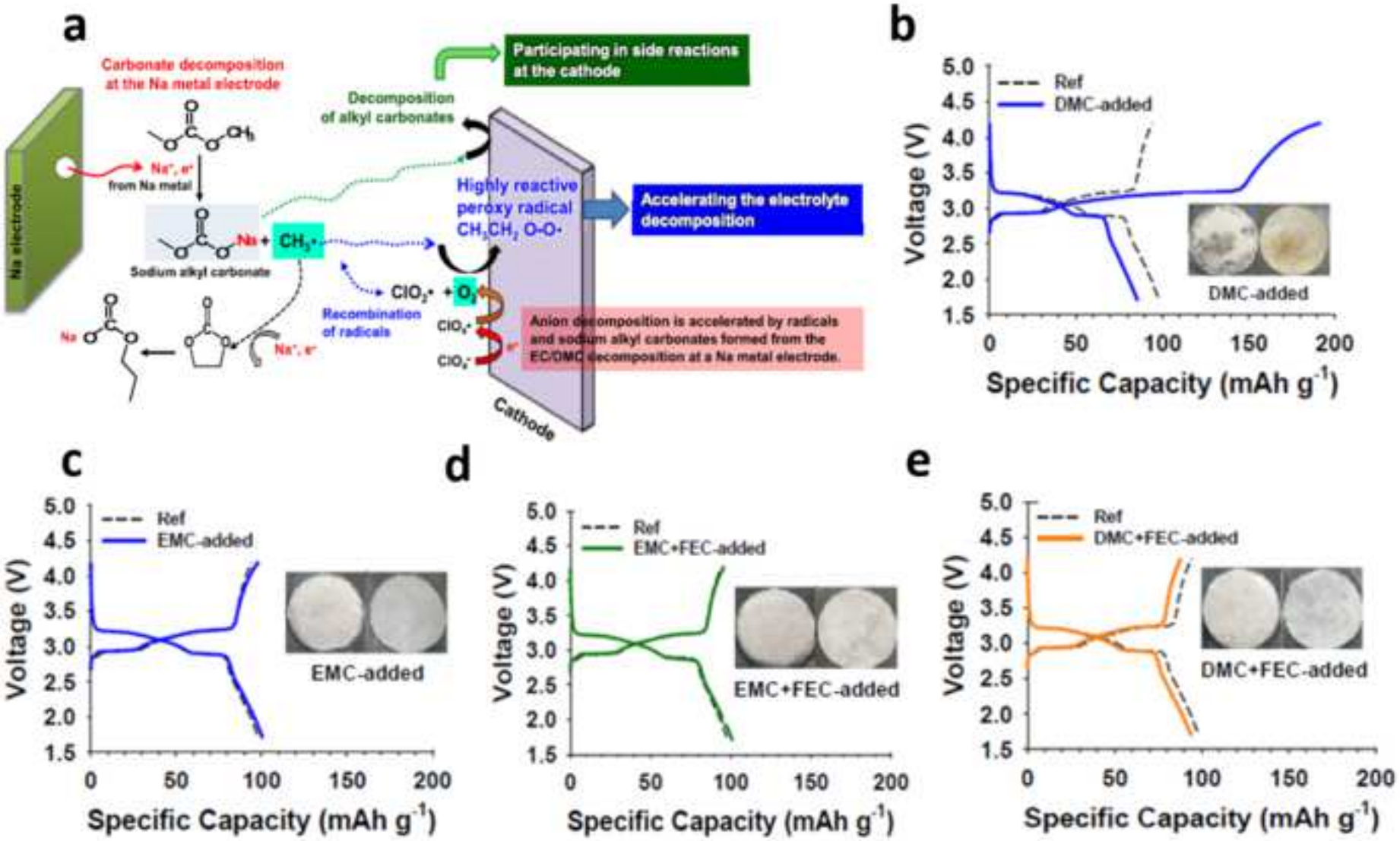

Table 1. Table comparing the unit call parameters of $Na_4M_3(PO_4)_2(P_2O_7)$ (M=Co, Fe, Ni,Mn)

Space group	$Pn2_1a$			
Space group no.	33			
Crystal System	orthorhombic			
M	Ref.	Cell parameters (Å)			Cell Volume ($Å^3$)
		a	b	c	
Ni	[47]	17.999(2)	6.4986(6)	10.4200(9)	1218.9(2)
Co	[49]	18.046(5)	6.533(2)	10.536(2)	1242.1(5)
Fe	[47]	18.07517(7)	6.53238(2)	10.64760(4)	1257.204(1)
Mn	[2]	17.991(3)	6.648(1)	10.765(2)	1287.6(3)

Table 2. The chemical composition of the solid-state prepared NFPP determined by XRD Rietveld refinement; Replotted with permission from ref. [97].

Sample	**XRD Rietveld refinement**		
	NFPP, %	$NaFePO_4$, %	$Na_2FeP_2O_7$, %
NFPP-600	56.7	25.3	18.0
NFPP-500	64.2	22.7	13.1
NFPP-450	89.1	10.9	-
NFPP-450 (quenching)	93.8	6.2	-
NFPP-400	61.8	28.9	9.3

Declaration of interests

☒ The authors declare that they have no known competing financial interests or personal relationships that could have appeared to influence the work reported in this paper.

☐The authors declare the following financial interests/personal relationships which may be considered as potential competing interests: